Evaluation of a concrete plug

-From the Dome Plug Experiment DOMPLU at Äspö HRL

Anders Kristiansson

June 2014
TRITA-BKN, Examensarbete 418, Betongbyggnad 2014
ISSN 1103-4297
ISRN KTH/BKN/EX--418--SE
Master Thesis in Concrete Structures

Royal Institute of Technology (KTH)
Department of Civil and Architectural Engineering
Division of Concrete Structures
Stockholm, Sweden, 2014

Abstract

In SKB's Äspö Hard Rock Laboratory (HRL) a full scale test of a concrete plug, part of a sealing structure for the depository of spent nuclear fuel, has been carried out. The aim of this thesis is to evaluate the behavior of the concrete plug and how it corresponds to assumptions made during the design. The concrete plug is dome shaped, un-reinforced and casted in situ with low-pH concrete. It will be exposed to high water and swelling pressures and designed for a life span of 100 years. During the first years it shall also prevent water leakage from the inside of the deposition tunnel. Before the pressure is applied, the concrete plug is assumed to de-bond from the rock due to autogenous and cooling shrinkage. The gap between the concrete and rock is then grouted during cooling and the concrete plug will hence be prestressed when the cooling is stopped.

The concrete plug is analyzed with the measurement data from the full scale test with comparisons to results from finite element simulations. The performed measurements include form pressure, internal strain and temperature, concrete plug displacements in the tunnel alignment, displacements relative to the rock and ambient temperatures. Two assumptions have been made during the evaluation; full bond to the rock or no bond to the rock. The results are also compared to two similar experiment that were previously performed.

The results indicate that the concrete did de-bond from the rock before grouting to some extent. It is plausible that a selective de-bonding was obtained. Due to high water leakage, were cables for the measurement equipment are drawn out from the concrete plug, the concrete plug was not exposed to the planed maximum pressure load. Results indicate that a water pressure is acting on the concrete plug from inside the rock slot which was not assumed during the design.

Keywords: DOMPLU, DOPAS, concrete plug, KBS-3V, measurement, full scale test, SKB, nuclear waste repository

Sammanfattning

I SKB:s Äspölaboratoriet har ett fullskaleförsök på en betongplugg, del av ett pluggsystem för förvaret av kärnavfall, utförts. Syftet med denna uppsats var att utvärdera betongpluggens beteende under fullskaleförsöket och hur det förhåller sig till gjorda antaganden under dess utformning. Betongpluggen är kupolformad, oarmerad och platsgjuten med låg-pH-betong. Höga vatten- och svälltryck kommer verka på betongpluggen som är utformad för en livstid på 100 år. Under de första åren ska den även motverka läckage från insidan av deponeringstunneln. Innan trycklasten läggs på är det antaget att betongpluggen släpper från berget till följd av autogen krympning och kylning. Utrymmet mellan betongen och berget injekteras och betongpluggen kommer således vara förspänd efter att kylningen upphört.

Betongpluggen är analyserad med mätdata från fullskaleförsöket som jämförts med resultat från finita element analyser. Mätningarna inkluderar formtryck, inre töjningar och temperaturer, deformationer i tunnelriktningen, deformationer relativt berget och lufttemperatur utanför betongpluggen. Två antaganden har gjorts under utvärderingen; att betongen är fast i berget eller att den är fri från berget. Resultaten jämförs även med två liknande fullskaleförsök som utförts tidigare.

Resultaten tyder på att betongpluggen till viss del släppt från berget innan injekteringen. Det är troligt att den släppt på vissa ställen och på andra inte. På grund av för högt vattenläckage där de ingjutna mätinstrumentens kabelgenomföring utförts, kunde inte betongpluggen belastas till det maximala tryck som var planerat. Resultaten tyder på att ett vattentryck verkar på betongpluggen mellan berget och betongen vilket inte var antaget under konstruktionen.

Nyckelord: DOMPLU, DOPAS, betongplugg, KBS-3V, mätningar, fullskaleförsök, SKB, kärnavfallsförvaring

Preface

This thesis was carried out in 2014 at the Division of Concrete Structures, Department of Civil and Architectural Engineering at the Royal Institute of Technology (KTH) in Stockholm, Sweden. The project was initiated by Dr. Richard Malm who also supervised the project.

I would like to express my sincere gratitude and thankfulness to Dr. Richard Malm for letting me take part of the project and for his advises and guidance.

The finite element analyses presented in this thesis is by a very large extent a work by Doctoral Student Tobias Gasch. I would like to express my sincere gratitude and thankfulness to Tobias Gasch for letting me use his model and for all his advises and guidance.

Stockholm

Anders Kristiansson

Contents

Chapter 1

Introduction

1.1 The Repository

SKB (Svensk Kärnbränslehantering AB) are researching on a method for storing spent nuclear fuel in the final repository in Forsmark, Sweden. The repository shall contain the spent nuclear fuel and isolate it from the biosphere. In addition, if the containment is breached, it shall prevent and retard the dispersion of radioactive substances so that the ionising radiation does not cause harm. (SKB (2010))

In the main alternative, KBS-3V, the nuclear waste is stored in a system of tunnels in rock at a depth of 470 meters. The tunnel system consists of a horizontal transport tunnel, shaped like a horseshoe, with horizontal deposition tunnels excavated perpendicular to the transport tunnel. Vertical deposition holes are excavated approximately 6 meters apart in the floor of the deposition tunnels. Nuclear waste, stored in copper canisters, are placed in the vertical deposition holes and embedded in a bentonite clay buffer. When all the vertical deposition holes of a deposition tunnel are used, the deposition tunnel needs to be sealed off from the transport tunnels and the rest of the deposition facility. This is done by filling the deposition tunnel with bentonite clay and sealing it with a plug system. When all the nuclear wastes are deposited, the transport tunnels and shafts are filled with swelling clay. A figure of the principle of the deposition facility is shown in Figure 1.1. (Malm (2012))

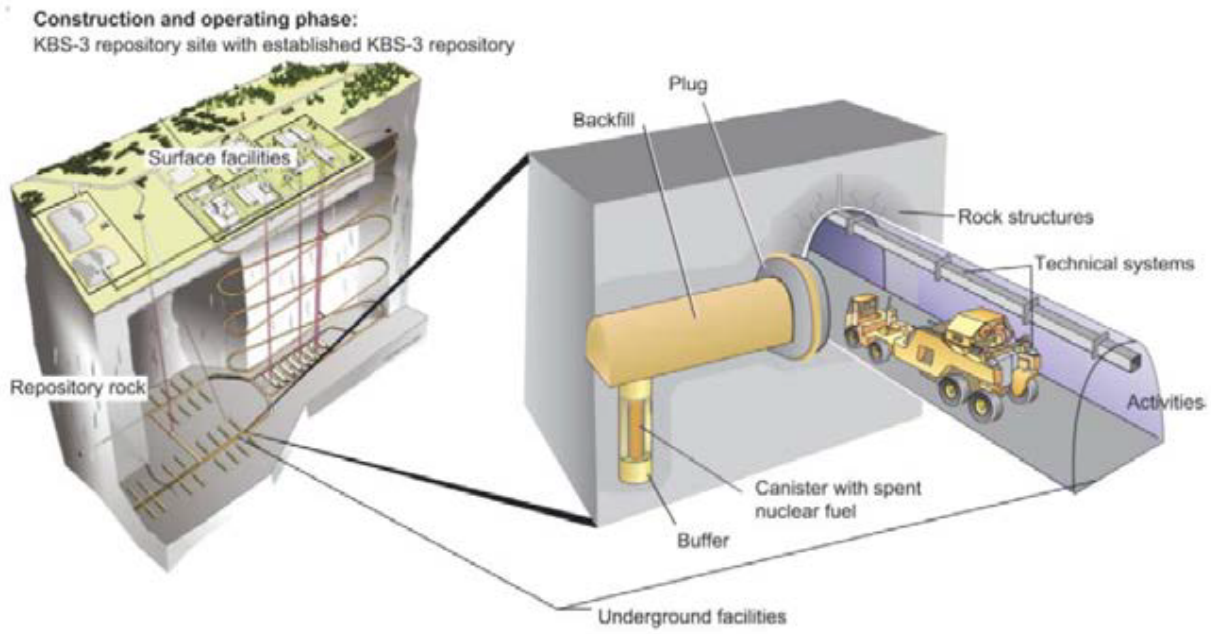

Figure 1.1: Principle of deposition facility. From Malm (2012)

1.2 Plug system

The plug system is designed for a lifespan of 100 years and shall maintain its function until the transport tunnels are filled and the natural geohydrological conditions are retained. The main purpose of the plug system is to create a watertight seal and prevent leakage from the deposition tunnel into the transport tunnel. A figure of the principle design of the plug system is shown in Figure 1.2. The plug system contains the following layers: (Malm (2012))

- Delimiters; to separate different layers in the plug design.
- A filter; to drain the tunnel while the concrete plug is cast and matures and also for controlled wetting of the bentonite seal.
- A bentonite seal; used as a watertight seal in the plug system.
- Concrete plug; described in Section 1.3.

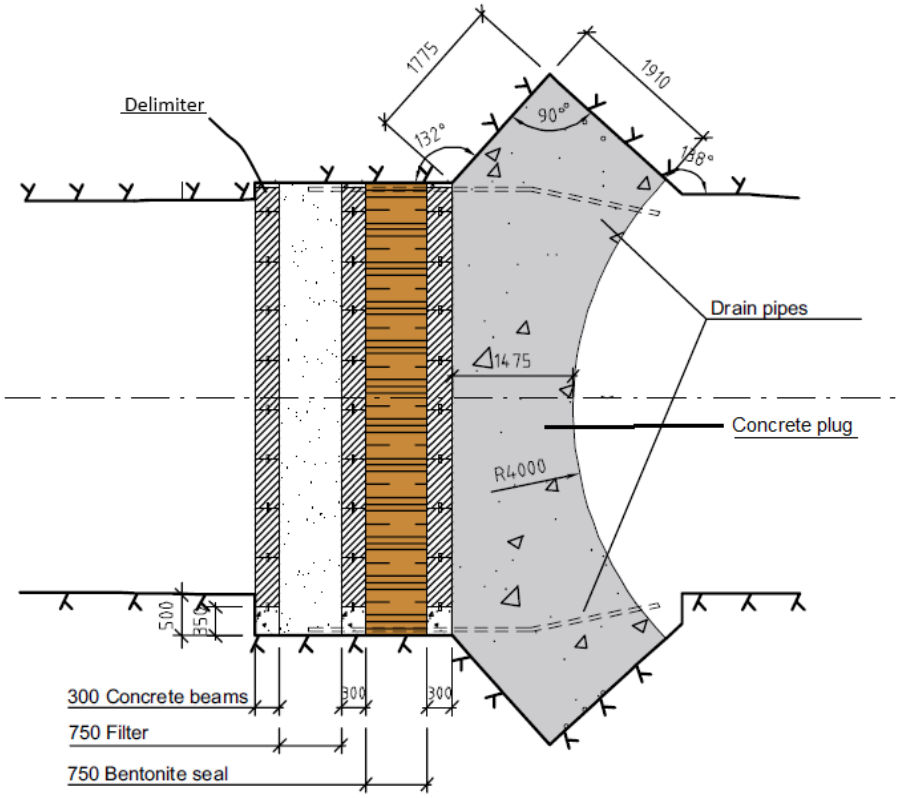

Figure 1.2: Plug system. Dimensions are different in the full scale test. Modified from Malm (2012).

1.3 Concrete plug

The main purpose of the concrete plug is to resist the loads acting on the structure. The largest external loads comes from the swelling of the bentonite clay inside the deposition tunnel and the hydrostatic water pressure from the inside of the deposition tunnel. Further, the concrete plug must be watertight until the bentonite seal is saturated and has reached homogenization. (Malm (2012))

The bentonite clay is sensitive to chemically basic materials. To minimize the negative effects on the swelling of the bentonite clay, the concrete plug is cast with a low-pH concrete; here defined as concrete with pH-value below 11. Normal concrete have typically a pH-value above 12.5. Low-pH concrete has a larger amount of autogenous shrinkage (shrinkage under sealed conditions). If the concrete plug was reinforced, cracks could occur due to shrinkage restraint. The concrete plug is therefore unreinforced. The concrete plug has a dome shaped design and is cast in-situ. (Malm (2012))

For further reading about the choice of the design of the concrete plug it is referred to Malm (2012).

1.4 Full scale test

The purpose of the full scale test is to ensure that the design of the plug system works as intended and fulfills the performance requirements. Further, the test will be used to evaluate the structural behavior of the concrete plug and verify calculations and assumptions used during the design.

The concrete plug with the design described in Section 1.3 was casted in Äspö Hard Rock Laboratory in March 2013. The test includes all the material layers in the plug system as described earlier. About three months after casting, the concrete plug is cooled to obtain an extra shrinkage in addition to the obtained autogenous shrinkage. The gap between the concrete plug and the rock surface is grouted from the upstream side of the concrete plug (the side of the deposition tunnel, subjected to pressure). The cooling is then shut off. This is done to obtain a pre-stressing of the concrete. (SKB (2013))

Measurements of pressures, temperatures, strains and deformations are continuously registered during the test period.

1.5 Previous tests

A number of tests for similar purposes have been carried out earlier. The design and materials in these tests differ from the test evaluated in this thesis. Their results can however still serve for comparisons. The most relevant tests are described in Sections 1.5.1 and 1.5.2.

1.5.1 Prototype Repository

The Prototype Repository experiment was carried out in full scale to test the engineered barriers and their interaction to the host rock. The test was separated in two sections. The first section was installed during summer and autumn 2001 and the second section was installed during spring and summer 2003 in the Äspö HRL. (Johannesson et al. (2006))

The inner section (Section I) contained four vertical deposition holes with copper canisters surrounded by a bentonite buffer. The canisters were equipped with electrical heaters to simulate the heating from the nuclear waste. The sections were separated by a concrete plug (Plug I). The outer section (Section II) contained two deposition holes and was sealed with a concrete plug (Plug II). A principle layout of the tested deposition tunnel is shown in Figure 1.3. The tunnels were backfilled with a mixture of bentonite and crushed rock. (Dahlström (2009))

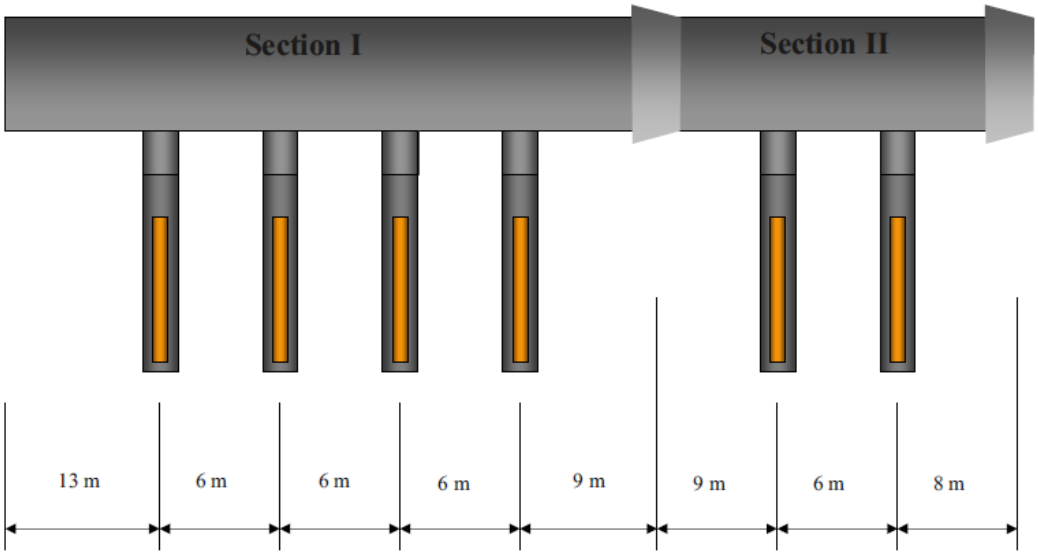

Figure 1.3: Layout of the Prototype Repository test. Plug I to the left and Plug II to the right. From Dahlström (2009)

The concrete plugs are dome shaped with v-shaped abutments. The plug was casted with self compacting concrete and reinforced with minimum reinforcement according to the used design code. A cooling system was installed together with the reinforcement. After curing of the concrete, the plug was cooled about 10-12 °C and the gap between the concrete and rock, caused by autogenous shrinkage of the concrete and shrinkage from the cooling, was grouted via pre-installed grouting tubes. The cooling was then stopped.

Plug II was instrumented with the following: (Dahlström (2009))

- 6 joint meters at the concrete - rock interface, measuring the deformation between the plug and rock.
- 6 strain gauges installed parallel to each joint meter, measuring the strain in the concrete.
- 12 rebar strain gauges embedded in the concrete, measuring strain in the concrete.

Drainage of the inner part of Section I and through Plug II were closed during November 2004. This led to drastic increase of the pressure in the backfill and buffer which led to failure of one of the heaters. Due to this, the drainage was opened again with a subsequent slow saturation of the backfill and buffer and a low pore pressure in the tunnel, according to Malm (2012). Hence, the plug was never exposed to the planed pressure but a maximum pressure of 1.6 MPa. The measured pressure acting on the plug is shown in Figure 1.4. (Dahlström (2009))

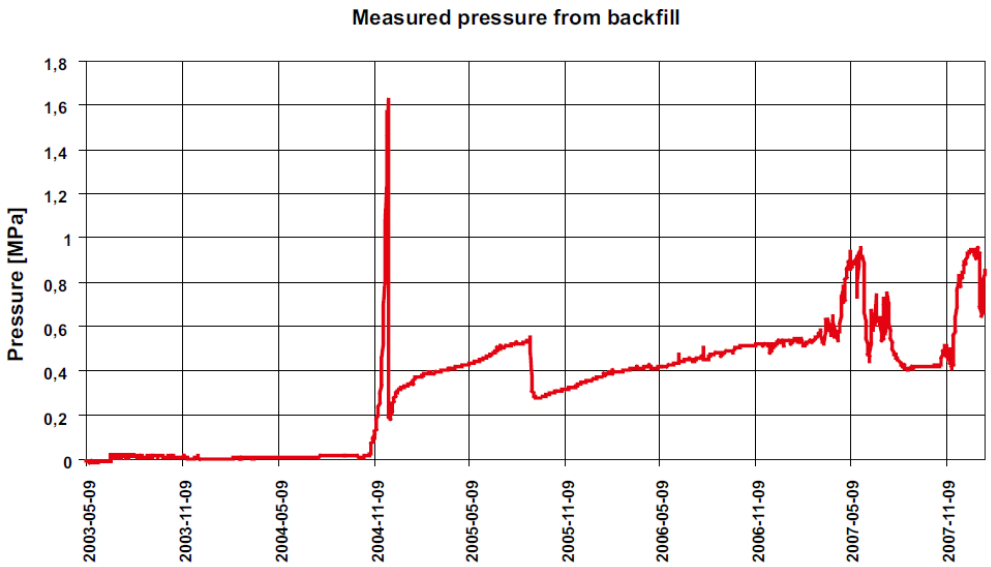

Figure 1.4: Measured pressure acting on Plug II. From Dahlström (2009)

Joint meter measurements showed an increase of the gap in the concrete - rock interface perpendicular to the rock of 0.15 to 0.24 mm when the plug was cooled prior to grouting. This was close to the expected, according to Dahlström (2009). Instruments parallel to the tunnel axis showed no increase of the gap in the concrete - rock interface. According to Dahlström (2009), this was probably due to the high pressure from the backfill behind the plug. Long term deformation measurements of the interface indicated an increase of the width perpendicular to the rock surface, which was expected due to the grouting of the interface. Measurements of the interface width parallel to the tunnel axis indicate compression but their corresponding strain gauges do not indicate compression. A reason for this might be that the plug had deformed or slipped according to Dahlström (2009).

The rebar strain gauges inside the plug showed small tension during casting before being compressed to stresses around -2 MPa as the temperature decreased. The cooling before grouting caused the plug to additional compression of around -1.4 to -2.2 MPa. Long term measurements show compression in the whole plug with stresses from around -2.8 to -4.9 MPa. (Dahlström (2009))

1.5.2 Tunnel Sealing Experiment

In the tunnel sealing experiment (TSX) an unreinforced concrete plug was tested in full scale, at the Underground Research Laboratory in Manitoba, Canada. The concrete used was a Low Heat High Performance concrete (LHHPC).The plug was casted in situ in the 3.5 m high and 4.4 m wide elliptical tunnel cross section. The plug was casted in wedge shaped keys, excavated in the rock. A figure of the concrete plug is shown in Figure 1.5.(Martino et al. (2006))

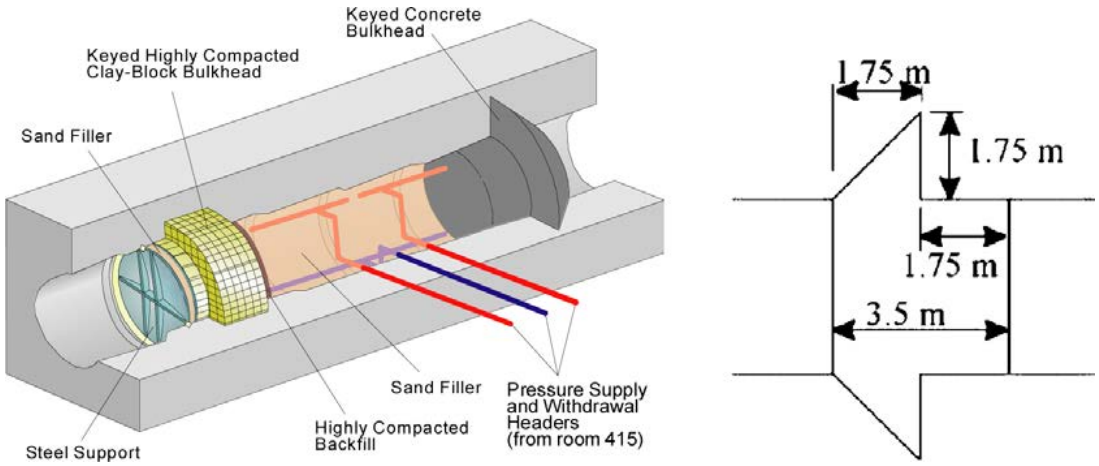

Figure 1.5: Test set-up (right) and concrete plug (left) in the TSX. From Malm (2012).

The plug was equipped with sensors monitoring deformation, temperatures, interface displacement as well as acoustic emissions and velocity. The tunnel was filled with sand and water and a system supplying pressurized water controlled the pressurization. When the pressurization began, it was found that the seepage past the plug was too large. The pressure was therefore reduced and grouting of the interface through pre installed grouting tubes was performed. The pressure was increased again in steps to a final pressure of 4 MPa where it was held constant during heating of the upstream side of the plug. The temperature was increased to approximately 50 °C and 65 °C in two steps before cooling and draining of the tunnel. (Martino et al. (2006))

Volume reduction during cooling caused a partial separation of the concrete from the rock. Within two weeks after casting, three cracks developed at the intersection of the keyed and unkeyed segments of the plug. According to Martino et al. (2006) this indicated tensile forces in the concrete due to a combination of shrinkage and selective de-bonding in the concrete-rock interface. The acoustic amplitude and velocity after the grouting indicated that these cracks were injected successfully. During the pressurization, most of the cracks were associated with the concrete-rock interface, however, a relatively low number of cracks occurred during pressurization. Displacements measured at the plug face indicated a maximum displacement of approximately 0.25 mm in the downstream direction at the final pressurization. (Martino et al. (2006))

1.6 Aim and scope of the thesis

The full scale test in Äspö HRL is carried out to verify that the plug system fulfills the requirements and behaves as expected during the design. This thesis treats the evaluation of the behavior of the concrete plug based on measurements from this test and comparisons to results from finite element calculations.

The thesis includes evaluation of the following:

- Form pressure during casting.
- Strains and stresses in the concrete plug.
- Displacements of the concrete plug in the tunnel alignment and displacements relative to the rock.
- Temperature of the concrete plug and ambient temperatures.

The results are discussed in Chapter 7 with focus on the behavior of the concrete plug and how it corresponds to what was expected.

The results from this thesis will be used to verify structural calculations and assumptions made during the design of the concrete plug.

1.7 Delimitations

This report focus on the evaluation of the concrete plug in the full scale test. Other materials and layers in the plug system are described in the report but are not evaluated. Measurements of the pressure in the bentonite seal are used but is not evaluated in this report nor is its validity.

The main focus for the evaluation in this report is on the measurement data. FE calculations are used but are only partly made by the author of this report. Calculations are made with the assumptions of either no bond to the rock or full bond to the rock before the grouting takes place. A selective de-bonding is not included in the calculations.

The behavior of the concrete plug is discussed with measurements as the main base. The behavior is thus treated in the extent of which conclusions that can be drawn from the measurement results. One assumption is that the concrete plug carries the load through arch action. This is not evaluated in this report. Further, creep is not included in the stress calculations based on strain measurements.

1.8 Structure of the thesis

Each chapter is briefly described below to get an overview of the structure of this thesis.

In Chapter 2, the plug system with its layers and their function requirements and properties are presented. The concrete plug is presented in depth with material composition and properties while other layers in the plug system are presented briefly.

Chapter 3 gives an overview of the full scale test. The purpose of the test is presented as well as the test procedure and the installation of the concrete plug. Also, the measurements performed in the full scale test are presented. This includes an brief description of the instrumentation of the concrete plug. The instrumentation of the concrete plug is further described in Chapter 4. This chapter presents the measurement sensors types and their properties, installation and positions.

The methodology is described in Chapter 5. Filtering of the measurement data is described with brief explanations of the used filtering methods. Temperature compensation for the strain gauges are described as well as stress calculations. The methods for finding the measurement reference points are described and the chosen reference points are presented. The chapter also include descriptions of the FE models used for the evaluation of the concrete plug.

The results are presented in 6. The results are divided in two time periods. Results during the casting and grouting period is presented in the first section and results during the pressurization period are presented in the second section. Measurement results for temperature, joint meters, LVDT displacements, stress and strain are presented with results from 3D FEM simulations. From the 2D FEM simulations, strain results and LVDT displacement results are presented for one sensor respectively. Measured form pressure during cating is also presented.

The results are discussed in Chapter 7. The measurement results are compared to results from the FEM simulations and previously performed experiments. The plausible behavior of the concrete plug is discussed and compared to assumptions made during the design. The chapter also contains a discussion of the validity of the results and suggestions for further research.

Chapter 2

Plug System and Concrete Plug

In this chapter the layers of the plug system and their function requirements and properties are described.

2.1 Plug system

The plug system shall keep the backfill in place and be a watertight barrier preventing axial flow from the deposition tunnel and erosion of the bentonite buffer. It must also resist the loads acting on it and maintain its function during the entire time that the repository facility is in use. Hence, the plug system should be designed for a lifespan of 100 years.

The plug system, shown in Figure 1.2, includes the following parts, according to Malm (2012), from the upstream side (the side of the deposition tunnel, subjected to pressure) to the downstream side (the side of the transportation tunnel):

1. Delimiter
2. Filter
3. Delimiter
4. Bentonite seal
5. Delimiter
6. Concrete plug

2.1.1 Delimiters

The delimiters consist of prefabricated concrete beams. The delimiters are used to separate and facilitate the installation of the different layers. (Malm (2012))

2.1.2 Filter

The filter consist of expanded clay aggregate and crushed rock. The filter is used to buffer water and allow for artificially controlled wetting of the bentonite seal through drainpipes. Drainage from the deposition tunnel can thereby be performed until the concrete plug has reached sufficient strength and contact grouting has been performed. Assuming that the concrete beams can move in the tunnel direction and that the filter is compressible, the filter also reduce the swelling pressure from the backfill and assist to create an evenly distributed pressure on the concrete plug. (Malm (2012))

2.1.3 Bentonite seal

The bentonite seal is the main layer to create a watertight system and prevent leakage from the deposition tunnel. During saturation of the installed bentonite, the bentonite will swell and penetrate cracks in the rock. The artificial wetting from the drainpipes and filter ensures a fast and homogenous saturation of the bentonite seal. (Malm (2012))

2.2 Concrete plug

2.2.1 Functional requirements

The concrete plug shall support the bentonite seal and transfer the loads from the hydrostatic pressure at repository depth and the swelling pressure from the backfill to the surrounding rock. It may take several years before the bentonite seal has saturated and fully obtained its sealing function. During this time, the concrete plug is an important barrier to prevent leakage from the deposition tunnel. It is hence important that no cracks going through the entire thickness develops in the concrete plug. Such a crack may lead to high leakage due to the large hydrostatic pressure and thereby risk erosion of the buffer and backfill material. (Malm (2012))

2.2.2 Geometry

The concrete plug is dome shaped, casted into a slot excavated as an octagon around the tunnel surface. Its dimensions can be seen in Figure 2.1.

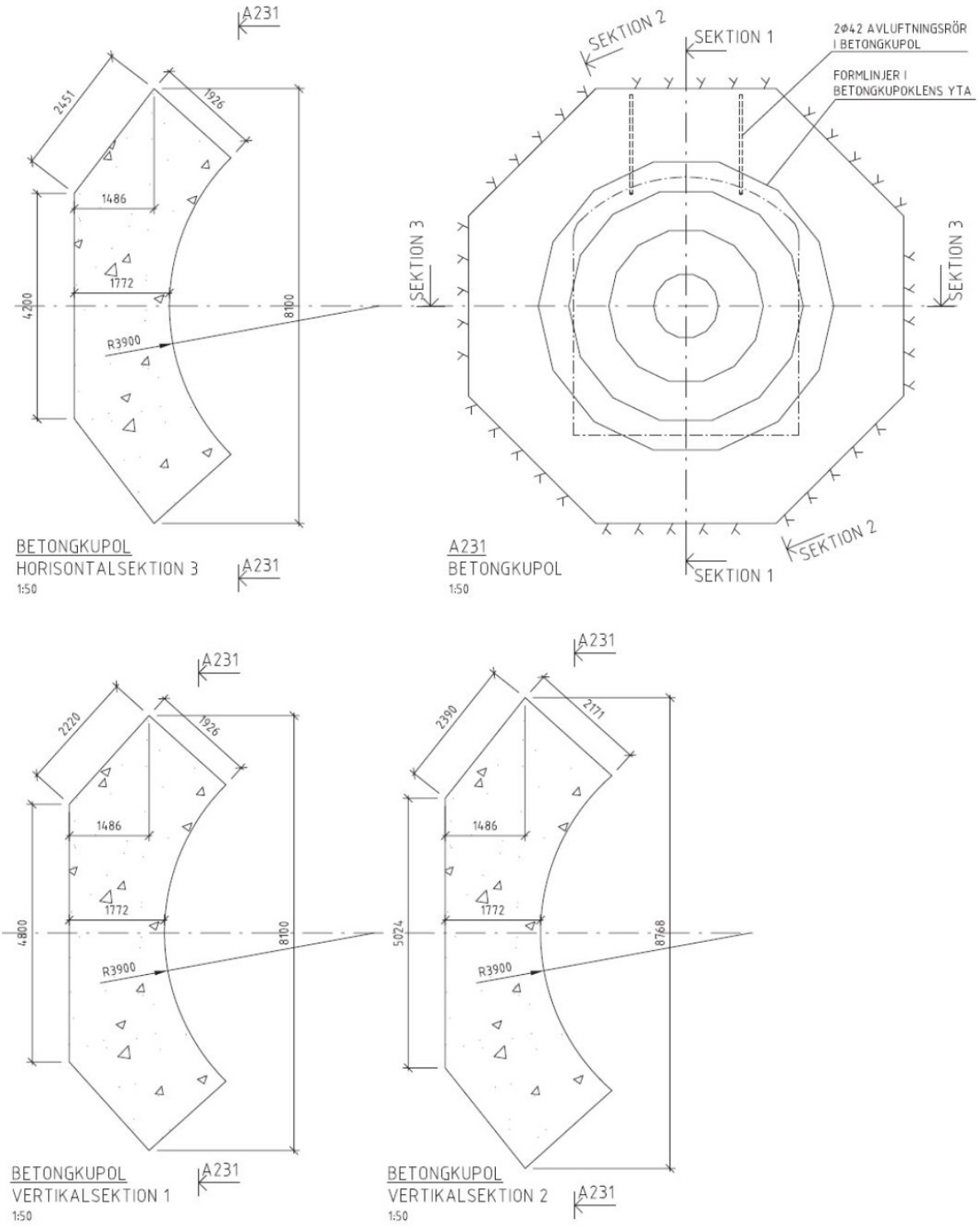

Figure 2.1: Concrete plug dimensions. From Malm (2014).

2.2.3 Composition and properties

In initial studies of the concrete plug, it was found that mainly compressive stresses occurred and that only the minimum amount of reinforcement according to design codes was required. It was later decided by SKB that low-pH concrete should be used for the concrete plug to minimize negative effects on the bentonite clay. The low-pH concrete developed for the concrete plug showed a large amount of autogenous shrinkage that could cause cracking due to the restraining forces from reinforcements. Further studies showed that it would be possible to design a concrete plug without any reinforcement. An un-reinforced dome shaped low-pH concrete plug was therefore chosen for the conceptual design. (Malm (2012))

A low-pH self-compacting concrete was developed and tested by the Swedish Cement and Concrete Research Institute (CBI). Theoretical and experimental methods to examine the concrete properties were also carried out at Luleå University of Technology (LTU). Two concrete recipes with different binder contents were tested; B200 with 200 kg/m^3 and B300 with 300 kg/m^3 (Vogt et al. (2009)). Concrete B200 was chosen for the concrete plug in the full scale test (Malm (2012)).

Mix design

To lower the pH value, about 40% weight of the cement in the binder was replaced by silica fume. The chosen method to obtain self compacting properties was to increase to amount of paste by adding filler. Limestone filler was chosen since this is the most commonly used filler material in Sweden. The fine aggregate was considered to have a high influence on the quality of the concrete. Natural sand of high quality from the Äspö area with a well distributed grading curve and rather high amount of fine material was selected. The course aggregate was considered to be of less importance and crushed rock of average quality was chosen. Superplasticizer was also added. For more information about the mix design it is referred to Vogt et al. (2009). The composition of B200 is given in Table 2.1.

Table 2.1: Mix composition of concrete B200. From Vogt et al. (2009).

Cement CEM I 42.5 MH/SR/LA	120 kg/m^3
Silica fume (densified)	80 kg/m^3
Water	165 kg/m^3
Limestone filler L25	369 kg/m^3
Sand 0-8 mm	1037 kg/m^3
Gravel 8-16 mm	558 kg/m^3
Glenium 51	6.38 kg/m^3
water/cement	1.375
water/binder	0.825
water/powder	0.29

Heat development

The heat development during curing was measured by CBI in a semi-adiabatic calorimeter. The measurement showed a temperature increase of 7 °C. This is according to Vogt et al. (2009) a low value compared to $40 - 45$ °C for ordinary concrete.

When testing at concrete factory, cylindrical steel moulds with diameter 0.85 m and height 3 m were filled with concrete. A temperature increase was measure to about 10 °C during curing.

Shrinkage

The concrete plug will be casted in an environment with high relative humidity. Water will probably be present on the upstream concrete surface, at least until the bentonite seal has reached homogenization. The downstream surface will be covered by a plastic sheet to accumulate water passing the concrete plug in order to measure the leakage of water. The concrete will hence be subjected to a relative humidity of almost 100%. The main part of the shrinkage will therefore be a consequence of autogenous shrinkage and drying shrinkage will have a minor influence. (Malm (2012))

The shrinkage was examined with three methods in Vogt et al. (2009). Shrinkage under sealed conditions, i.e. autogenous shrinkage, was considered since this is valid for a large part of the concrete plug.

Method 1 measured volume change of a sample in a tight flexible latex membrane submerged in water. The change in volume was measured by the change in weight (reduced buoyancy, according to Archimedes' principle). The measurement started about 30 minutes after mixing. This method showed a large volume change during the first 6 h. After 48 h a volume change of approximately -0.6% was measured.

Method 2 used a digital dilatometer. The concrete specimen was casted into a flexible plastic tube and was placed into a measuring frame. Measurements started about one hour after mixing and continued over a long time period. The measurement registered a shrinkage of about 0.75 mm/m during the first 24 h and 1.2 mm/m after 4.5 months, i.e. a large part of the shrinkage occurred during the first 24 h.

Method 3 was a modified Swedish standard test in accordance with SIS (2000). Beams were demoulded one day after casting. Half of the beams were sealed with gas-tight butyl tape and half of the beams was stored with a free surface in 50% RH. Measurements of shrinkage and weight started 24 h after casting. The sealed beams lost almost no weight while the unsealed beams lost a large amount of water according to Vogt et al. (2009). Shrinkage after a long time period was approximately 0.17 mm/m for the sealed beams.

According to Vogt et al. (2009), method 2 was the only suitable method for the early autogenous shrinkage. However, the plastic tube in method 2 later allowed

water to evaporate. The most realistic description of the autogenous shrinkage may therefore be a combination of method 3 with method 2 used for the first 24 h. It was also concluded that the shrinkage goes on for a long time period. Equation (2.1) for the shrinkage after 24 h was developed in Vogt et al. (2009) to fit the results from method 3.

$$y = 0.0238Ln(x) + 0.003 \tag{2.1}$$

where y is the shrinkage in mm/m and x is the time in days.

Malm (2012) estimated the shrinkage contribution to the gap between concrete and rock before grouting after 90 days with shrinkage values according to Vogt et al. (2009). Since a large part of the autogenous shrinkage occurs during the first 24 h, the casting rate was taken into account as 0.5 m/h with a total casting time of 16 h. Since the concrete plug is assumed to release from the rock, free shrinkage was assumed. The resulting gap from shrinkage can be seen in Figure 2.2.

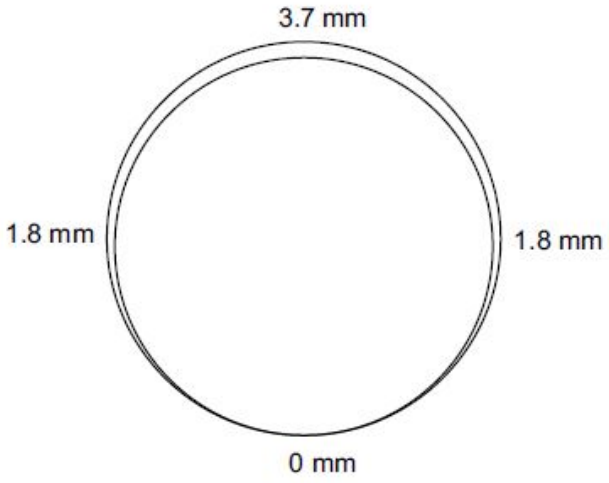

Figure 2.2: Estimated gap between concrete plug and rock from shrinkage after 90 days. From Malm (2012).

Strength

It was found that in contrast to ordinary concrete, the compressive strength keeps increasing after 28 days of curing. The design age was set to 90 days after curing. The characteristic compressive strength for a cylinder with 150 mm diameter and height 300 mm, f_{ck}, was calculated to 54 MPa in accordance with Eurocode EN 1992-1-1:2004. The mean compressive strength, f_{cm}, was calculated to 62 MPa.

The tensile strength calculation was based on uniaxial tensile tests of cylinders with 68.5 mm diameter at the age of 115 days. Only two specimens were tested. The characteristic tensile strength, f_{ctk}, was calculated to 2.9 MPa and the mean tensile strength, f_{ctm}, was calculated to 3.3 MPa. (Vogt et al. (2009))

Young's modulus and Poisson's ratio

The development of the Young's modulus was tested and evaluated at LTU with different methods for young and mature concrete. Young concrete was here defined from casting and the first month thereafter, and mature was defined as the age of external loading (here about three months) to the time of interest for long-term effects.

In the evaluation of the Young's modulus for young concrete, the rate of loading was taken into account. For mature concrete, a test procedure in accordance with Swedish standard SIS (2005) was used. Equation (2.2) was used to describe the development of the Young's modulus with parameters chosen to agree with the test results. The evaluated trend curve and test results from Vogt et al. (2009) are shown in Figure 2.3.

$$E_c(t) = \left[exp\left\{ S_E \left(1 - \sqrt{\frac{28 - t_{SE}}{t_0 - t_{SE}}} \right) \right\} \right]^{0.5} \cdot E_{28d} \tag{2.2}$$

where,
t_0 is the equivalent age at loading [days]
t_{SE} is the equivalent time where deformations start to create stresses [days]
E_{28d} is the elastic modulus at equivalent time of 28 days [GPa]
S_E is the shape parameter for the growth of the elastic modulus [-]

The Poisson's ratio, based on compression tests, was evaluated by Vogt et al. (2009) to $v = 0.27$.

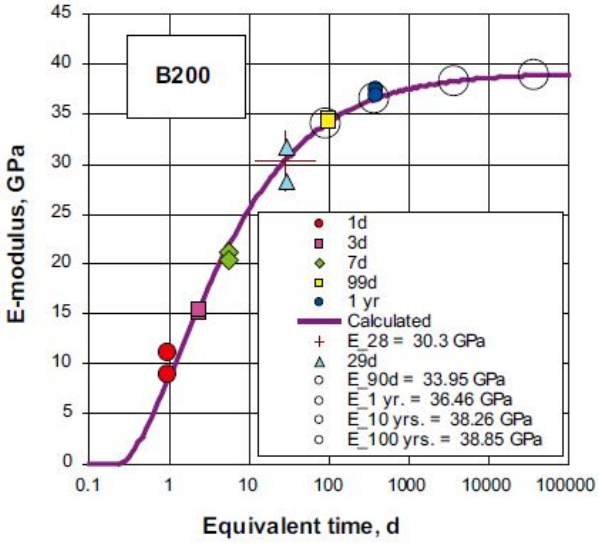

Time at loading	E_{cm}, GPa
28 d	30.3
90 d	33.9
1 yr.	36.5
10 yrs.	38.3
100 yrs.	38.8

Figure 2.3: Elastic modulus evaluation result. From Vogt et al. (2009)

Thermal deformation

Tests were performed to determine the deformation of concrete at variable temperatures, see Vogt et al. (2009). The thermal deformations were measured indirectly by separating the autogenous shrinkage and the thermal deformation of newly cast concrete. This was accomplished by a fitting technique based on the measured total deformation for a 0.7 m wall structure temperature curve, were the thermal dilation coefficient was chosen as constant. The obtained thermal dilation coefficient was $11.1 \cdot 10^{-6} / \,^{\circ}\mathrm{C}$ for concrete B200.

Concrete - rock bond strength

The bond strength between the concrete and sawed rock was tested by Magnusson (2013). Tests were performed 10, 28 and 90 days after casting. The tests indicated that the mean horizontal bond strength was 4.4 MPa and the mean vertical bond strength was 2.9 MPa at 90 days after casting. The bond strength was hence slightly lower than the mean concrete tensile strength of 3.3 MPa evaluated in Vogt et al. (2009).

2.2.4 Loads acting on the concrete plug

Water pressure

The nominal value of the pressure from the groundwater is based on the vertical distance from the groundwater level to the deposition tunnel. This is set to 5 MPa in the project for a depth of 500 m. According to hydraulic calculations for the site of the final repository, the water pressure inside the backfill of the plug system will be about 3 MPa at a maximum. Due to hydrogeological inhomogeneous properties of the rock, a conservative design value would be to chose the maximum hydrostatic pressure of 5 MPa. (Malm (2012))

Swelling bentonite

Bentonite clay swell during its saturation. The expected swelling pressure in the backfill is 6 - 10 MPa. However, by reducing the density of the backfill closest to the plug system, the pressure on the concrete plug can be reduced. Compaction of the filter during swelling of the bentonite will also reduce the pressure. The concrete plug is designed to withstand an expected swelling pressure equal to 2 MPa with a design value of 4 MPa. (Malm (2012))

Thermal loads

The spent nuclear fuel in the copper canisters in the repository will cause a temperature increase in the surrounding rock. The temperature increase will cause compressive stresses in the concrete plug due to restrained thermal expansion of the concrete as well as expansion of the rock.

Different approaches to calculate the temperature increase, as summarized in Malm (2012), have indicated a temperature increase of about +25 °C at the position of the concrete plug. According to Malm (2012), the thermal expansion may however have a beneficial effect of the concrete plug since it would counteract the tensile stress from the shrinkage of the concrete. The most conservative approach would therefore be to neglect thermal expansion completely.

Another, still conservative, approach would be to use a minimum temperature increase as shown in Table 2.2. (Malm (2012))

Table 2.2: Minimum temperature increase from nuclear fuel. From Malm (2012).

Time [years]	Temperature [°C]
0	+0
1	+0
10	+2
100	+7

Prestressing of the concrete plug

It is assumed that the autogenous shrinkage in combination with cooling of the concrete will cause the concrete plug to de-bond from the rock surface creating a gap between the rock and concrete plug. The concrete plug would hence be subjected to free shrinkage and may be considered as stress free before the grouting stage.

After 90 days of curing, the concrete plug will be cooled by the installed cooling equipment. The cooling was estimated by Malm (2012) to result in a temperature decrease of about $6.6 - 7.6\,^{\circ}\mathrm{C}$. The subsequent thermal shrinkage of the concrete plug will increase the gap between the concrete plug and rock with about 0.5 mm.

The gap will then be grouted from pre-installed grouting tubes. After the grouting is performed, the cooling is stopped and the temperature increase will cause the concrete plug to expand. The concrete plug will hence be subjected to prestressing related to the thermal shrinkage before grouting. Malm (2012) estimated this prestress, in accordance with Equation (2.3), to be approximately 2.2 MPa in the radial direction of the concrete plug. (Malm (2012))

$$\sigma = E \cdot \Delta T \cdot \alpha \tag{2.3}$$

where,
σ, is compressive stress,
$E = 33.9$ GPa, is the Young's modulus,
$\Delta T = 6.6\,^{\circ}$C, is the temperature decrease,
$\alpha = 10^{-5}1/\,^{\circ}$C, is the thermal dilation coefficient.

Shrinkage

Although a large part of the shrinkage will occur prior to the prestressing, some shrinkage will occur afterwards and cause tensile stresses in the concrete. This does, however, not mean that tensile stresses will occur in the concrete due to e.g. prestressing and the pressure load. Figure 2.4 shows the shrinkage occurring from 90 days to 100 years calculated with Equation (2.1).

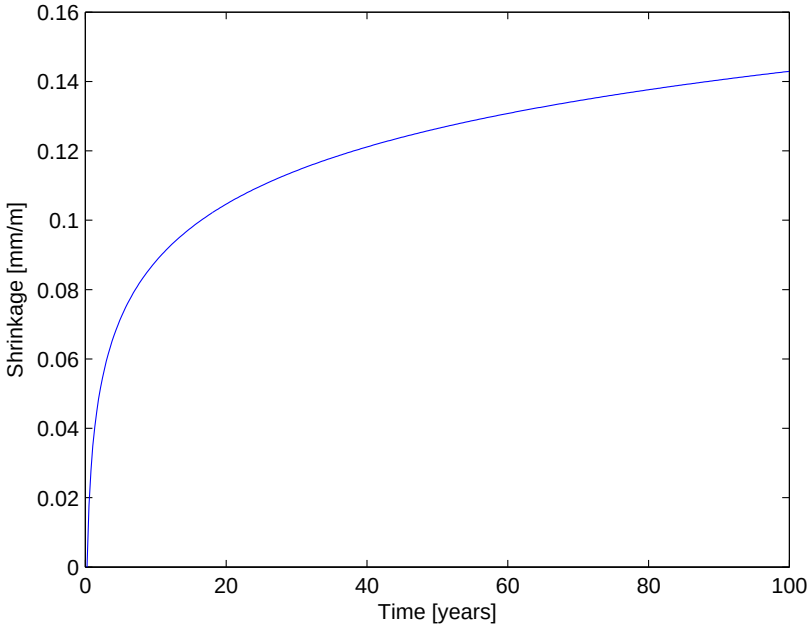

Figure 2.4: Shrinkage from 90 days to 100 years.

Chapter 3

Full scale test

This chapter gives a brief description of the full scale test to give an overview of the test. This includes its different stages, the purpose of the test, construction methods and the instrumentation.

3.1 Purpose of the full scale test

The full scale test is part of the EU DOPAS (Full-Scale Demonstration of Plugs and Seals) project. The DOPAS project aim to improve the knowledge about possible designs and strategies of plugs and seals in geological disposal facilities. The test dealt with in this thesis, denoted DOMPLU in the DOPAS project, is the first of five experiments. Other experiments will take place in France, Finland, Czech Republic and Germany. (IGD-TP (2014))

The main purpose of the full scale test is to verify that the plug system fulfills the requirements and behaves as expected during the design. The installation of the whole plug system is tested. The full scale test will for example show if the filter is capable to drain the tunnel while the concrete plug is hardening and until contact grouting is performed. The saturation of the bentonite seal and the amount of leakage from the plug system is also tested. (Malm (2012))

3.1.1 Purpose of the instrumentation of the concrete plug

Malm (2013a) stated some of the most important subjects to evaluate about the concrete plug as the following:

- The assumption that the concrete plug de-bond from the rock due to its early autogenous shrinkage during the first months and the cooling before the contact grouting.
- The assumption that the concrete plug is stress free before the contact grouting.

- The cooling effect from the cooling equipment and the temperature in the concrete plug during hydration and before contact grouting.
- The magnitude of water pressure and pressure from swelling bentonite acting on the concrete plug.
- Stresses and strains in the concrete plug due to the loading pressure.
- The deformations of the concrete plug, to capture the behaviour of the concrete plug and that it carries the load through arch action.

3.2 Test procedure

3.2.1 Installation of the concrete plug

Pre casting

The deposition tunnel is excavated by drill and blasting. A v-shaped slot is sawed out in the rock in an octagonal shape around the tunnel. The concrete wall closest to the concrete plug is covered with two plies of geotextile to remove cohesion between the concrete wall and the concrete plug. Pipes for contact grouting and drainage, cooling equipment and measurement instruments are installed before the prefabricated formwork is assembled in different segments. The formwork is prepared with holes for the pouring of the concrete and for cables from the measurement instruments. The formwork is designed for a full hydrostatic pressure from the concrete with design values of 160 kPa at the lower edge, 30 kPa at the upper edge and linear variation in between. (Palmer and Magnusson (2012))

Casting

The transportation of the concrete from the factory to the concrete pump was about 2 h. The concrete was poured under pressure from underneath the concrete surface inside the formwork, except for the lowest part due to geometrical reasons. (Palmer and Magnusson (2012))

According to Malm (2013c), the casting started on 2013-03-13 around 09:40. The casting was finished around 20:30 the same day, i.e. the total casting time was about 10.5 h. The concrete temperatures at delivery are presented in Table 3.1.

Table 3.1: Concrete temperature at delivery. From Malm (2013c).

Truck	1	2	3	4	5	6	7	8	9	10	11	12	13
Concrete temperature (°C)	9.2	9.1	9.3	9.7	9.7	9.7	9.1	9.3	9.5	9.4	9.5	8.9	8.9

Once the lowest temperature gauge indicated an increase of 1 °C, the cooling started at 7 °C. The cooling was continued until either the highest measured temperature

by the strain gauge thermocouples was 17 °C lower than the maximum measured temperature or less than 2 °C higher than the surrounding temperature for more then 24 h. The full cooling schedule can be seen in Appendix C. The formwork was removed after about 21 days. (Palmer and Magnusson (2012))

Contact grouting

After 90 days of curing the concrete plug is assumed to have de-bonded from the rock. The concrete plug was planed to be cooled to a temperature of about 5 °C. In combination with the autogenous shrinkage this should create a gap between the concrete and rock of about 4.2 mm at the top of the concrete plug, according to Malm (2012). 3.7 mm would be from autogenous shrinkage and approximately 0.5 mm would be from cooling.

Contact grouting was performed through three grouting pipes in two steps. The cooling was then stopped gradually. (Swedenborg (2011))

3.2.2 Loading steps

It was planned to increase the pressure gradually to a final pressure of 10 MPa, (Malm (2012)). However, when the pressure had reached about 4 MPa, the water leakage from the plug system was too large to increase the pressure further. The applied pressure has stayed on a level of 4 MPa after the decision not to increase it further.

3.3 Measurements

3.3.1 Water leakage

Water tightness is an important criteria in the plug system design. The water leakage is therefore measured in the full scale test. The downstream surface of the concrete plug is covered by a plastic sheet to accumulate the water that passes though and around the concrete plug. (Malm (2012))

3.3.2 Pressure from water and bentonite

Water pressure and swelling pressure from the bentonite in the bentonite seal have been measured with several sensors. These measurements are not evaluated in this thesis but the results are used for the evaluation of the concrete plug. Information about the evaluation and measurements of the pressure can be found in Malm (2014). The mean value of the total pressure is shown in Figure 3.1.

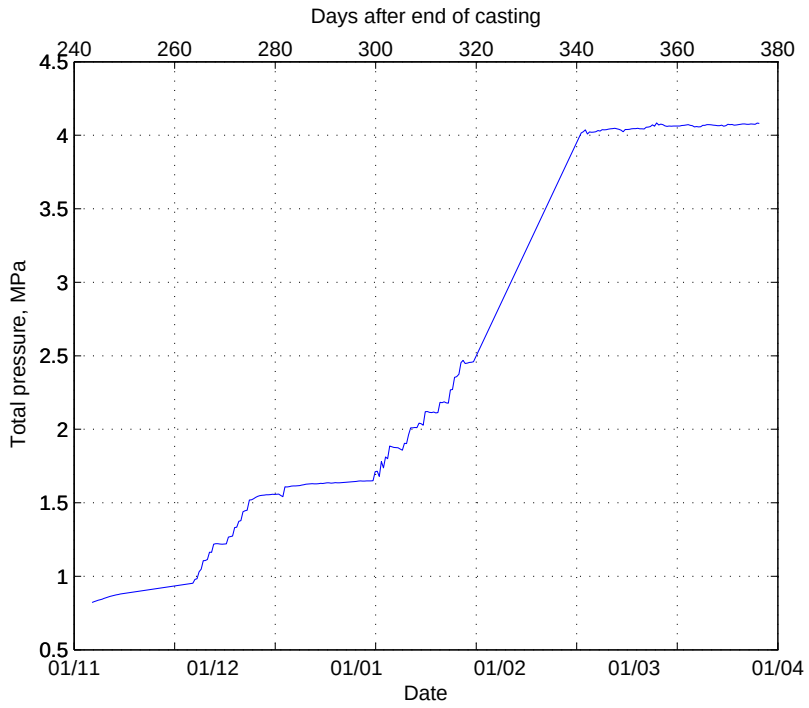

Figure 3.1: Measured mean total pressure in bentonite seal.

3.3.3 Instrumentation of the concrete plug

The concrete plug in the full scale test is instrumented with:

- 6 joint meters
- 3 LVDT meters
- 23 TML strain gauges, 14 include thermocouple
- 4 Geokon strain gauges, all include thermocouple
- 2 PT thermocouples

The joint meters measure the relative displacement between the concrete plug and the rock surface. These are placed between the concrete plug and the rock; 2 parallel to the tunnel direction, one vertical in the tunnel roof and three perpendicular to the contact.

The LVDT meters measure the deformations on the outside surface of the concrete plug. These are installed after the formwork is removed.

Two different manufacturers of the strain gauges are used to get reliable results even in the case that one of the manufactures strain gauges would be less reliable. The TML and Geokon strain gauges are mounted inside the concrete plug. Six of the

strain gauges are placed parallel to each joint meter and the rest at different places and in different directions in the concrete plug. All four Geokon gauges and 14 of the TML gauges also measures temperature. The temperature is thus measured at 18 locations inside the concrete plug. This gives the possibility to follow the strain and temperature variation in the concrete plug during different stages such as hydration and cooling. Also, two temperature gauges are placed on the outside of the plug system to measure the ambient temperature. These sensors are of model Pentronic Pt100. The form pressure is also measured by five sensors. (Malm (2013a))

Chapter 4

Instrumentation

This chapter presents the measurement instruments used for the concrete plug. Their positions are given together with some specifications and their purpose. The specifications are presented to give the reader an understanding of the measurements precision.

In order to understand the instrument specifications, a brief explanation of the terminology is given below.

Capacity - The maximum strain or load that a transducer can measure and still maintain specifications.

Rated Output (RO) - Output voltage when maximum load (capacity) is applied to a transducer. RO is often expressed as output voltage generated per applied voltage to the transducer. This is used to calculate the measured strain.

Non-linearity - Maximum deviation of an output curve to an ideal linear calibration curve.

Temperature range - Range of temperature that can be applied continuously without causing permanent destructive change to the transducer.

(TML Co., Ltd. (2013))

4.1 Form pressure sensors

The form pressure is measured by five sensors installed in the formwork. These sensors are of type Wika S10. Metal sockets were installed in the formwork and the sensors were fixed in these. Specifications are given in Table 4.1. (Malm (2013b))

The sensors were placed as close as possible to the theoretical positions shown in Figure 4.1.

Table 4.1: Wika S-10 specifications. From Malm (2013b).

Capacity	0-4 bar
Accuracy	0.25%
Temperature range	0 to +80 °C

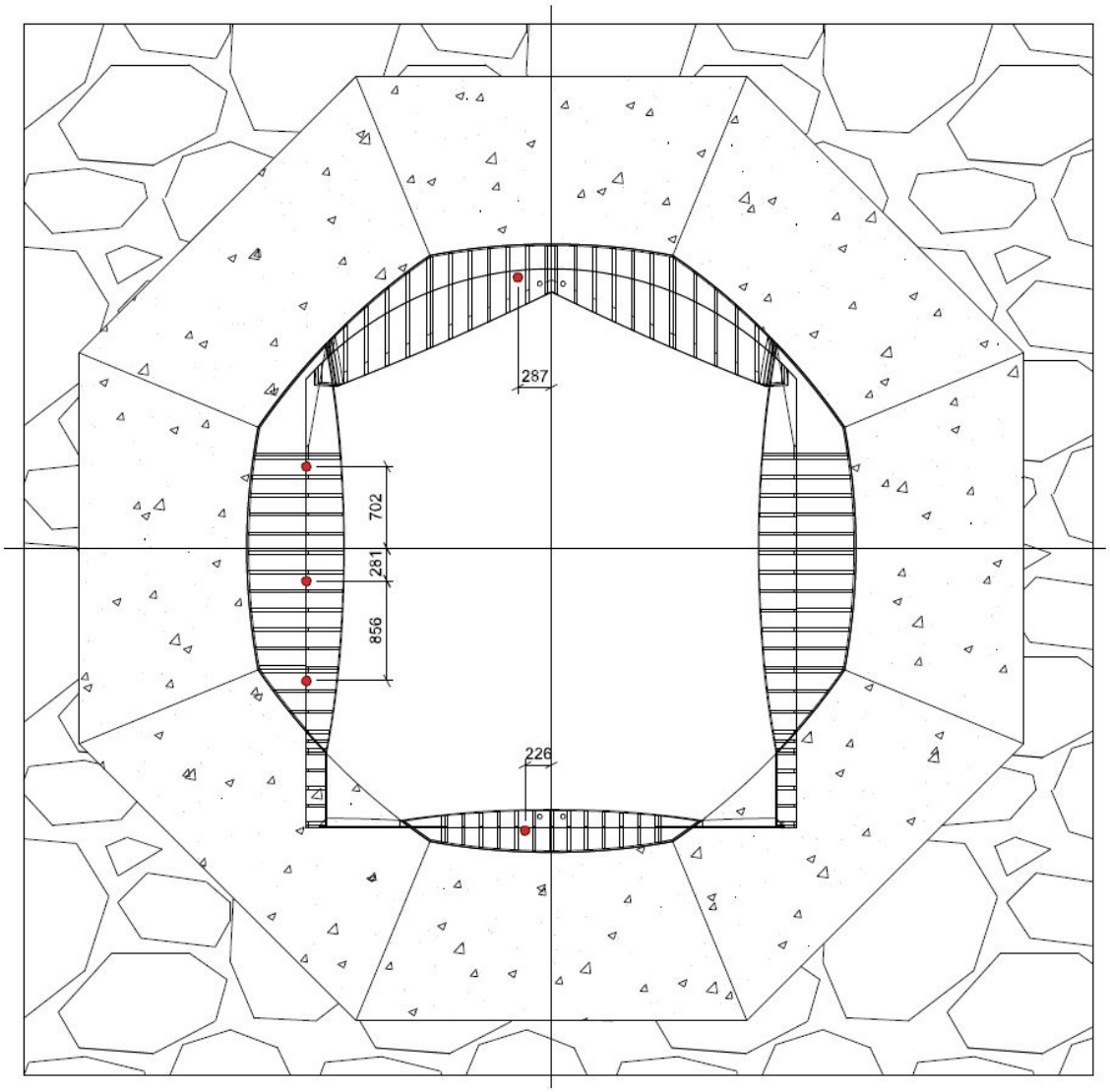

Figure 4.1: Theoretical placement of form pressure sensors. From Malm (2013b).

4.2 Ambient temperature sensors

Two temperature gauges are placed on the downstream side of the plug system to measure the ambient temperature. These sensors are of model Pentronic Pt100. During curing and until the formwork was removed, these sensors were placed close to the cooling machines. After the formwork was removed, the sensors were placed between the concrete plug and the plastic sheet. PT01 was placed relatively close

to the center of the concrete plug while PT02 was placed close to the rock at mid height. (Malm (2013b))

4.3 Strain gauges

Most of the sensors were installed on short reinforcement bars attached to the cooling pipes. 11 sensors were placed at different depths in the center of the concrete plug. These were mounted on spiders on a rod as shown in Figure 4.2. Sensors installed close to the rock were attached to reinforcement bars bolted into the rock as can be seen in Figure 4.3.

Figure 4.2: Strain gauges mounted on spiders on a rod. From Malm (2013b).

Figure 4.3: Strain gauges attached to reinforcement bars bolted into the rock. From Malm (2013b).

Table 4.2 presents approximate positions of all strain gauges in the coordinate system shown in Figure 4.4. The placements of all sensors were controlled with a total station. Sensor ST08 was planned to be placed in section 4. However it was found that this sensor was placed on the upstream side of the concrete plug, i.e. in section 1, close to a cooling pipe. This was not corrected and the concrete plug was casted with sensor ST08 at the misplaced position. The planned positions can be seen in Figure 4.5. Even though the concrete plug is circular in this figure, it is octagonal in reality. (Malm (2013b))

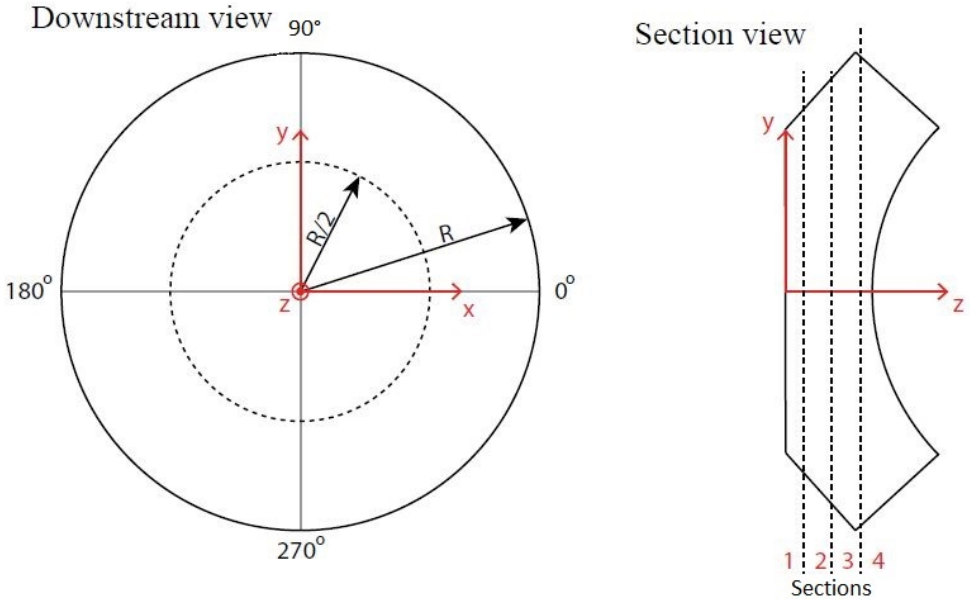

Figure 4.4: Strain gauge position coordinate system. Reproduced from Malm (2013b).

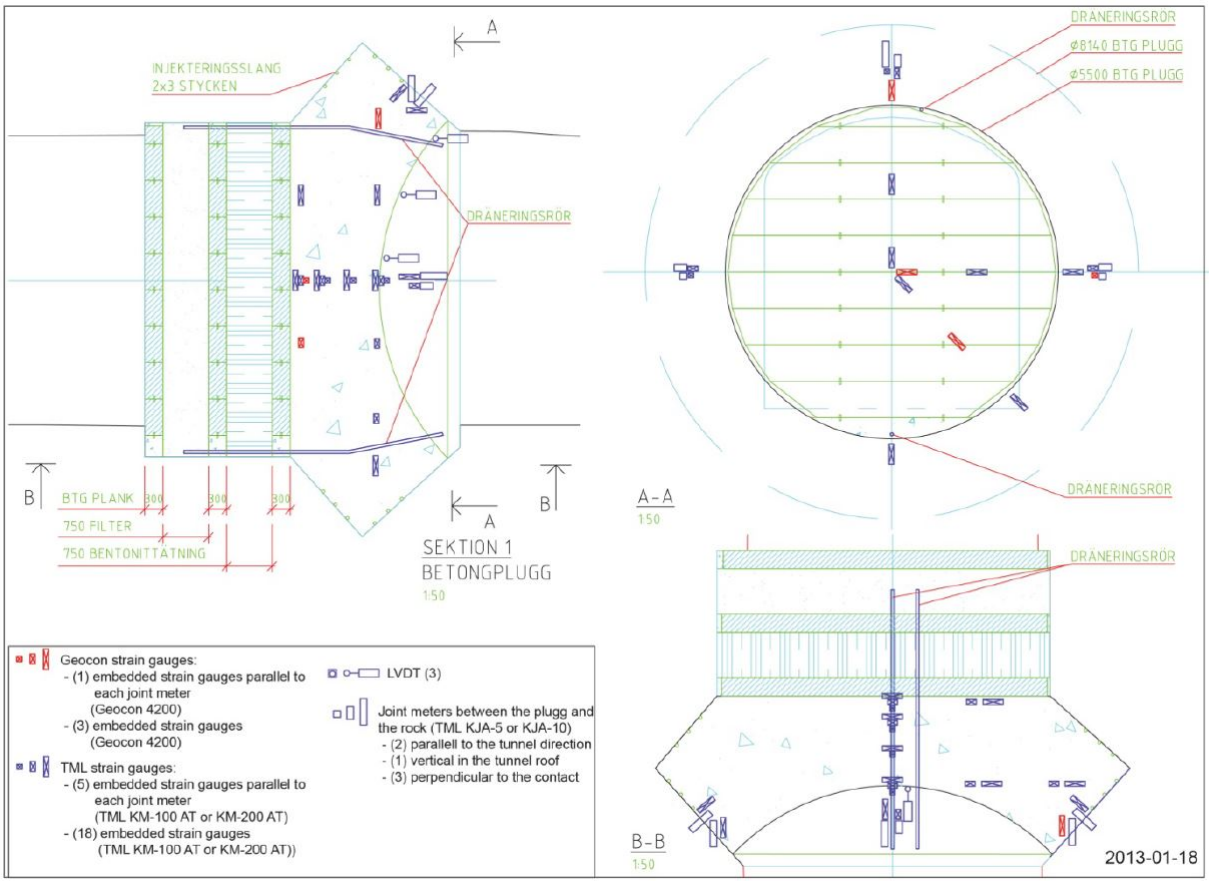

Figure 4.5: Planned positions of strain gauges and joint meters. From Malm (2013a).

Table 4.2: Strain gauge positions. From Malm (2013b).

Name	Manufacturer	Section	Direction	Placement	Note
ST01	Geokon	1	0°	center	Incl. temp.
ST02	TML	1	315°	center	Incl. temp.
ST03	TML	1	90°	center	Incl. temp.
ST04	TML	2	0°	center	
ST05	TML	2	315°	center	Incl. temp.
ST06	TML	2	90°	center	
ST07	TML	3	0°	center	
ST08	TML	1	270°	1 radius	Incl. temp.
ST09	TML	3	90°	center	Incl. temp.
ST10	TML	4	0°	center	Incl. temp.
ST11	TML	4	315°	center	Incl. temp.
ST12	TML	4	90°	center	
ST13	TML	1	0°	0.5 radius	Incl. temp.
ST14	Geokon	1	315°	0.5 radius	Incl. temp.
ST15	TML	1	90°	0.5 radius	
ST16	TML	4	0°	0.5 radius	Incl. temp.
ST17	TML	4	315°	0.5 radius	Incl. temp.
ST18	TML	4	90°	0.5 radius	Incl. temp.
ST19	TML	4	0°	1 radius	
ST20	TML	4	315°	1 radius	
ST21	Geokon	4	90°	1 radius	Incl. temp.
ST22	TML	4	180° (9 o'clock)	Perpendicular to the rock	Incl. temp.
ST23	TML	4	180° (9 o'clock)	Upstream direction	
ST24	TML	4	90° (12 o'clock)	Perpendicular to the rock	Incl. temp.
ST25	TML	4	90° (12 o'clock)	Upstream direction	
ST26	TML	4	0° (3 o'clock)	Perpendicular to the rock	Incl. temp.
ST27	Geokon	4	0° (3 o'clock)	Upstream direction	Incl. temp.

4.3.1 TML sensors

Twenty-three of the strain gauges are manufactured by TML (Tokyo Sokki Kenkyujo). Fourteen of these are also equipped with thermocouple to measure temperature. The gauges measuring temperature are of model KM-100AT and the gauges only measuring strain are of model KM-100A. The gauge can be seen in Figure 4.6.(Malm (2013b))

The KM series strain transducers are designed to measure strain in materials such as concrete. They are ideally suited for measuring strains during the very early stages of curing and produce excellent stability for long-term strain measurements, according to TML Co., Ltd. (2013). Specifications for the TML transducers are given in Table 4.3.

Figure 4.6: Strain gauge KM-100A by TML. From Malm (2013b).

Table 4.3: TML KM-100A and KM-100AT specifications. From Malm (2013b).

Capacity	$\pm 5000 \times 10^{-6}$
Rated output	2.5 mV/V
Non-linearity	1% of RO
Temperature range	-20 to +80 °C

4.3.2 Geokon sensors

The four installed Geokon sensors installed in the concrete plug are of model 4200 and can be seen in Figure 4.7. The Geokon 4200 are a type of vibrating wire embedment strain gauges and are designed for direct embedment in concrete. A steel wire is tensioned between two end blocks. Strains in the concrete will cause the two end blocks to move relative to each other and alter the tension in the wire. The tension is measured by plucking the wire and measure its resonant frequency of vibration using an electromagnetic coil. The gauges provide excellent long term stability and resistance to the effect of water. The gauges incorporate a thermistor measuring temperature. Geokon 4200 specifications are given in Table 4.4. (Malm (2013b))

Figure 4.7: Strain gauge 4200 by Geokon. From Malm (2013b).

Table 4.4: Geokon 4200 specifications. From Malm (2013b).

Capacity	$\pm 3000 \times 10^{-6}$
Non-linearity	$< 0.5\%$ of capacity
Temperature range	-20 to +80 °C

4.4 Displacement sensors

Three LVDT (Linear Variable Differential Transformer) sensors are installed on the downstream side of the concrete plug. The sensors measure the displacement of the concrete plug relative to the rock. The sensors are of model WA manufactured by HBM. The sensors are mounted on a scaffolding beam structure, mounted after the formwork was removed. In order to measure the horizontal displacement, wedges were attached on the concrete surface, see Figure 4.8. LVDT01 was placed on the center of the concrete plug, LVDT03 on the top of the concrete plug and LVDT02 was placed in between. The placement of the sensors is shown in Figure 4.8. (Malm (2013b))

The HBM WA has high mechanical durability and is insensitive to rough conditions. Specifications are given in Table 4.5. (HBM (2009))

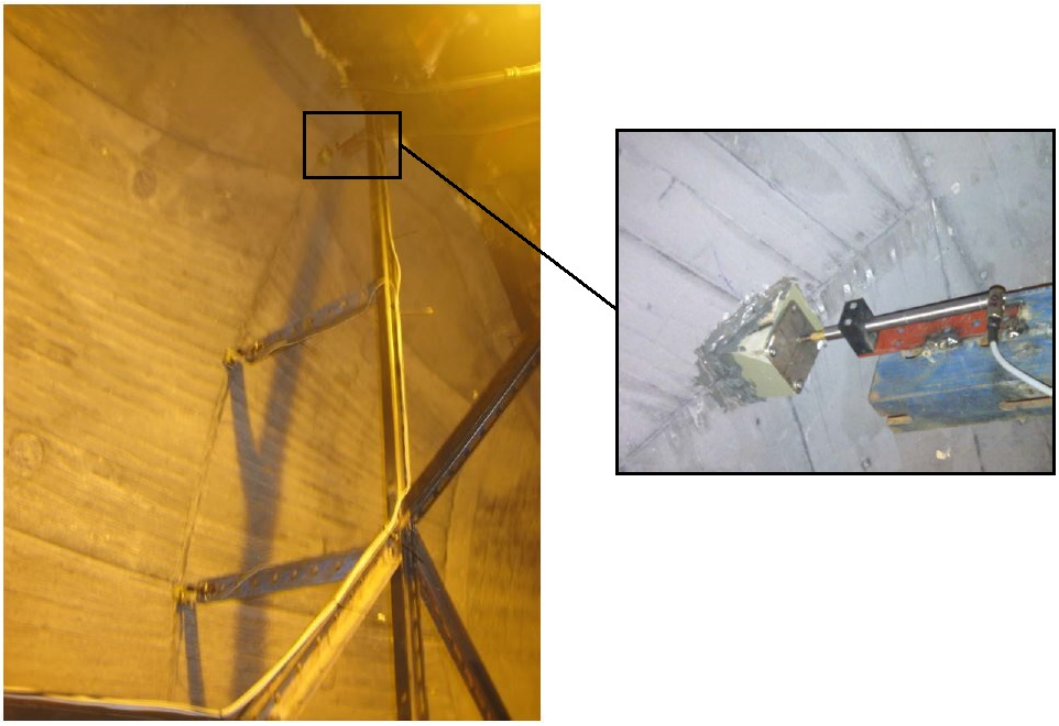

Figure 4.8: LVDT sensors placement. Reproduced from Malm (2013b).

Table 4.5: LVDT specifications. From HBM (2009).

Capacity	10 mm
Rated output	80 mV/V
Linearity deviation	$< \pm 0.2\%$ to $\pm 0.1\%$ of capacity
Temperature range	-20 to +80 °C

4.5 Joint meters

The six joint meters used are of model KJA-A manufactured by TML. The sensors are used to measure the relative displacement between the concrete and the rock at the concrete-rock interface. The sensors were placed at the interface to the right, left and top of the concrete plug. Two sensors were placed at each position. The displacement perpendicular to the rock was measured at each of the three positions. On the left and right side, the displacement in the tunnel alignment was measured and at the top, the vertical displacement was measured. The placements of the sensors are given in Table 4.6 with the coordinate system in Figure 4.4. The placement can also be seen in Figure 4.5. Specifications of the joint meters are given in Table 4.7.(Malm (2013b))

Table 4.6: Joint meter positions. Modified from Malm (2013b)

Name	**Section**	**Direction**	**Placement**
JM01	4	180° (9 o'clock)	Perpendicular to the rock
JM02	4	180° (9 o'clock)	Upstream direction
JM03	4	90° (12 o'clock)	Perpendicular to the rock
JM04	4	90° (12 o'clock)	Vertical direction
JM05	4	0° (3 o'clock)	Perpendicular to the rock
JM06	4	0° (3 o'clock)	Upstream direction

Table 4.7: Joint meter specifications. From Malm (2013b).

Capacity	10 mm
Rated output	1 mV/V
Non-linearity	1% of RO
Temperature range	-20 to +80 °C

When installing a sensor, a hole was drilled in the rock and a socket was mounted. The sensor was then attached to the socket. The installation is illustrated in Figure 4.9. (Malm (2013b))

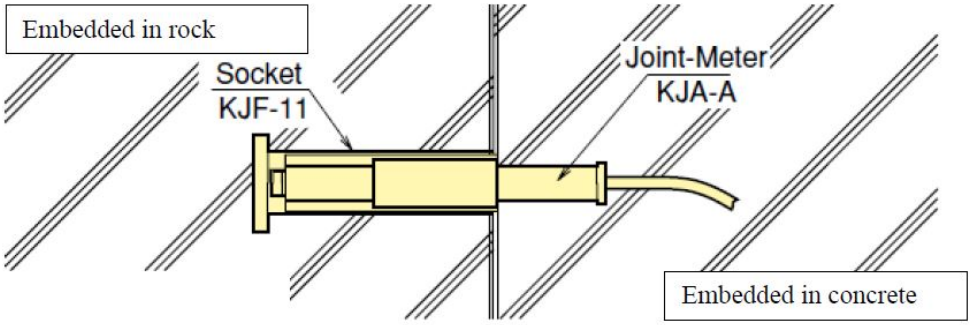

Figure 4.9: Joint meter installation. From Malm (2013b).

Chapter 5

Methodology

5.1 Softwares

The measurement data is treated with the software MATLAB from The MathWorks Inc. MATLAB is used for digitally filtering the measured data, analysis of the data and for result plots.

The measured results are compared with results from FEM (Finite Element Method) calculations. The FEM software used is ABAQUS ver. 6.12-1 from Dassault Systèmes Simulia Corp.

5.2 Filtering

The data from the measurement equipment is contains background noise. The noise sources in the test can, for example, be the cooling equipment and work in nearby tunnels. Noise can also be a result of random error in the measurement and data acquisition equipment.

In the case of noise originated from the cooling equipment, and assumed that this noise has a sinusoid behaviour with a frequency and amplitude, the noise could thereby be detected in an analysis of the signal in the frequency domain. This frequency component can then be attenuated with a digital filter. In order for this to be possible, the Nyquist criterion will have to be fulfilled. The Nyquist criterion states that a component (for instance noise) of a signal only can be reproduced correctly in the frequency domain if it is sampled with a sample rate greater than twice the frequency of the component. The sample rate in the full scale test is very low, with one sample approximately every 5 minutes. Noisy signals from e.g. the cooling equipment can therefore not be detected in an analysis in the frequency domain and filtering out frequency components of the signal will do no good. (Hewlett-Packard Co. (1994))

The measurement data are therefore filtered with smoothing filters to remove the

noisy appearance. Two different kinds of smoothing filters are used for the different measurement sensors; Savitzky-Golay smoothing filter and robust locally weighted regression (rlowess in MATLAB).

5.2.1 Savitzky-Golay smoothing filter

The Savitzky-Golay smoothing filter (sgolayfilt in MATLAB) smooth data by fitting a polynomial curve of a specified order to a specified number of samples (span). The fitting is done with a least square fit that minimize the mean-square error. The middle sample in the span is then replaced by its smoothed value. A thorough explanation is given by Orfanidis (2010).

The Savitzky-Golay filter is used for TML strain and temperature measurements, joint meters and the ambient temperature.

5.2.2 Robust locally weighted regression

The robust locally weighted regression with a linear polynomial is called rlowess in MATLAB. This filter smooth data with use of regression weights and robust weights for each data point in a given span. The regression weights are calculated for each data point in the span and specifies the amount of influence each data point has on the smoothed point. The largest influence is assigned to the point being smoothed and points outside the span have no influence. The robust weight are also calculated for each point in the span. In this method, lower weight (or importance) is assigned to outliers (points that deviate by a large degree from other points in the span). A data point outside an interval of six mean absolute deviations of the span is assigned zero weight. The smoothed value is given by a weighted linear least square regression with a linear polynomial. Further reading can be found in Cleveland (1979).

Robust locally weighted regression is used for Geokon strain and temperature measurements and LVDT displacement measurements.

5.2.3 Strain gauges

The TML strain measurements was filtered with a cubic (3rd order) Savitzky-Golay smoothing filter with a span of 15 points. This filter proved to remove some of the noise but still kept the behaviour of sudden and large changes. It is important to keep these sudden and large changes, in order to determine when the sensor bond to the concrete, further described in Section 5.5. If the point when the sensor can be said to have bond to the concrete had been filtered out, it would not be possible to perform further analysis with the filtered data. The filtered data was however displaced somewhat in the time domain. Filtered and original data from TML sensor ST13 are shown in Figure 5.1.

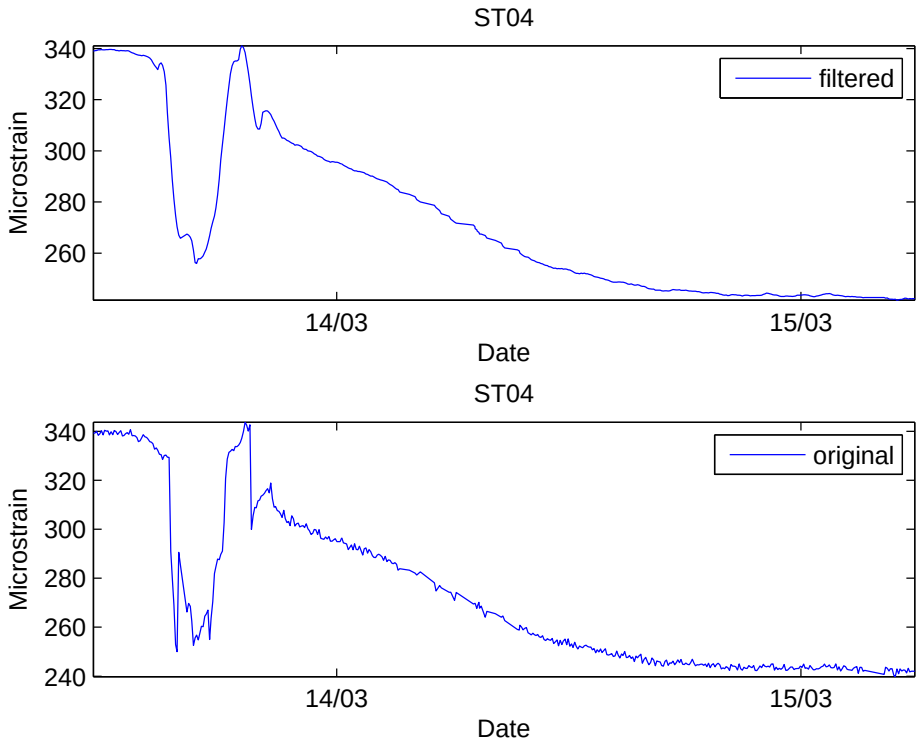

Figure 5.1: Filtered (top) and original (bottom) data from TML sensor ST13.

The Geokon sensors were filtered with robust locally weighted regression. The Geokon measurements all had occasional spikes in the measurement data. The use of the robust weighting factors in rlowess removed the spikes completely. Except for the spikes, the Geokon measurements had low noise level and the filtered data followed the original data well. Filtered and original data from Geokon sensor ST27 are shown in Figure 5.2.

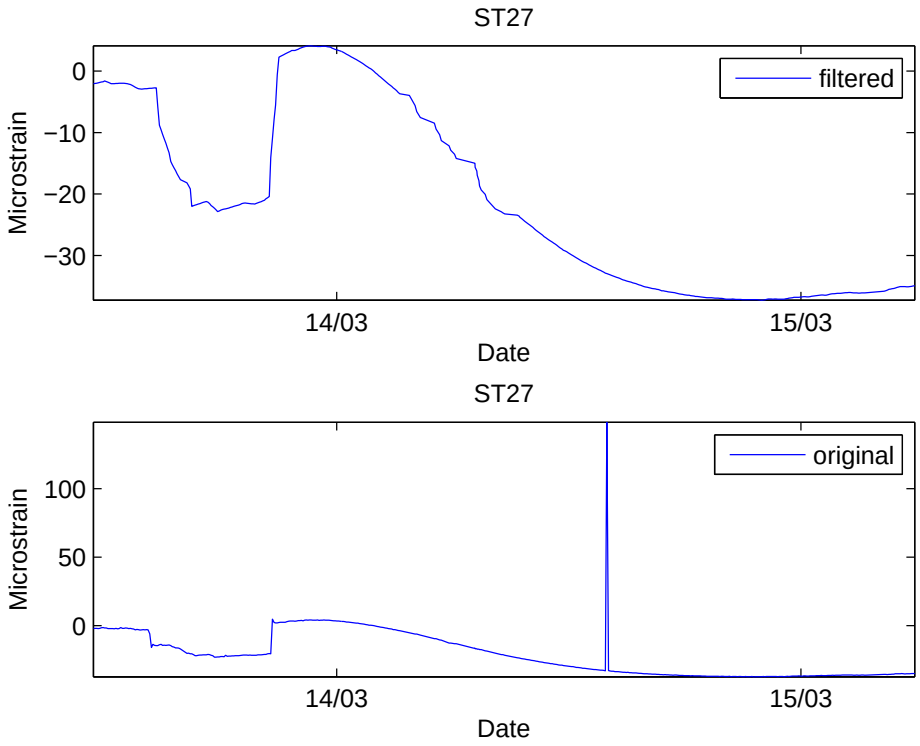

Figure 5.2: Filtered (top) and original (bottom) data from Geokon sensor ST27.

5.2.4 Temperature measurements

The temperature measurements from the TML sensors were filtered with a cubic Savitzky-Golay filter with a span of 17 points. This filtered out noise sufficiently and there was no sudden and large changes in the measurements that made the filtered curve to differentiate from the original by a large degree. Filtered and original temperature measurements from TML sensor ST13T are shown in Figure 5.3.

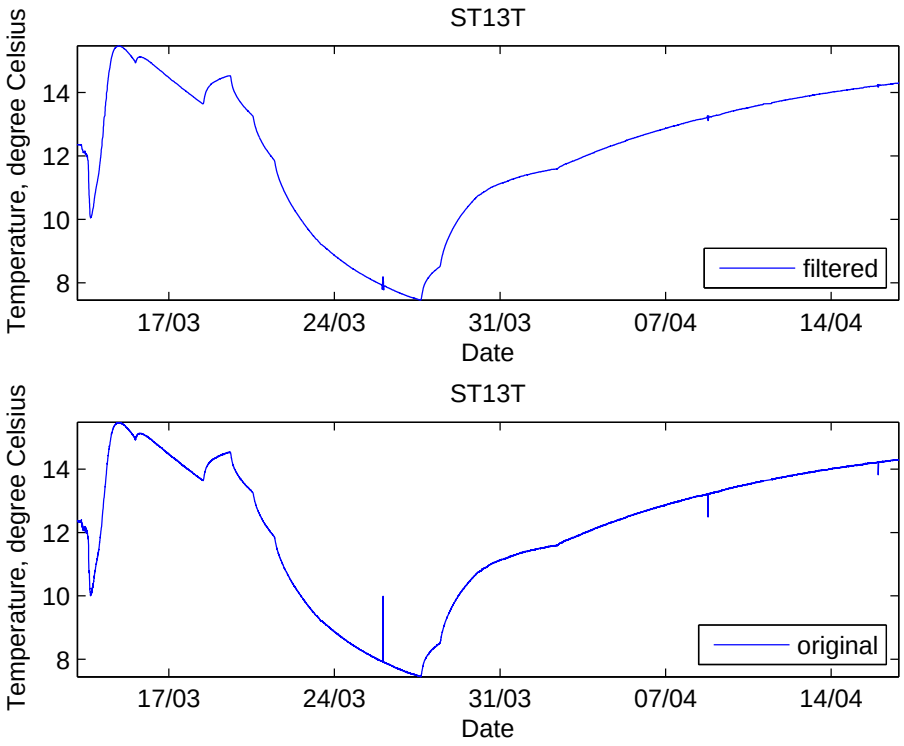

Figure 5.3: Filtered (top) and original (bottom) temperature data from TML sensor ST13T.

As for the strain measurement, the Geokon temperature measurements had occasional spikes in the data, as can be seen in Figure 5.4. This data was therefore also filtered with the same rlowess filter as the Geokon strain data.

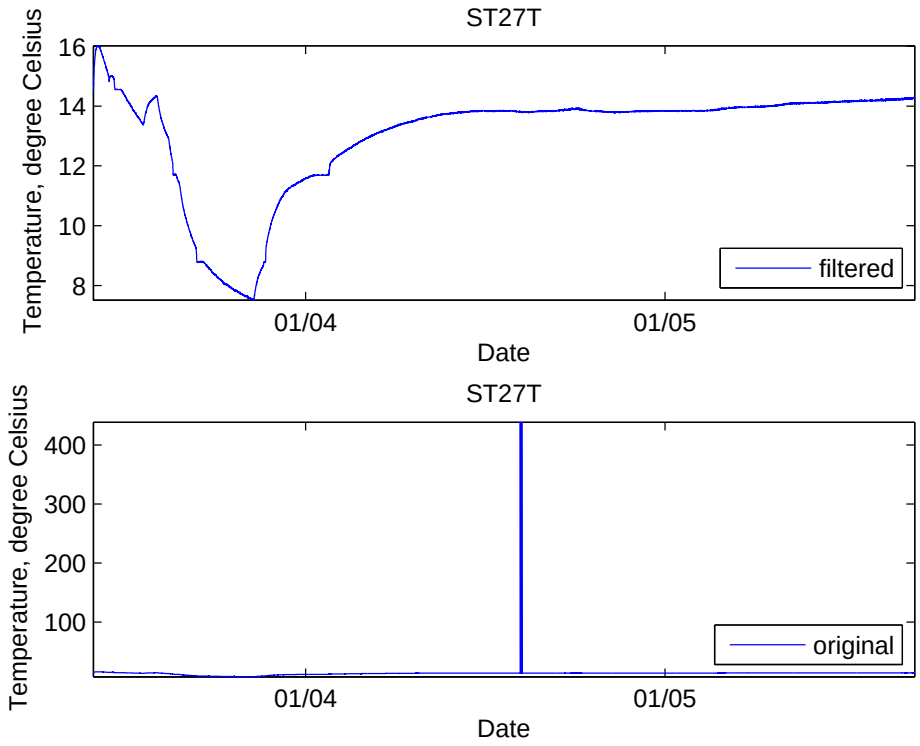

Figure 5.4: Filtered (top) and original (bottom) temperature data from Geokon sensor ST27T.

The ambient temperature measurements showed occasional large deviations. A quintic (5th order) Savitzky-Golay filter with a span of 61 point smoothed these deviations in a fulfilling way. Filtered and original data from sensor PT01 are shown in Figure 5.5.

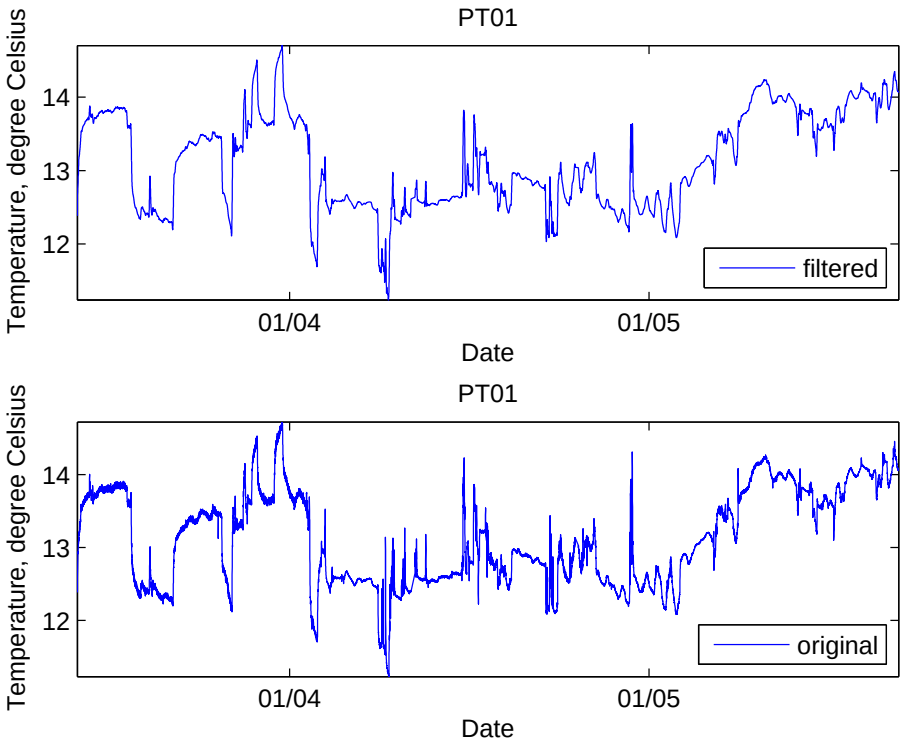

Figure 5.5: Filtered (top) and original (bottom) temperature data from sensor PT01.

5.2.5 Joint meters and LVDT sensors

The joint meters gave results with a large amount of noise. The noise was best filtered out with a quintic Savitzky-Golay filter with a span of 71 points. The filtered curve still followed the evident displacements in the original curve, as can be seen in Figure 5.6.

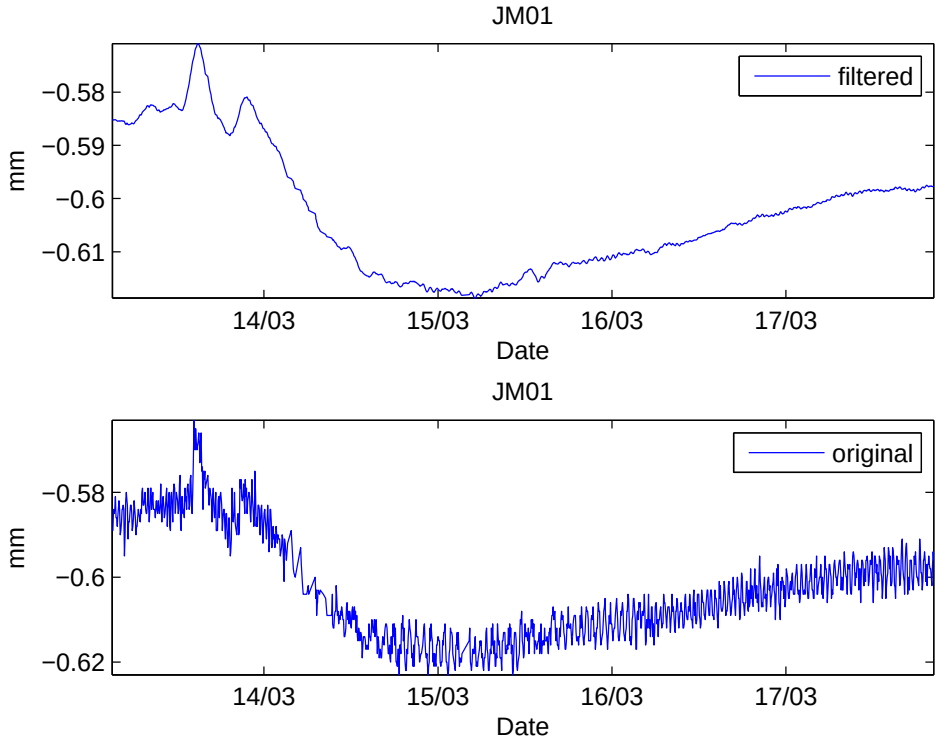

Figure 5.6: Filtered (top) and original (bottom) data from joint meter JM01.

The LVDT sensors gave occasional spikes in the results. This data was therefore filtered with an rlowess filter with a span of 5 points. Filtered and smoothed data from sensor LVDT01 can be seen in Figure 5.7.

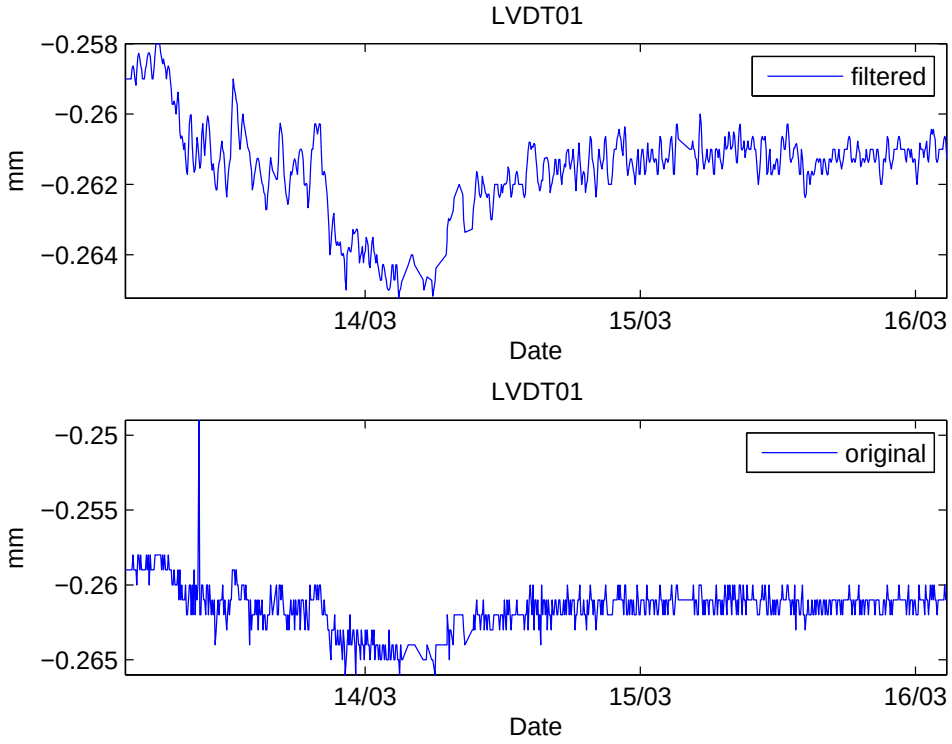

Figure 5.7: Filtered (top) and original (bottom) data from sensor LVDT01.

5.3 Temperature compensation of strain measurements

Change of temperature influence the strain gauge resistance and hence the strain measurement output. To compensate for this, the measured strain must be temperature compensated according to Equation (5.1). (Malm (2013b))

$$\epsilon = \epsilon_0 + C_1 \cdot \Delta T \tag{5.1}$$

where,
ϵ is the real strain
ϵ_0 is the measured calibrated strain
C_1 is the strain gauge temperature compensation factor
ΔT is the temperature change

The temperature compensation factor for the TML strain gauges are supplied with each gauge and are shown in Table 5.1. According to Geokon Inc. (2013), the temperature compensation factor for the Geokon strain gauges can be set to $12.2^{-6}\,^{\circ}\mathrm{C}^{-1}$, which is the coefficient of expansion for steel.

The temperature compensated strain calculated according to Equation (5.1) refers to the actual strain or the strain that can be measured or observed otherwise. When

calculating the stress in the concrete, assumptions has to be made whether the concrete is restrained or free to expand/shrink. This is discussed later in this chapter.

Table 5.1: Temperature compensation factors for TML strain gauges. From Malm (2013b).

Temperature compensation factors ($10^{-6}\,°C^{-1}$)					
ST02	9.7	ST10	9.1	ST19	10.1
ST03	9.5	ST11	9.3	ST20	9.3
ST04	9.7	ST12	10.3	ST22	9.9
ST05	9.3	ST13	9.2	ST23	9.3
ST06	9.7	ST15	10.0	ST24	9.8
ST07	9.3	ST16	10.1	ST25	9.4
ST08	9.2	ST17	9.6	ST26	9.7
ST09	9.7	ST18	9.1		

5.4 Stress calculations

The concrete plug is assumed to act linear elastic, hence Hook's law according to Equation (5.2) can be applied.

$$\sigma(t) = E_c(t) \cdot \epsilon(t) \tag{5.2}$$

where,
$\sigma(t)$ is the stress, [Pa]
$E_c(t)$ is the elastic modulus, [Pa]
$\epsilon(t)$ is the strain, [m/m]

The development of the elastic modulus, $E_c(t)$, have been estimated based on the tests performed by Vogt et al. (2009). The elastic modulus is calculated according to Equation (5.3), with parameters chosen to correspond to the plotted trend curve previously shown in Figure 2.3.

$$E_c(t) = \left[exp\left\{ S_E \left(1 - \sqrt{\frac{28 - t_{SE}}{t_0 - t_{SE}}} \right) \right\} \right]^{0.5} \cdot E_{28d} \tag{5.3}$$

where,
t_0 is the equivalent age at loading [days]
$t_{SE} = 0$ is the equivalent time where deformations start to create stresses [days]
$E_{28d} = 30.3$ is the elastic modulus at equivalent time of 28 days [GPa]
$S_E = 0.487$ is the shape parameter for the growth of the elastic modulus [-]

According to Malm (2013b), it can be assumed that the elastic modulus starts to develop after the whole concrete plug is casted and this is why t_{SE} is assumed to be zero.

Measured strain is temperature compensated using Equation (5.1). This strain equation refers to the real strain or the strain that could be observed. This assumes

that the concrete is free to expand due to thermal expansion. However, if the concrete is fully restrained to expand due to bond to the rock, the strain used for stress calculations needs to account for the thermal expansion coefficient of concrete. In Geokon Inc. (2013), Equation (5.4) is given to temperature compensate the strain for stress calculation in the case of a restrained body.

$$\epsilon = \epsilon_0 + (C_1 - C_2) \cdot \Delta T \tag{5.4}$$

where C_2 is the thermal dilation coefficient of the concrete. Other parameters were previously explained in Section 5.3. The thermal dilation coefficient is set to $11.1 \cdot 10^{-6}/\,^{\circ}\mathrm{C}$ as presented in Section 2.2.3.

An explaining example for Equation (5.4) is given in this paragraph. Assume a thermal increase of $+1\,^{\circ}\mathrm{C}$. This would lead to an expansion of the steel vibrating wire in the Geokon strain gauge in the order of 12.2 microstrain resulting in a strain measurement of -12.2 microstrain. If the concrete is fully restrained, no expansion could take place so the real strain is zero. The real strain can hence be calculated according to Equation (5.1). However, the restrained thermal expansion causes compressive stresses in the concrete. The equivalent strain of this stress is equal to $-C_2 \cdot \Delta T = 11.1$ microstrain. The compensated strain for both the strain gauge and the strain from the restrained condition is hence calculated according to Equation (5.4).

Stress calculations have been performed for both the fully restrained condition and the condition of no restraint, and compared to FEM calculations. This comparison is performed in order to analyse if the concrete has released from the rock prior to grouting or not.

5.5 Measurement reference point

The time when a measurement sensor can be said to have bonded to the concrete and hence have started to measure the strains is called the measurement reference point. In this thesis the reference measurement point is referred to as the zero level, i.e. the point when the strain is zero and which the magnitude of later occurring strains is relative to. Determining when the sensors have bonded to the concrete is therefore of great importance in order to evaluate the induced stresses in the concrete plug.

5.5.1 Joint meters

As seen in Figure 5.8, there is a similar behavior between neighboring sensors during the time of casting. A consistent behavior for all six sensors can however not be observed until the readings have become stable. The joint meters are therefore assumed to have bonded to the concrete at the time when they register stable readings. The time of bond for the joint meters are presented in Table 5.2. As

seen in the table, sensors JM01, JM02, JM05 and JM06 bond at similar times while sensors JM05 and JM06 bond later. The four earlier bonding sensors are placed at the sides of the concrete plug while the other two are placed at the top of the concrete plug. An earlier bond could therefore be expected for the sensors at the sides.

As mentioned in Section 3.2.1, the casting was finished around 20:30 on March 13, i.e. the bonds occurred after the casting was finished.

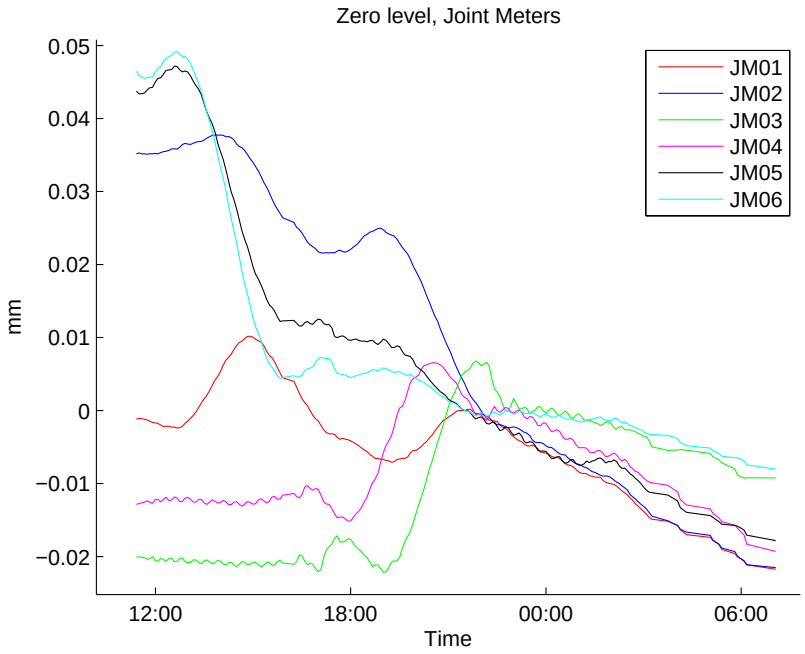

Figure 5.8: Joint meter readings during casting and early curing.

Table 5.2: Time of estimated bond for the joint meters.

Joint Meter	Time of bond
JM01	13/3 21:30
JM02	13/3 22:00
JM03	13/3 22:45
JM04	13/3 22:30
JM05	13/3 21:30
JM06	13/3 21:30

5.5.2 Strain gauges

For determining the zero level for the strain gauges, three approaches were analysed. In all approaches, the measured strains from sensors at similar positions were compared to each other and to results from FEM calculations. Sensors at similar positions should, according to the FEM calculations, give similar results.

Approach 1: Bond at hydration

In approach 1 it was assumed that a sensor bonded at the time of hydration of the concrete, i.e. when the temperature started to increase. Sensors not measuring temperature were assigned the same zero level as the closest sensor at the same height measuring temperature. Although the point when the temperature started to increase was very obvious and easy to pick out, the following strain comparisons between sensors at similar positions differed to a large extent. This approach was therefore discarded.

Approach 2: Bond at sudden strain change

In approach 2 it was assumed that a sensor bonded at the time of a sudden change of strain before the measurements became stable. The registered strain from all sensors changed because of the pouring of the concrete. Right before the registered strain became stable, most sensors (except for ST22) registered a sudden change in strain. The zero level was assigned to the point of the sudden change. Sensor ST22 was assigned the zero level at the same time as ST23 which was positioned next to it. Comparisons between sensors at similar positions indicated that both the magnitude of the sudden change of strain and the consequent strain measurements differed to a large extent. This approach was therefore also discarded.

Approach 3: Zero level at similar behavior

In approach 3 it was assumed that sensors at similar positions, pointing in the same direction would behave in a similar manner after they had bonded to the concrete. As seen in Figure 5.9, the horizontal sensors behave in a similar manner around 21:00 on the day of casting. Sensors ST01, ST07 and ST19 becomes stable after a sudden increase of strain and the others becomes stable after a sudden drop.

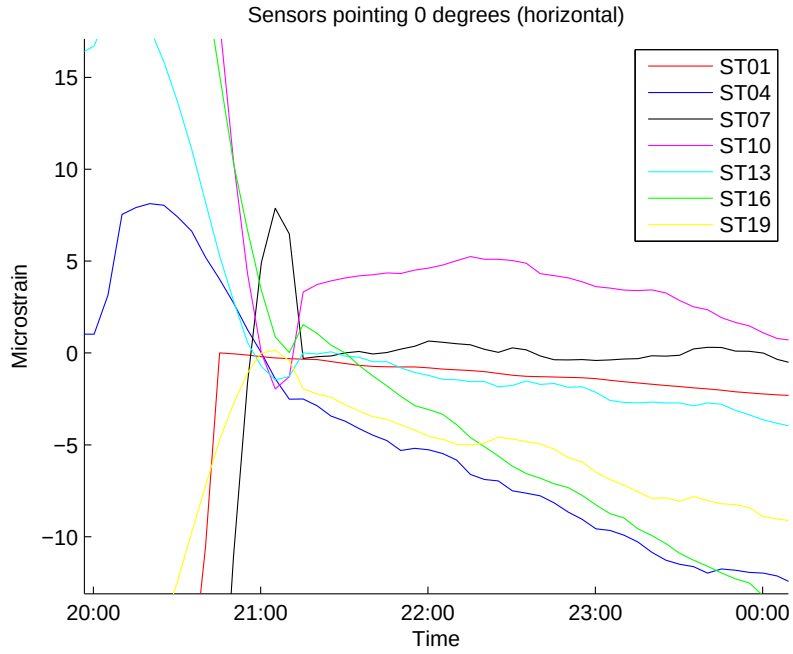

Figure 5.9: Horizontal strain gauges.

Figure 5.10 and 5.11 show that the stable behavior for the vertical sensors and sensors in a 45 degree angle also occurred around 21:00 on the day of casting. It can also be seen that most of the sensors become stable after a sudden drop.

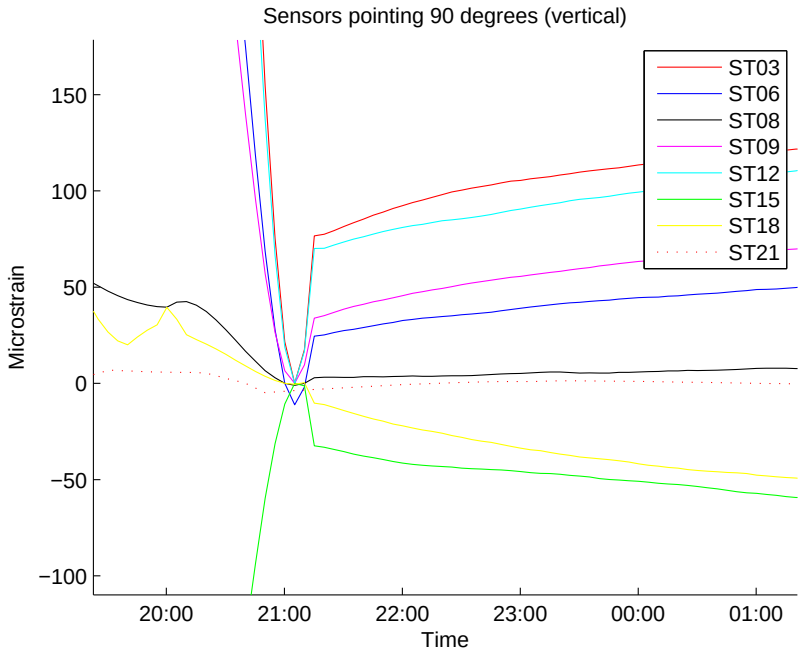

Figure 5.10: Vertical strain gauges.

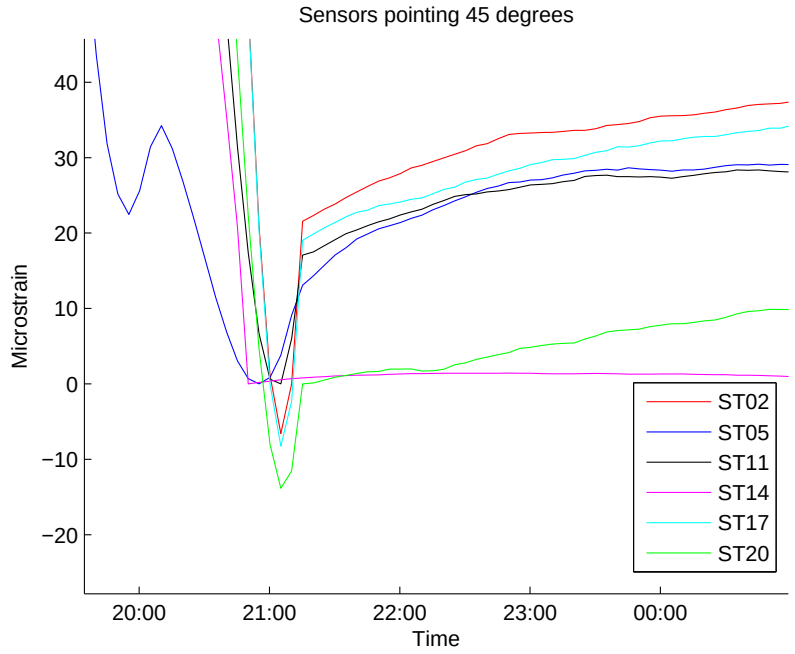

Figure 5.11: Strain gauges in a 45 degree angle.

In Figure 5.12, the sensors close to the concrete-rock interface are shown. It can be seen that the sensors in the top (ST24 and ST25) behave differently than the sensors at the sides after they have become stable around 21:00 on the day of casting.

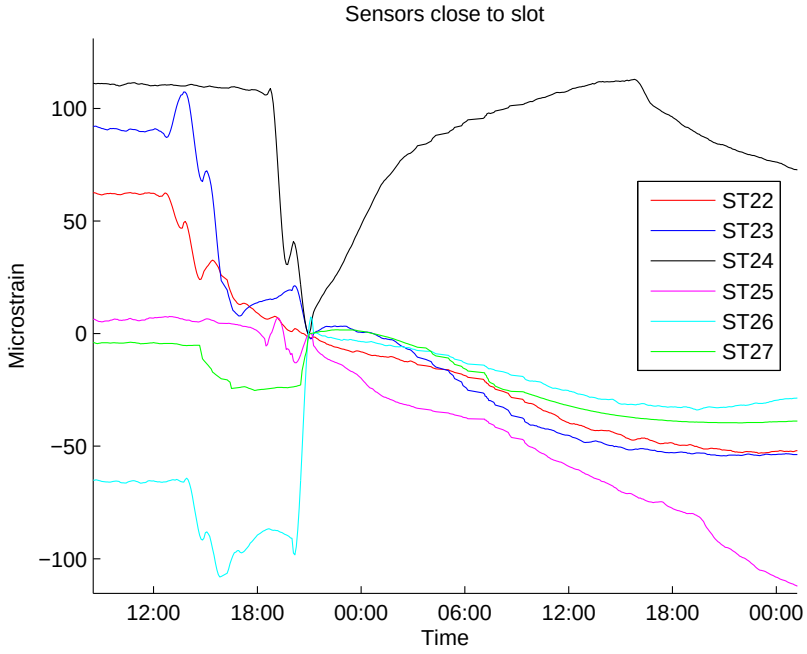

Figure 5.12: Strain gauges close to the slot.

Strain measurements from sensors ST01-ST03 are plotted with FEM results, assum-

ing no bond in Figure 5.13 and full bond in Figure 5.14.

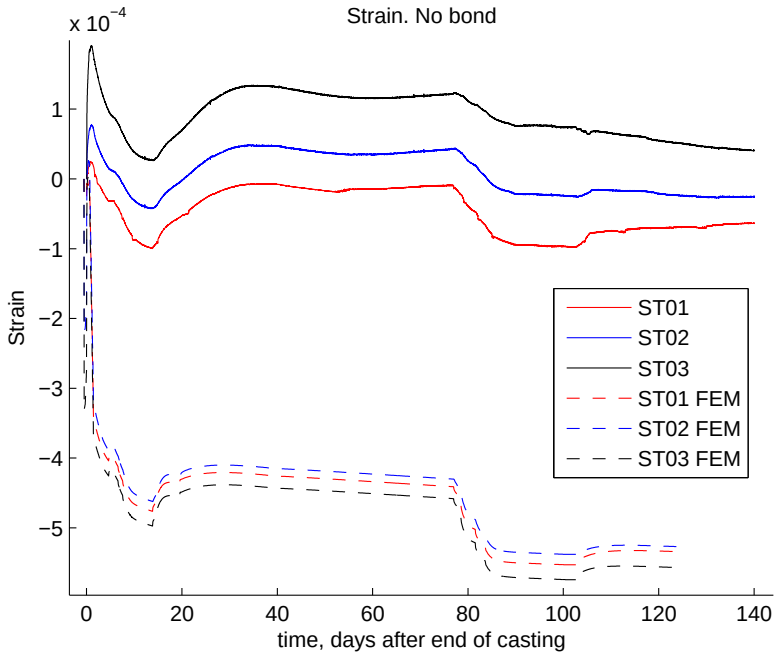

Figure 5.13: Strain from measurements and FEM calculation assuming no bond. Approach 3.

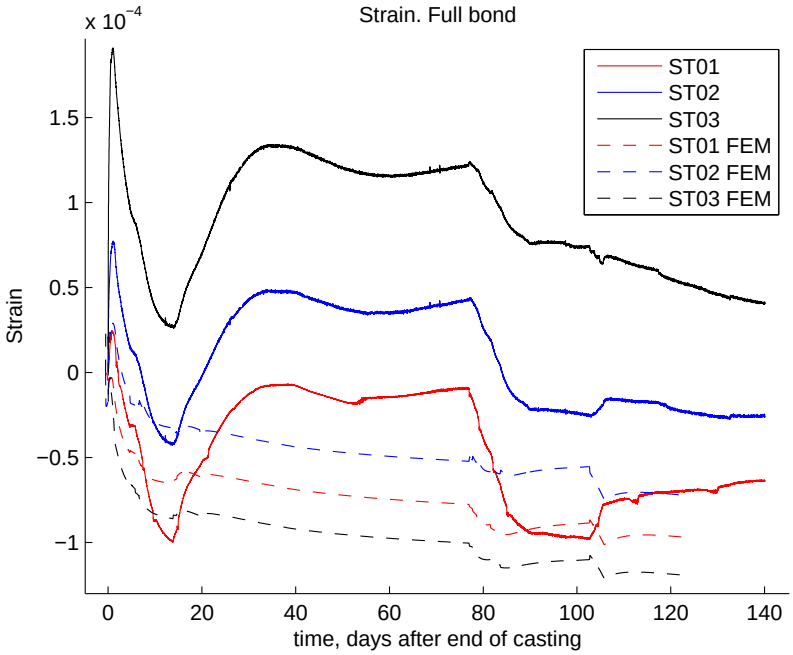

Figure 5.14: Strain from measurements and FEM calculation assuming full bond. Approach 3.

The FEM results show that the sensors should indicate a compressive state of the

concrete but this is not the case for all the sensors. The sensors also show relatively large differences compared to each other. It was therefore decided to test a modified approach, referred to as approach 3.1. Figure 5.9 to 5.12 show that some of the sensors indicate an increase of strain after the curves have become stable. This increase is in different magnitude for different sensors. However, it was found that there is a correlation of the time when this increase stops and the direction and position of the sensors. The zero levels were therefore tested for the time when the strain stopped to increase. The zero level times, or the times of bond, with this approach are shown in Table 5.3.

Table 5.3: Time of bond. Approach 3.1.

Sensors in 45 degrees		**Sensors close to slot**	
Sensor	*Time of bond*	*Sensor*	*Time of bond*
ST02	14/3 02:00	ST22	13/3 20:40
ST05	14/3 01:00	ST23	13/3 21:15
ST11	14/3 01:00	ST24	14/3 15:50
ST14	13/3 23:00	ST25	13/3 21:00
ST17	14/3 03:00	ST26	13/3 21:30
ST20	14/3 04:00	ST27	13/3 21:05
Vertical sensors		**Horizontal sensors**	
Sensor	*Time of bond*	*Sensor*	*Time of bond*
ST03	14/3 09:00	ST01	13/3 20:45
ST06	14/3 08:00	ST04	13/3 21:00
ST08	14/3 01:00	ST07	13/3 21:30
ST09	14/3 08:00	ST10	13/3 22:30
ST12	14/3 08:00	ST13	13/3 21:15
ST15	13/3 21:15	ST16	13/3 21:30
ST18	13/3 21:00	ST19	13/3 21:00
ST21	13/3 23:30		

The horizontal sensors indicate no increase in strain, or that the increase stop soon after the end of casting. Sensors in a 45 degree angle stop to indicate increase in strain around 02:00 on March 14 (the day after casting). Vertical sensors stop to indicate increase in strain around 08:00 on March 14 with few exceptions. The strain increase from ST08 is small and stops at 01:30 on March 14. This sensor is positioned in the bottom of the concrete plug and an earlier bond to the concrete can therefore be expected. The strain from ST15 and ST18 do not increase after the curves have become stable. Also, the Geokon sensor ST21 registers a small strain increase which stops at 23:30 on March 13 even though it is positioned above the center of the concrete plug. This can be due to an earlier bonding for this type of sensor. Geokon sensors ST01 and ST14 also seem to bond to the concrete earlier than their neighboring TML sensors. This may be due to the large flanges of the Geokon sensors.

Figure 5.15 and 5.16 show the measured strain with zero levels from approach 3.1 and the strain from FEM calculations for sensors ST01-03 assuming no and full

bond. As seen in these figures, the measured strain better correspond to each other and they indicate compressive strain or strain close to zero. This is also valid in comparisons for sensors at all the other positions.

Since approach 3.1 yield the most consistent and reasonable strain behavior, the zero levels from this approach are chosen for further analysis.

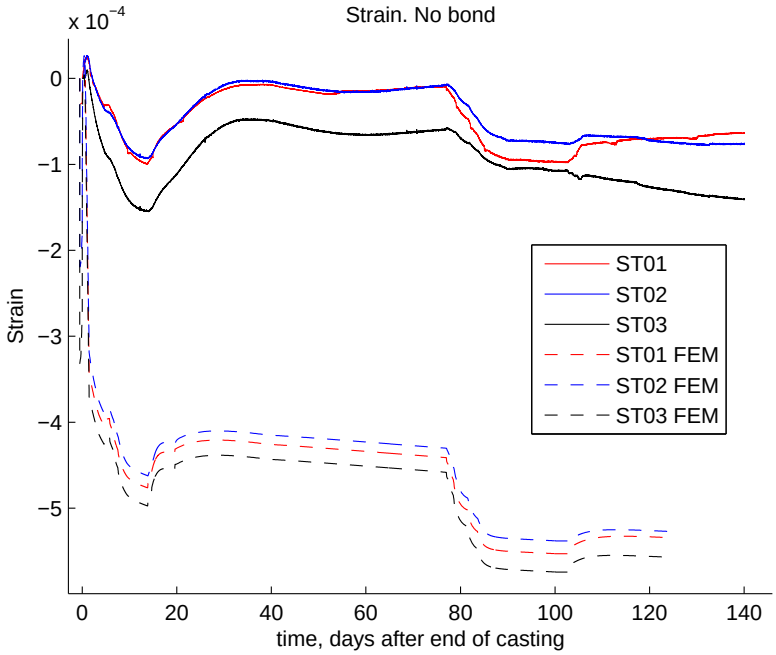

Figure 5.15: Strain from measurements and FEM calculation assuming no bond. Approach 3.1.

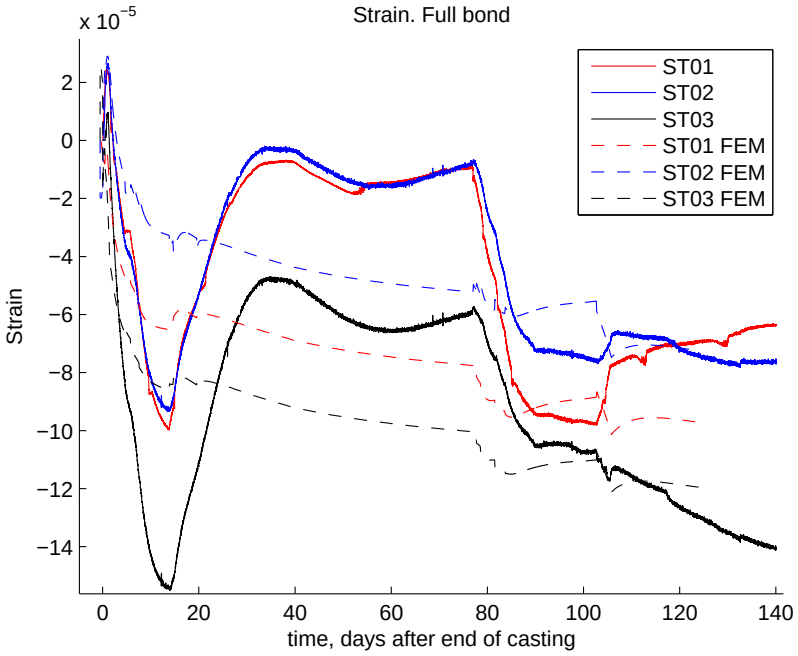

Figure 5.16: Strain from measurements and FEM calculation assuming full bond. Approach 3.1.

5.6 FEM Calculations

FEM calculations are performed for comparison to the measured results. This allows for a better evaluation of measurements and the actual behavior of the concrete plug and made assumptions.

A previously built 3D model and performed calculations by KTH doctoral student Tobias Gasch, presented in Malm (2014), are used and built on with pressure loads from water and swelling bentonite. The calculations performed by Tobias Gasch are made until the end on the grouting stage. The 3D FE model and calculation is hence to a large extent a work by Tobias Gasch.

The stress and strain results during the loading sequence obtained from the 3D FE model did not resemble the ones from measurements, see Section 6.2. A 2D FE model was therefor built by Tobias Gasch and tested with different conditions, see Section 5.6.2.

5.6.1 3D FE model

Boundary conditions

Two different boundary conditions are used for separate simulations. One simulation assumes no bond between the rock surface and the concrete plug before the grouting.

Full bond is assumed at both concrete-rock contact faces in the slot after grouting. In the other simulation, full bond is assumed both prior to and after grouting. The models had approximately 180,000 variables. (Malm (2014))

Geometry and element types

The concrete plug is modeled as a vertical symmetry plane in full scale with sensors placed at their planed positions, i.e. the misplaced sensor ST08 is placed in section 4 instead of section 1. The FE model can be seen in Figure 5.17.

The concrete, rock and grout are modelled with 8-node linear brick elements (C3D8 in ABAQUS). Sensors are modelled with 2-node linear 3D truss elements (T3D2 in ABAQUS) and the cooling pipes are modelled with 2-node diffusive heat transfer link elements (DC1D2 in ABAQUS) embedded in the concrete. (Malm (2014))

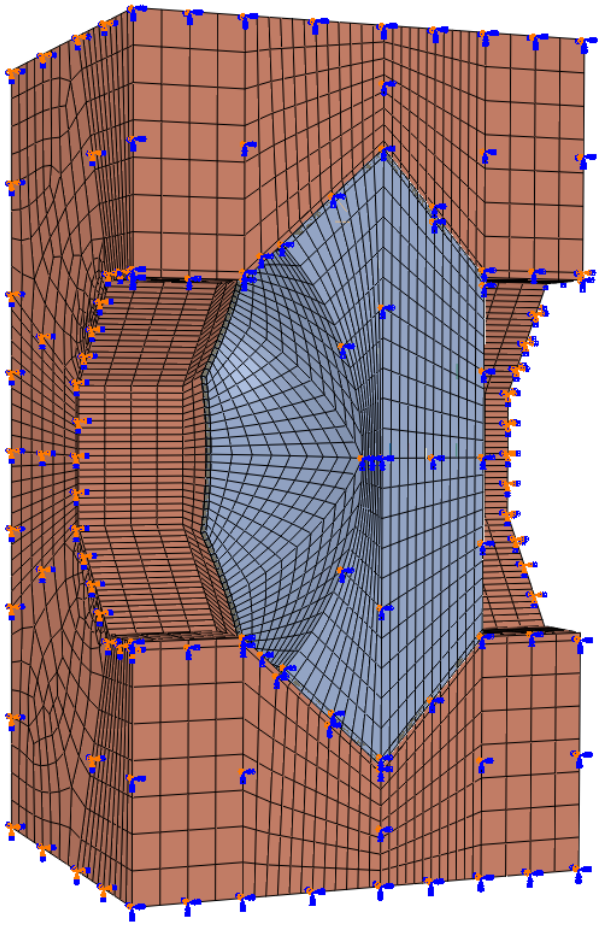

Figure 5.17: 3D FE model.

Casting, Curing and Grouting sequence

The early shrinkage of the concrete is accounted for as well as the slow casting rate with an assumed value of 0.5 m/h. It is assumed that no real shrinkage occurs

until the whole concrete plug is casted, since concrete will be poured to the top. The shrinkage effect of the first poured concrete is hence less than the last poured concrete. The shrinkage is defined according to the testing results in Vogt et al. (2009), with results from method 2 for the first 24 h and Equation (2.1) after 24 h.

The development of the elastic modulus is also modeled according to the test results from Vogt et al. (2009), i.e. according to Equation (5.3) with parameters chosen to correspond to the trend curve. The parameters are here the same as the ones used for the stress calculations based on measurements except for parameter t_0, see Section 5.4. This parameter was chosen to 0.5 in the FE simulation.

Parameters for the varying curing temperature are chosen by comparisons with thermal measurements obtained from casting tests in a cylindrical mould and concrete cube in Vogt et al. (2009) and separate FE simulations of these tests. The cooling pipe elements are assigned prescribed temperatures to simulate the actual cooling sequence, which can be seen in Appendix C. The surrounding rock is assigned a temperature of 15 °C which correspond to the average temperature in the tunnel at the Äspö laboratory.

The grouting sequence is modeled by changing the properties of layers between the rock and concrete plug during the grouting cooling step. The grout material properties in the last step are shown in Table 5.4. (Malm (2014))

Table 5.4: FEM material properties

	Concrete	**Rock**	**Cooling pipes**	**Grout**
Density [kg/m^3]	2336	2600	7800	2400
Conductivity [W/(m· K)]	2.1	3.7	45	-
Specific heat [J/(kg· K)]	1000	900	384	-
E-modulus [GPa]	Varies	70	-	37.8
Poisson's ratio	0.27	0.2	-	0.27
Thermal expansion [1/K]	$1.11 \cdot 10^{-5}$	$8 \cdot 10^{-6}$	-	$1.11 \cdot 10^{-5}$

Loading sequence

Water pressure and swelling pressure from the bentonite in the bentonite seal have been measured with several sensors by SKB. The mean value of the total pressure is shown in Figure 3.1. The mean pressure is applied as a static uniform pressure, divided in 236 steps to capture the pressurization sequence, on the upstream surface of the concrete plug. The applied pressure is shown in Figure 5.18. The temperature is in this sequence assumed to be fixed and the same for all materials.

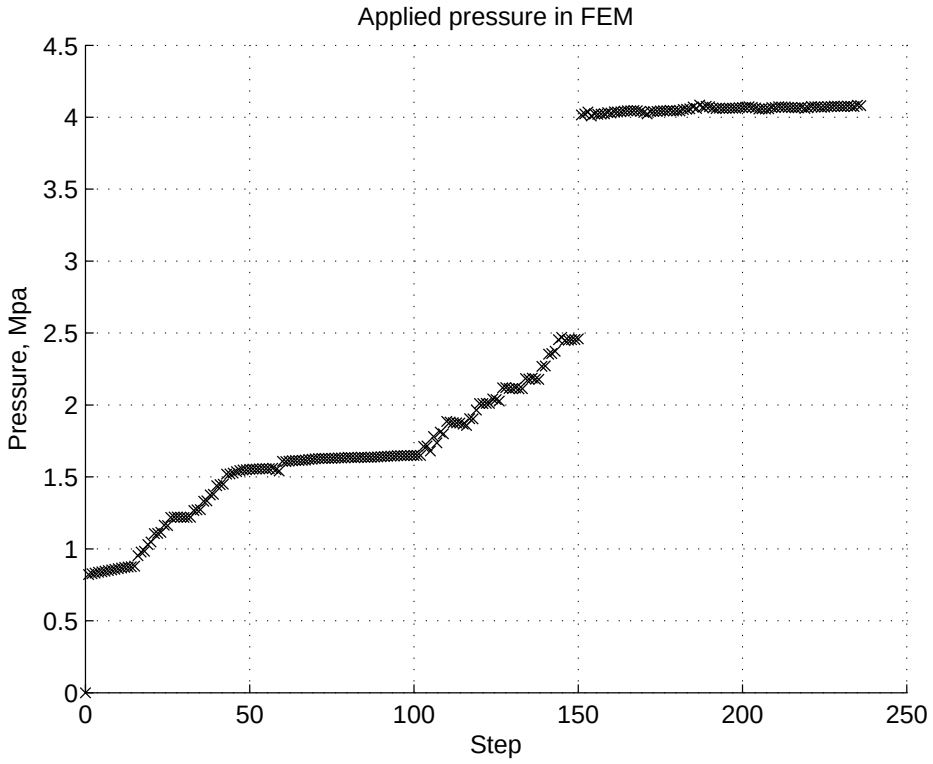

Figure 5.18: Applied pressure in FEM calculations.

Material properties

The strain gauges are assigned the same properties as the concrete to extract both strains and stresses. The material properties not previously discussed are shown in Table 5.4 and were obtained from Malm (2014).

5.6.2 2D model

The 2D FE model was built by Tobias Gasch and tested for three different cases. The models for each case are from here on denoted model 1, model 2 and model 3. The models with their conditions can be seen in Figure 5.19. Analogous to the 3D model, the concrete plug was modeled as a symmetry plane, i.e. cut in half. The Elastic modulus was set to 37.9 GPa. The models were tested for the pressurization sequence only, with no influences from the previous stages. The pressure was applied in the same order as for the 3D models; in 236 steps with magnitudes from Figure 5.18. The models had approximately 5000 variables.

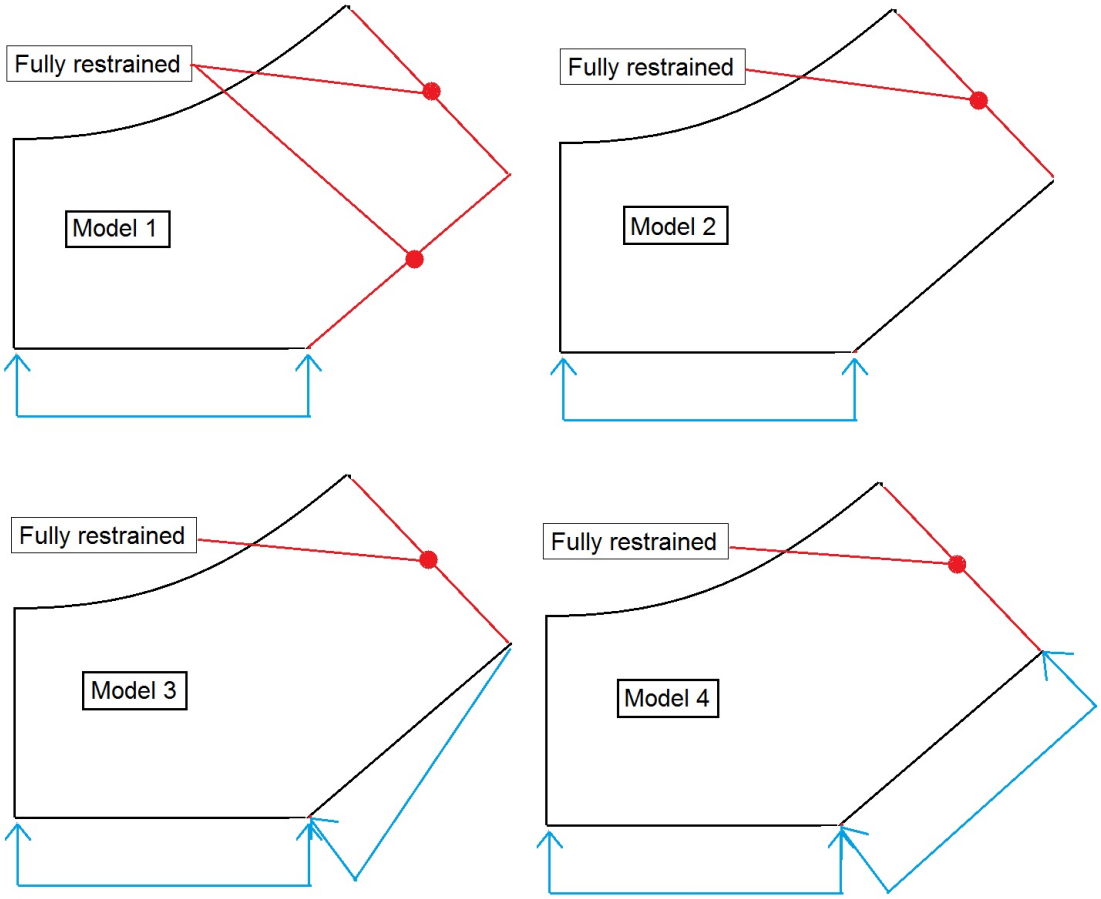

Figure 5.19: 2D FE models.

Model 1 was modeled as the 3D model with the concrete completely fixed to both sides of the slot. This corresponds to the boundary conditions used in the 3D model.

In model 2, the concrete was only fixed to the downstream side of the slot. The load was applied on the upstream surface as in model 1.

Model 3 had the same boundary condition as model 2 but a load was added to the upstream side of the slot. The load in the slot was applied with a linear decay to zero at the slot corner.

Also model 4 had the same boundary condition as model 2. In this model, the pressure applied on the upstream side of the concrete plug, was also applied to the entire length of the upstream side of the slot, i.e. with no decay as in model 3.

Chapter 6

Results

6.1 Casting and Grouting Period

In this section, the results from measurements and FE simulations from casting to grouting are presented. The whole grouting step is included, including the time after the cooling is stopped and the concrete plug temperature increase to the ambient temperature.

6.1.1 Form pressure

The form pressure was evaluated by Malm (2013b). The results are here presented to give a full view of the results concerning the concrete plug.

Figure 6.1 shows the measured form pressure during casting with sensor 1 placed at the bottom of the form work and sensor 5 at the top. Sensor 1 yield a highest value of 25 kPa which is significantly less than the design value of 160 kPa assuming hydrostatic pressure. All sensors reach a peak a few hours after they register a pressure increase and the pressure then decrease. It may therefore be concluded that the curing of the concrete starts before the whole concrete plug is casted and the full hydrostatic pressure will hence not occur at the bottom.

It can also be noted that a rapid and relatively large increase in pressure is registered by sensors 2 to 5 around the time of 20:35, as seen in Figure 6.2. The most likely reason for this was judged by Malm (2013b) to be an increased pouring pressure at the final stage of the casting to avoid possible air voids inside the concrete plug.

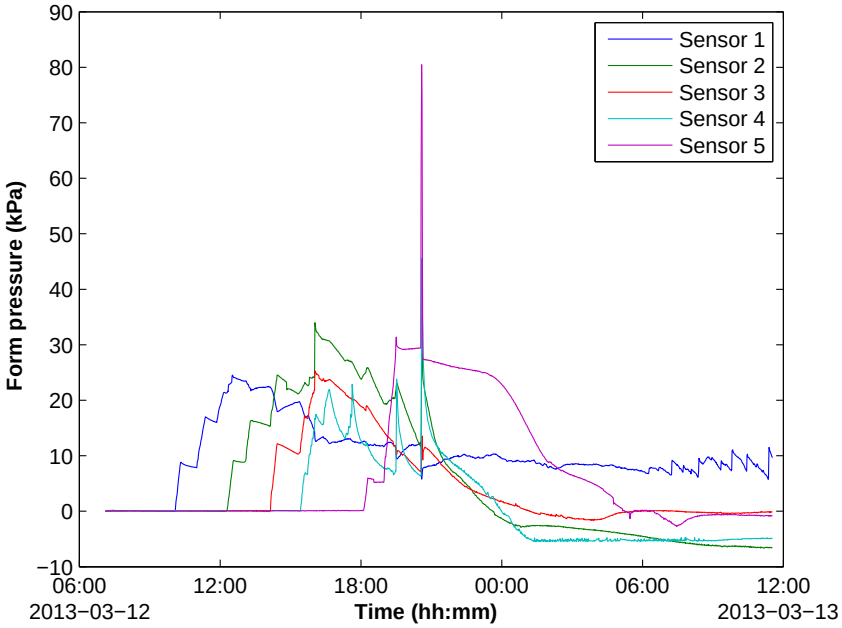

Figure 6.1: Measured form pressure during casting. (Malm (2013b)).

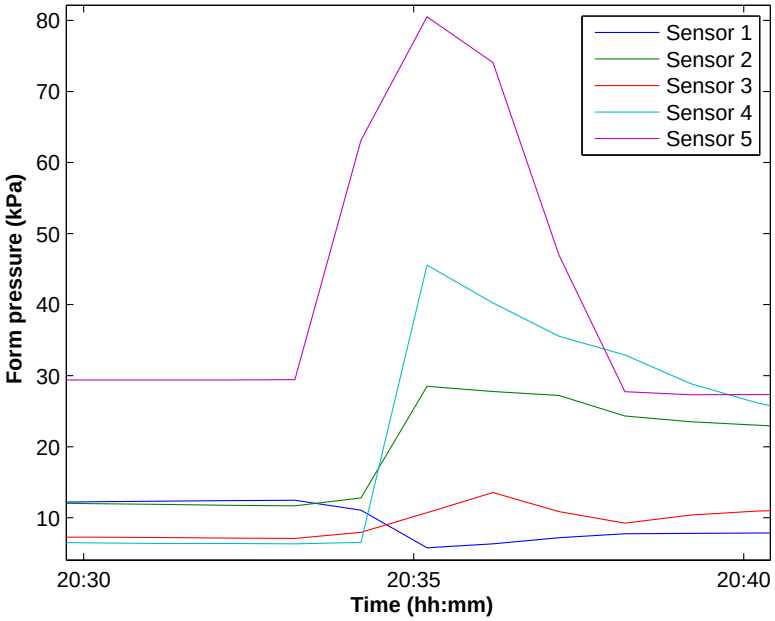

Figure 6.2: Registered rapid pressure increase. (Malm (2013b)).

6.1.2 Temperature

Measurement Results

Measured temperature by strain gauge thermocouples and ambient temperature gauges are presented in Figure 6.3. All thermocouples seem to have worked properly during the plotted time period of 2013-03-12 - 2013-07-30.

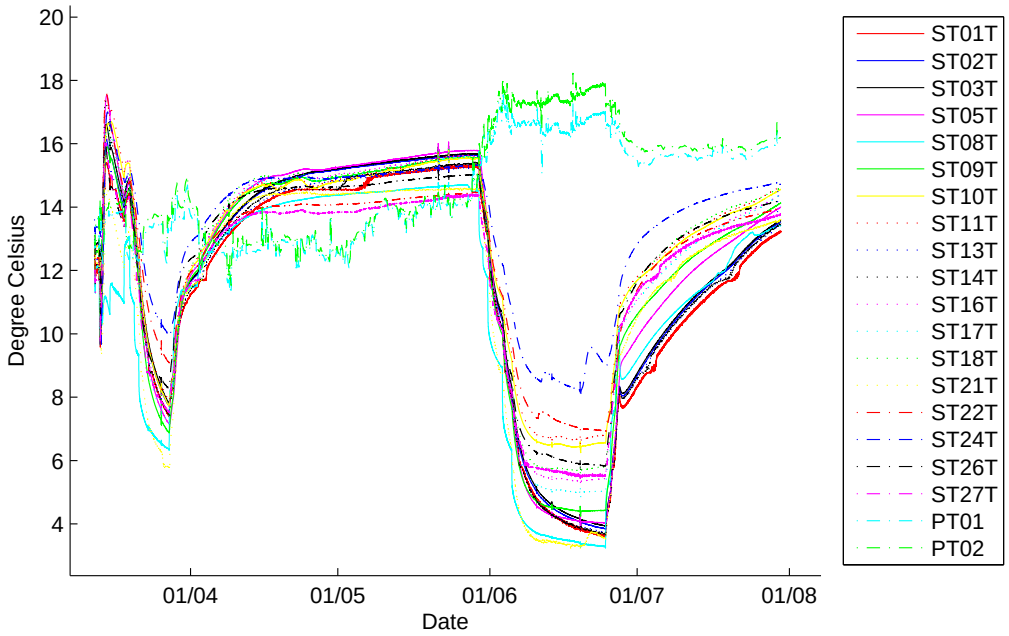

Figure 6.3: Measured temperatures from strain gauge thermocouples and ambient temperature gauges.

Before the casting begins, the measured temperatures are around 12-13 °C. When the concrete is poured and contacts the sensors, the temperatures drop to around 10 °C which is close to the delivered concrete temperature. The hydration of the concrete increase the temperatures to around 15-18 °C. A week after casting, the concrete plug is cooled gradually during about a week to a temperature of 6-10 °C before the cooling system is turned off.

The miss-placed sensor ST08T, that was placed close to a cooling pipe registered somewhat different temperatures than the other sensors due to its placement. It is especially apparent during the time period after casting to the second cooling that this sensor is affected by the temperature in the cooling pipe.

Before the grouting the concrete plug was cooled from about 14-16 °C to approximately 4-9 °C. The cooling thus resulted in a temperature decrease of approximately 8.5 °C.

The ambient temperature was around 13 °C until the cooling for the grouting. The

temperature was then increased to about 17 °C, probably due to the heat generated by the cooling machines.

FEM Result

The calculated temperature in the 3D FE analysis is shown in Figure 6.4. Figure 6.4 and 6.3 show that the FE temperature simulation correspond rather well to results from measurements. Excluding sensor ST08, the measured temperatures during hydration were between 15-18 °C. The corresponding FE results were in the magnitude of 14-18 °C.

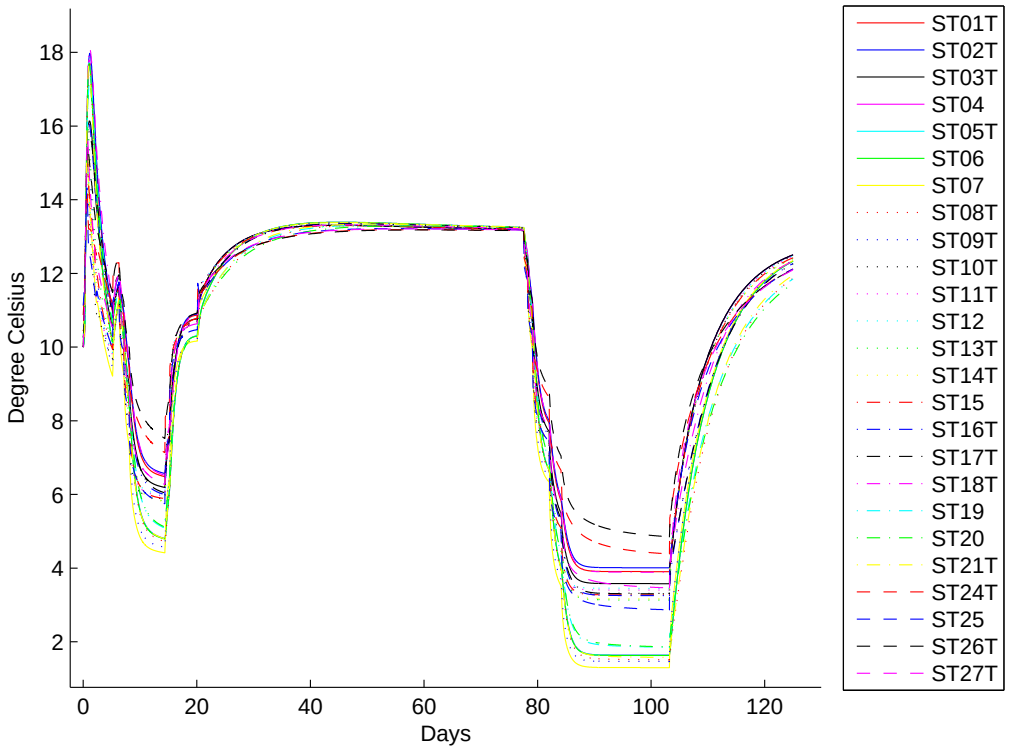

Figure 6.4: Temperature results from FEM.

The cooling after hydration resulted in temperatures about 2 °C lower in the FE simulation than the ones from measurements. The same is valid during the time when the concrete plug is cooled for grouting.

6.1.3 Joint meters

Measurement Results

Figure 6.5 shows the measured displacements in the concrete-rock interface from the time of bond to 2013-08-16. It also shows measured temperatures from sensor ST21T (positioned at the top of the concrete plug) for an easier orientation of the stages. Table 6.1 shows measurement results during four key stages for evaluating the displacement. For the grouting stage, the largest value during the period when the concrete plug temperature is around 6 °C is chosen. Positive values indicate gap.

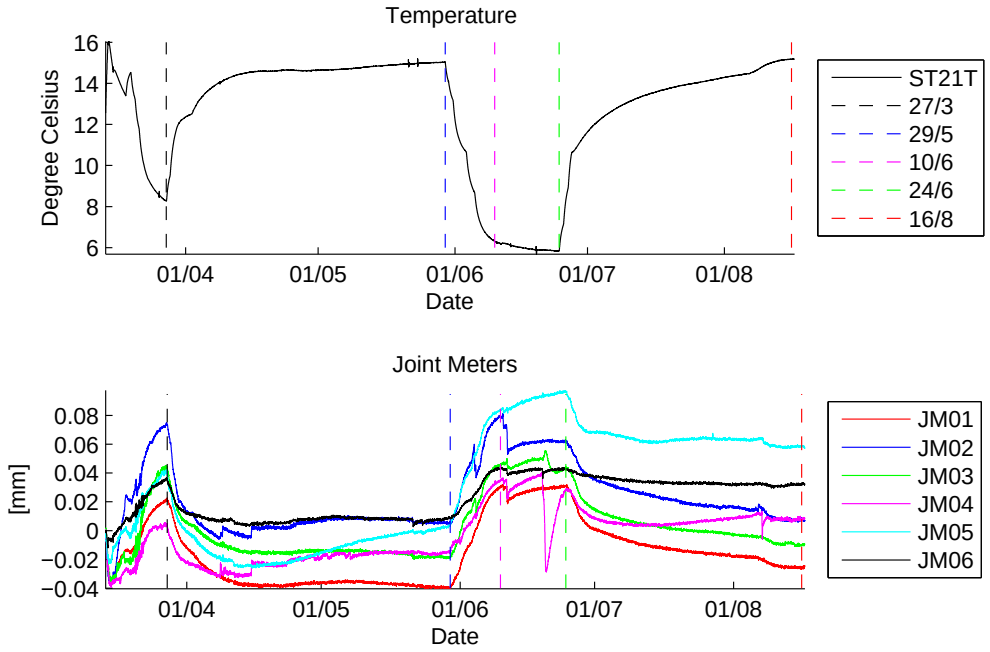

Figure 6.5: Measurements from joint meters.

Table 6.1: Joint meter measurement results during different stages.

	Cooling after hydration	**Pre cooling**	**Grouting**	**After grouting**
Date	27/3	29/5	10/6 to 24/6	16/8
Temp. [°C]	8	15	6	15
JM01 [mm]	0.02	-0.04	0.03	-0.03
JM02 [mm]	0.07	0.01	0.08	0.01
JM03 [mm]	0.04	-0.02	0.05	-0.01
JM04 [mm]	0.00	-0.01	0.04	0.01
JM05 [mm]	0.04	0.00	0.10	0.06
JM06 [mm]	0.04	0.01	0.04	0.03

FEM Result

Figure 6.6 shows the concrete-rock displacement from FE calculations at the positions of the joint meters. As seen in the figure, JM03 and JM04, placed at the top, yield similar values. The same goes for JM05 and JM06, placed at the side. Table 6.2 shows values over the same key stages as in Table 6.1.

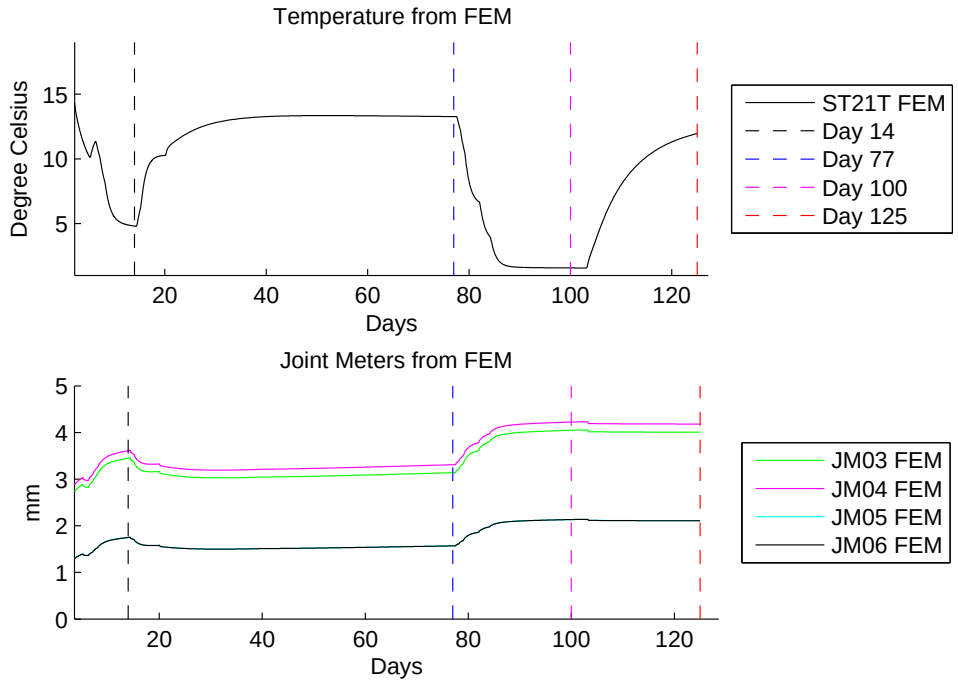

Figure 6.6: FEM results over concrete-rock displacement.

Table 6.2: FEM results during different stages.

	Cooling after hydration	**Pre grouting cooling**	**Grouting**	**After grouting**
Day	14	77	100	125
Temp. [°C]	5	13	2	12
JM03 [mm]	3.45	3.14	4.05	4.01
JM04 [mm]	3.61	3.31	4.22	4.18
JM05 [mm]	1.75	1.57	2.13	2.11
JM06 [mm]	1.75	1.57	2.13	2.11

Comparison

The results show that the cooling is affecting the measured displacement in the concrete-rock interface. The displacements are however very small compared to the FE results.

Comparing the values before the concrete plug was cooled for grouting and the values after grouting in Table 6.1, the difference is 0.00-0.06 mm. The corresponding values

from the FE simulation was 0.54-0.87 mm. The measured displacements from before the concrete plug was cooled for grouting to the grouting stage was 0.03-0.10 mm compared to 0.56-0.91 mm from FE calculations. The measured temperature went from 15 °C to 6 °C between these two stages. One may therefore question if the measured displacement is due to the impact the temperature difference may have on the joint meter sensors or if there is an actual displacement.

6.1.4 Strain

Strain is here referred to the real strain, i.e. the strain that could be observed, and does not include strain from restrained conditions. While the measured strain thus is the same for both the two assumptions of no and full bond between the concrete and rock, this is not the case for the FE simulations. The results from both cases and the FE simulations are therefore presented in separate sections.

Result plots for sensors ST01-03, positioned in the center of the concrete plug, and sensors ST22-27, positioned close to the slot, are presented in this section. Results from measurements are plotted with results from the FE simulations with negative values as compressive strains. Result plots for all sensors are presented in Appendix A.

Maximum, minimum and mean strain values are presented for three key stages; before cooling for grouting (76 days after casting), during grouting (95 days) and after grouting (124 days). Maximum, minimum and mean change of strain between the key stages are also presented. The maximum and minimum values in the tables does not necessarily indicate the largest and smallest strain values. For instance, in the case of measured strains of 10, -1 and -30 microstrain, the largest strain would be -30 and the smallest would be -1. However, in the tables in this chapter, the maximum value is 10 and the minimum is -30. The values denoted maximum and minimum hence refers to the boundary values of the strains.

Sensors ST23 and ST25 failed during the grouting stage and yielded large jumps in the result. The results from these sensors are therefore discarded after they had failed.

Assuming no bond

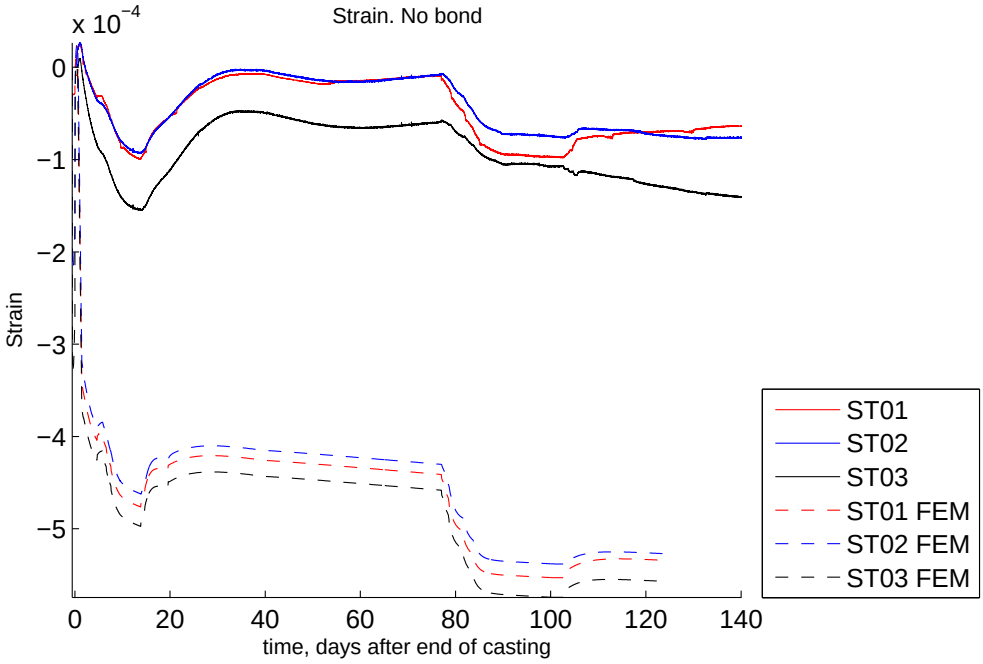

Figure 6.7: Strain for sensors ST01-03 from measurements and FE simulation assuming no bond.

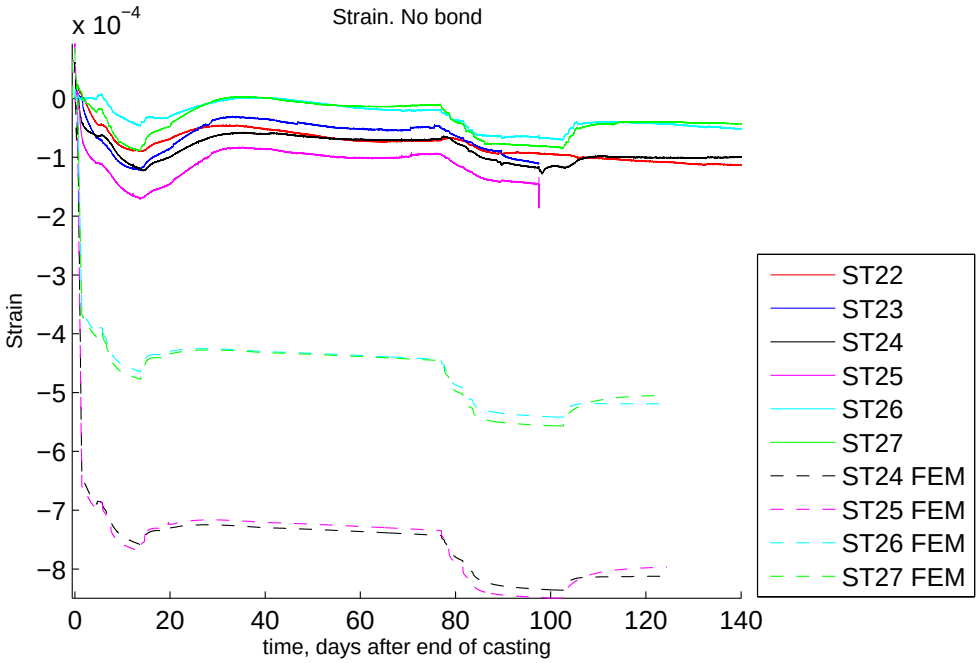

Figure 6.8: Strain for sensors ST22-27 from measurements and FE simulation assuming no bond.

Apart from that the strain obtained from the FE simulation is larger, as can be seen in Table 6.3, the measurements and the FEM curves in Figure 6.7 and 6.8 resemble each other with apparent strains caused by the temperature changes for the grouting sequence. As seen in Table 6.4, the change of strain during the first two stages was larger in the FE simulation. The same applies for the remaining strain after grouting, with ST08 being the only exception. This sensor registered a continuously increasing compressive strain for about 100 days after the grouting. All sensors indicated a sustained compressive strain after grouting, i.e. the registered strains were larger after grouting than before.

The measured change of strain between the last two stages were for some sensors positive and for others negative. The negative change of strain for many of the sensors in the center was also the result from the FE simulation. The negative change of strain was larger from measurements for all sensors. The sensors close to the slot indicated a negative change of strain both form measurements and the FE simulation with the exception of measurements from sensor ST22.

Table 6.3: Strain at three key stages assuming no bond.

	Micro-strain at key stages.		
	Stage 1 (day 76)	Stage 2 (day 95)	Stage 3 (day 124)
FEM max	-225.0	-351.9	-293.1
FEM min	-742.7	-847.2	-812.2
FEM mean	-462.2	-571.4	-556.1
Measured max	-8.3	-58.7	-39.7
Measured min	-123.1	-161.3	-203.8
Measured mean	-47.6	-101.6	-109.8

Table 6.4: Change of strain between key stages assuming no bond.

	From stage A to B. [micro-strain]		
	1 to 3	**1 to 2**	**2 to 3**
FEM max	-59.4	-90.2	60.9
FEM min	-124.8	-130.0	-22.9
FEM mean	-93.9	-109.2	-15.4
Measurements max	-16.1	-21.5	72.5
Measurements min	-110.7	-88.6	-47.8
Measurements mean	-64.0	-54.0	-10.1

Assuming full bond

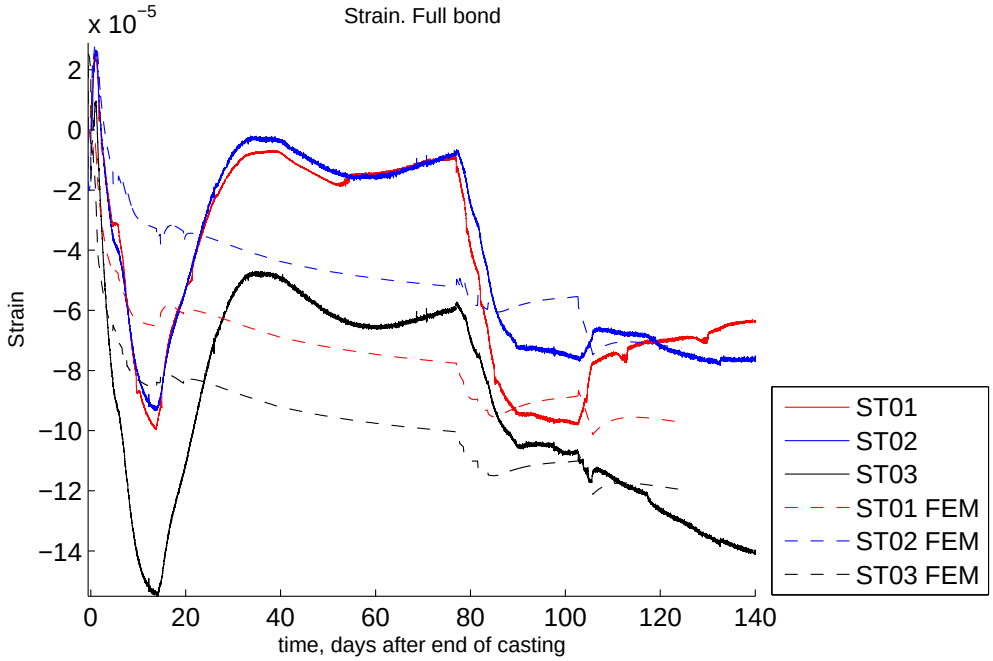

Figure 6.9: Strain for sensors ST01-03 from measurements and FE simulation assuming full bond.

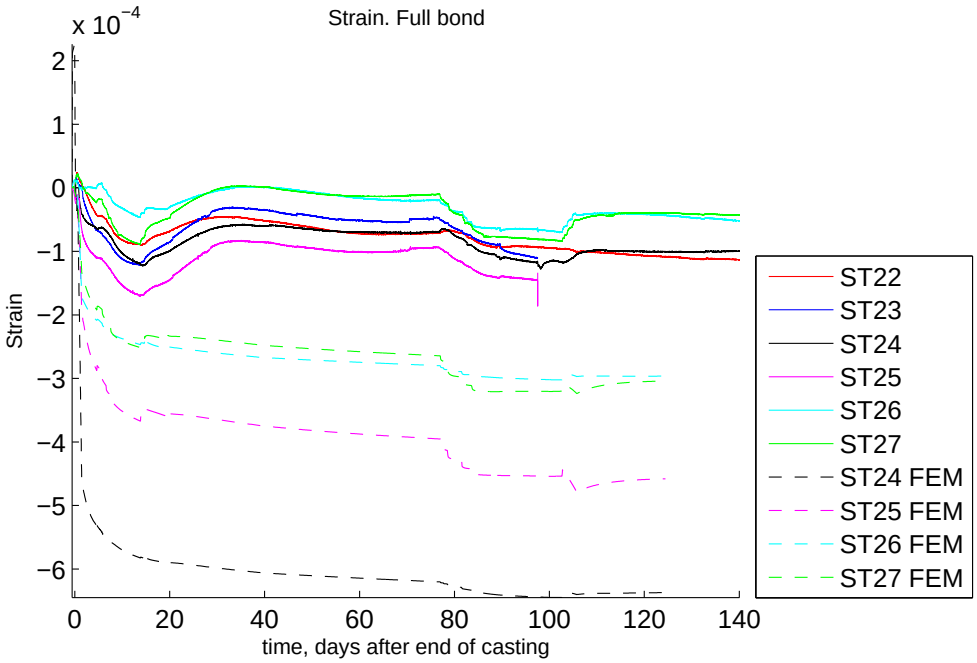

Figure 6.10: Strain for sensors ST22-27 from measurements and FE simulation assuming full bond.

The FEM curves in Figure 6.10 are similar to the curves from measurements. However, this is not the case in Figure 6.9 and several of the figures in Appendix A.

As seen in Table 6.5, analogous to the no bond case, the strains from the FE simulation are larger than the measured ones. While the measured results indicate compressive change of strain from before grouting to during grouting (stage 1 to stage 2), the FEM result indicate larger tensile strains at some positions. This can be seen in Table 6.6. It can also be seen in Table 6.6, that both measurements and the FE simulation indicate compressive change of strain from before to after grouting (stage 1 to stage 3). The compressive change of strain was larger from measurements between these two stages.

Table 6.5: Strain at three key stages assuming full bond.

	Micro-strain at key stages.		
	Stage 1 (day 76)	Stage 2 (day 95)	Stage 3 (day 124)
FEM max	120.4	155.4	104.0
FEM min	-619.9	-643.1	-637.0
FEM mean	-101.2	-113.5	-122.8
Measured max	-8.3	-58.7	-39.7
Measured min	-123.1	-161.3	-203.8
Measured mean	-47.6	-101.6	-109.8

Table 6.6: Change of strain between key stages assuming full bond.

	From stage A to B. [micro-strain]		
	1 to 3	**1 to 2**	**2 to 3**
FEM max	-14.6	36.9	56.6
FEM min	-63.1	-73.3	-54.0
FEM mean	-21.6	-12.3	-9.3
Measurements max	-16.1	-21.5	72.5
Measurements min	-110.7	-88.6	-47.8
Measurements mean	-64.0	-54.0	-10.1

6.1.5 Stress

As for strain, stress results are presented in two figures in this section for sensors ST01-03 and ST22-27. Negative values denotes compressive stress. All result plots can be found in Appendix B. Stress values are presented for the same three key stages as for strain.

Maximum, minimum and mean stress values are presented for the same key stages as the strain results in Section 6.1.4. Maximum, minimum and mean stress change are also presented. The same meaning of maximum and minimum values is valid in this section as in Section 6.1.4.

Assuming no bond

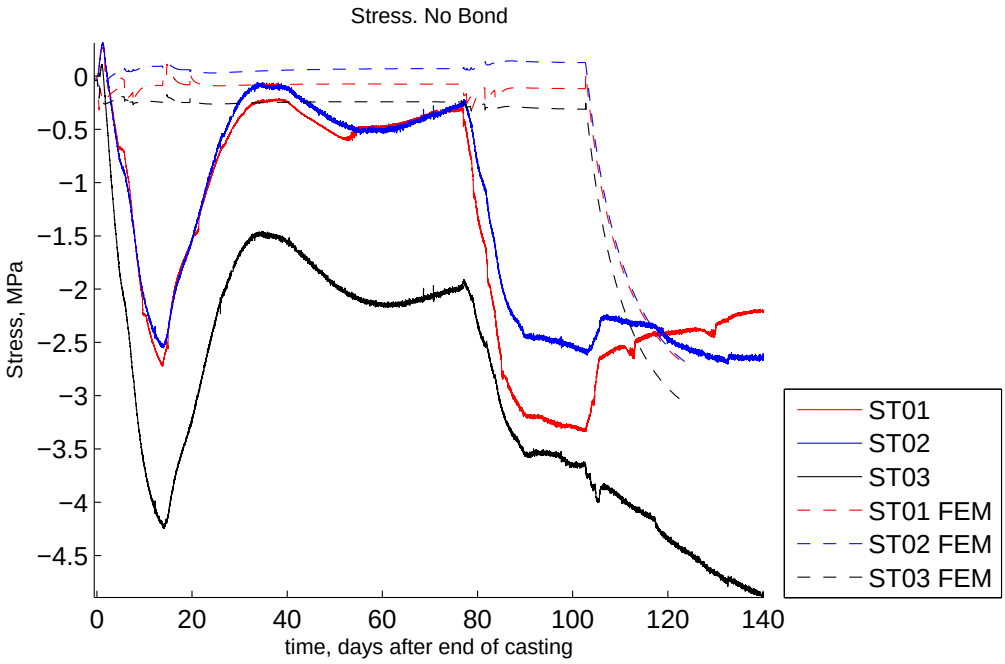

Figure 6.11: Stress for sensors ST01-03 from measurements and FE simulation assuming no bond.

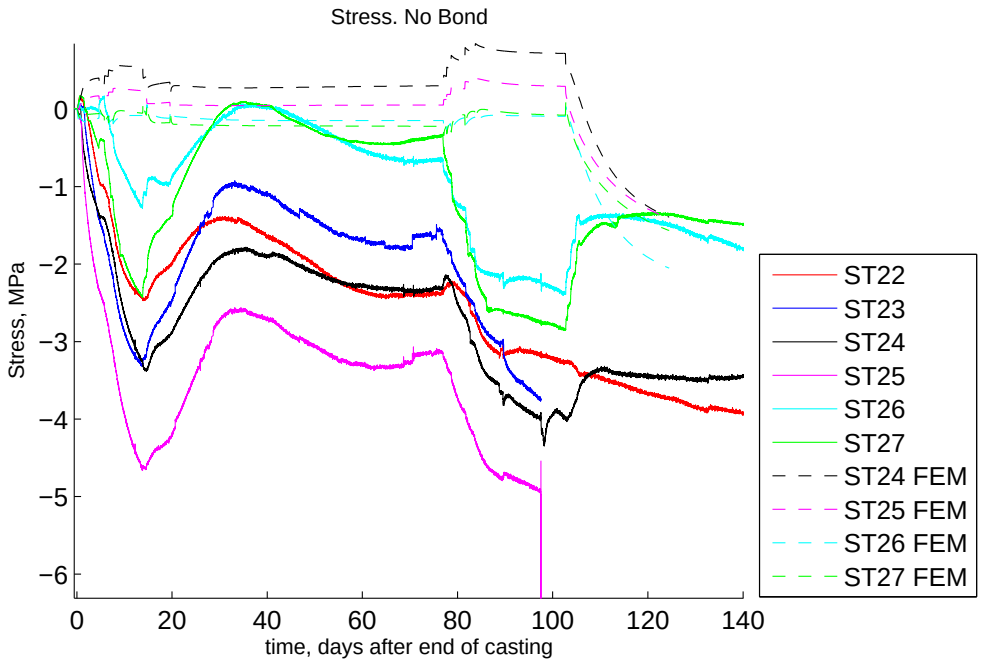

Figure 6.12: Stress for sensors ST22-27 from measurements and FE simulation assuming no bond.

As seen in Figure 6.11 and 6.12, results from measurements indicate larger change of stress during the cooling periods. It is also evident in Figure 6.12 that the FEM results indicate tensile change of stress between the first two key stages while the measured result indicate compressive change of stress. This is characteristic for most of the sensor positions as can be seen in the figures in Appendix B.

Table 6.7 shows the stress results obtained from measurements and the FE simulation at the three key stages with compressive stresses denoted as negative and tensile as positive. As seen in the table, the results from both measurements and the FE simulation indicate that the concrete plug is in a compressive state at all sensors positions at the post grouting stage (key stage 3).

Table 6.7: Stress at three key stages assuming no bond.

	Stress at key stages. [MPa]		
	Stage 1 (day 76)	Stage 2 (day 95)	Stage 3 (day 124)
FEM max	0.30	1.03	-1.26
FEM min	-0.62	-0.31	-4.24
FEM mean	-0.13	0.24	-2.68
Measured max	-0.28	-1.99	-1.37
Measured min	-4.11	-5.46	-7.02
Measured mean	-1.59	-3.44	-3.78

Table 6.8: Change of stress between key stages assuming no bond.

	From stage A to B. [MPa]		
	1 to 3	**1 to 2**	**2 to 3**
FEM max	-1.27	1.09	-1.49
FEM min	-3.70	-0.06	-4.33
FEM mean	-2.55	0.36	-2.92
Measurements max	-0.63	-0.77	2.41
Measurements min	-3.86	-3.04	-1.73
Measurements mean	-2.25	-1.85	-0.40

As seen in Table 6.8, the mean stress change from the FE simulation was tensile between the first two key stages (76 to 95 days after casting). The tensile changes of stress between the first two key stages are obtained from all FEM sensors except for sensors ST01 and ST03, positioned in the center close to the upstream surface. Measurements indicate a different behavior with compressive change of stress from all sensors during the same time period. Between the two first key stages the FE simulation indicate a change of stress of -0.06 to 1.09 MPa while the corresponding measured values are between -3.04 to -0.77 MPa.

From the grouting stage to the post-grouting stage (key stages 2 to 3), all FEM sensors indicate compressive change of stress while some of the measurement sensors indicate tensile and some compressive change of stress. The FEM change of stresses were between -4.33 to -1.49 MPa. The corresponding measured values were between -1.73 to 2.41 MPa.

The FE simulation indicated changes of stress between -3.70 to -1.27 MPa from before the concrete plug was cooled for grouting and after the concrete plug was grouted and the cooling was stopped (key stages 1 to 3). The corresponding measured values were between -3.86 to -0.63 MPa. Both measurements and the FEM simulation hence indicated a sustained compressive change of stresses at all sensor positions.

Assuming full bond

The results plotted in Figure 6.13 and 6.14 show a more similar stress behavior between the measurements and the FE simulation than the corresponding result plots for the no bond assumption. The resemblance is most apparent between the three key stages with the pre-grouting cooling causing tensile stress changes at all sensor positions. The FE simulation show a large tensile stress growth during the early age of the concrete which is could not be captured by the sensors.

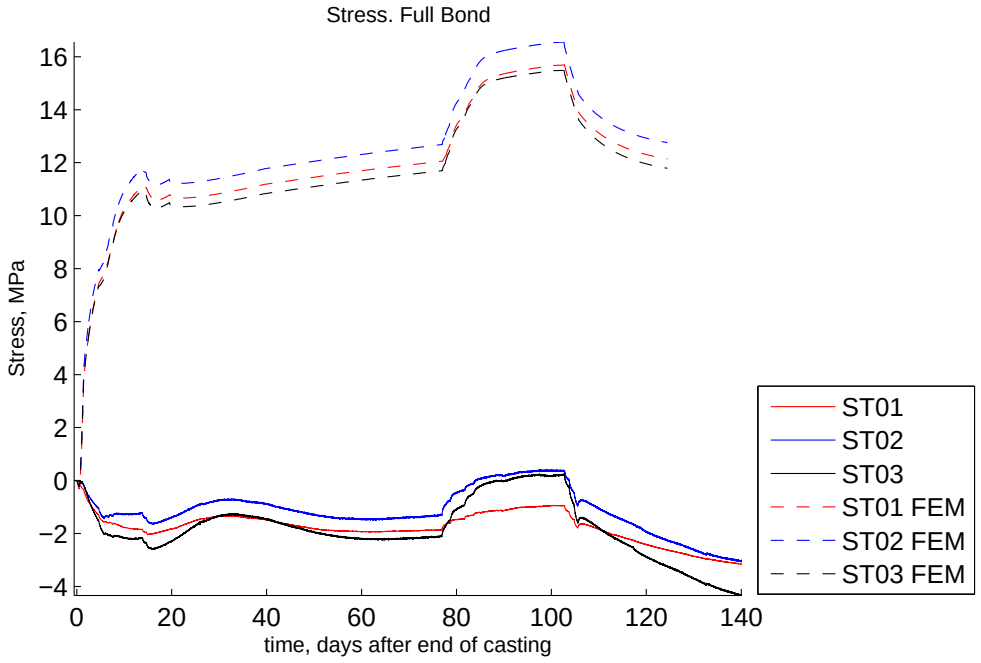

Figure 6.13: Stress for sensors ST01-03 from measurements and FE simulation assuming full bond.

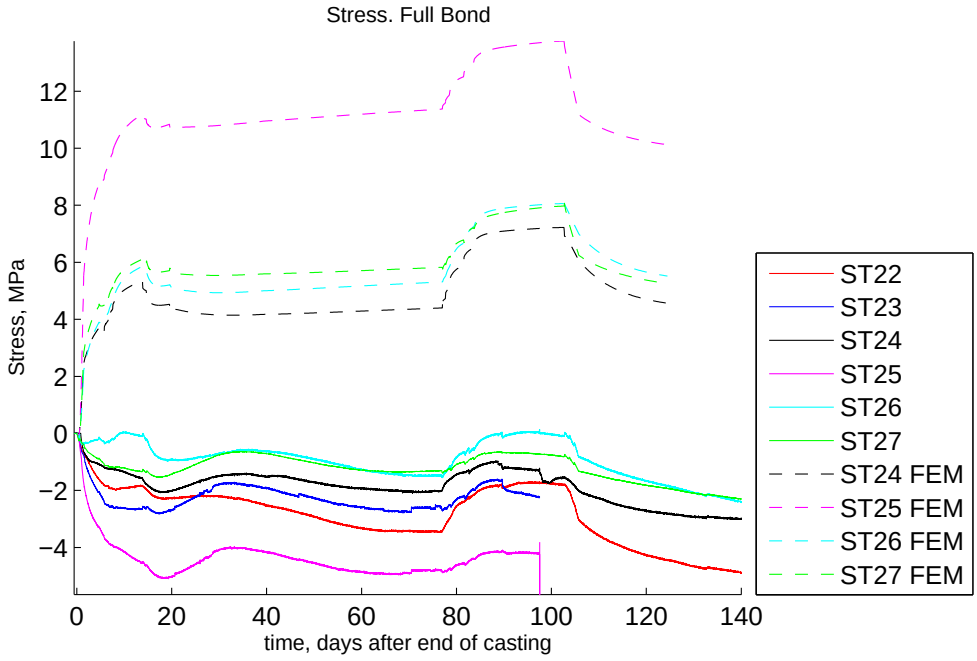

Figure 6.14: Stress for sensors ST22-27 from measurements and FE simulation assuming full bond.

Table 6.9 shows the stress results obtained from measurements and the FE simulation at the three key stages with compressive stresses denoted as negative and tensile as positive. As seen in the table, the tensile stresses from the FE simulation are larger than both the concrete tensile strength and the concrete - rock bond strength as presented in Section 2.2.3. In this case, the concrete plug would either crack or de-bond from the rock. The largest measured tensile stress of 0.63 MPa is lower than both the concrete tensile strength and the concrete - rock bond strength.

Table 6.9: Stress at three key stages assuming full bond.

	Stress at key stages. [MPa]		
	Stage 1 (day 76)	Stage 2 (day 95)	Stage 3 (day 124)
FEM max	18.42	23.81	18.79
FEM min	4.39	7.16	4.58
FEM mean	11.91	15.76	12.06
Measured max	-1.31	0.63	-1.81
Measured min	-5.45	-4.19	-7.58
Measured mean	-2.64	-1.12	-3.93

As seen in Table 6.10, between the first two key stages, the FE simulation indicated stress changes of 2.04 to 5.57 MPa while measurements indicated stress changes of 0.41 to 2.51 MPa. The stress changes from the grouting stage to the post-grouting stage (key stages 2 and 3) were between -1.69 to -5.22 MPa. The corresponding measured stress changes are between -0.82 to -4.40 MPa. The stress changes were

hence larger in the FE simulation than from measurements during both of the two periods.

Table 6.10: Change of stress between key stages assuming full bond.

	From stage A to B. [MPa]		
	1 to 3	**1 to 2**	**2 to 3**
FEM max	0.46	5.57	-1.69
FEM min	-1.23	2.04	-5.22
FEM mean	0.15	3.85	-3.70
Measurements max	-0.09	2.51	-0.82
Measurements min	-2.92	0.41	-4.40
Measurements mean	-1.38	1.52	-2.98

The obtained stress changes from key stage 1 to key stage 3 were between -1.23 to 0.46 MPa in the FE simulation. Compressive stress changes were obtained for sensors close to the slot in the upstream direction only, while all the other FEM sensors indicated a tensile stress change. Stress changes from measurements were between -2.92 to -0.09 MPa. All sensors hence indicated an obtained compressive stress change after the grouting.

6.2 Pressurization period

This section shows the results after the casting and grouting period as described in the previous section and continues to the end of available measurement data. This section hence include the pressurization of the concrete plug. As mentioned in Section 3.3.2, the pressure was measured in the bentonite seal. The resulting mean pressure is given in Figure 6.15 for the convenience and later reference.

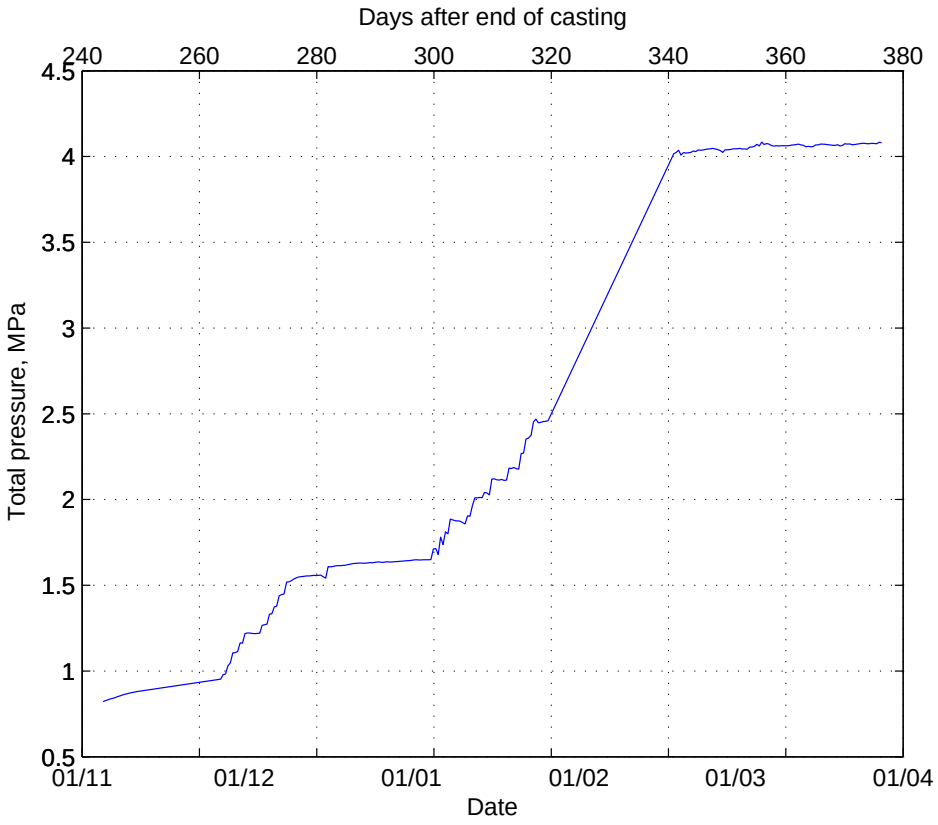

Figure 6.15: Mean total pressure measured in the bentonite seal.

6.2.1 Temperature

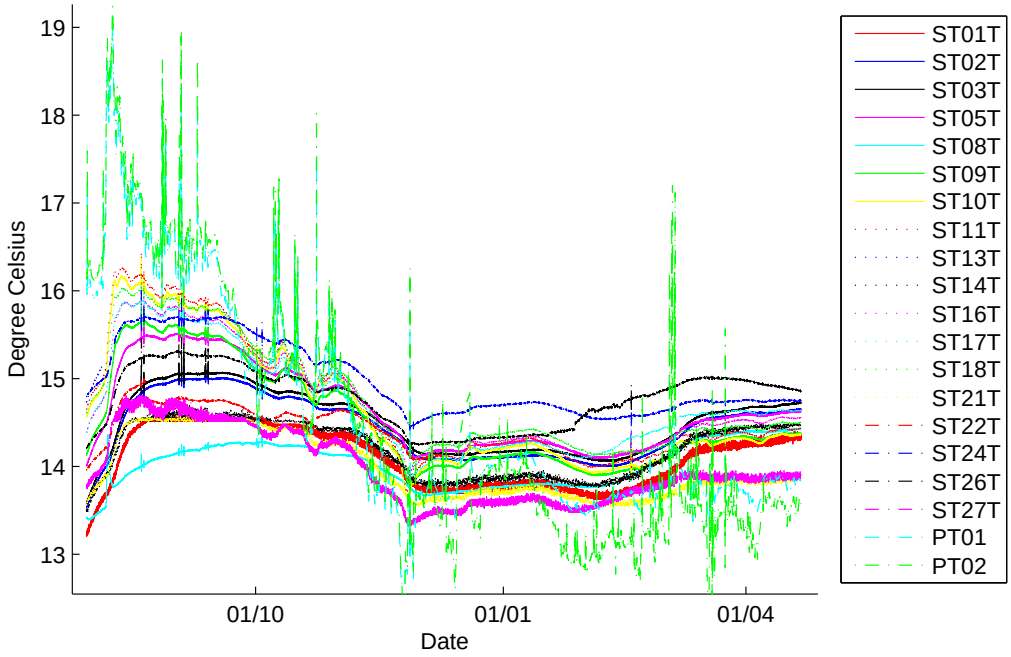

Figure 6.16: Measured temperature from strain gauge thermocouples and ambient temperature gauges.

Figure 6.16 continues the plot of measured temperatures in Figure 6.3. The figure shows that the temperature in the concrete plug was the same as the ambient temperature about three months after the cooling for grouting was stopped. The temperature in the concrete plug has since August 2013 been about 13-16 °C.

Sensor ST13T and ST22T were during this period damaged and yielded large jumps in the results. The results from these sensors presented in Figure 6.16 are therefore discarded after the sensors failed.

6.2.2 Joint meters

Measurements Result

As seen in Figure 6.17, the sensors at the top JM03 and JM04, indicated relatively large displacements between the 12th and 13th of February. These sensors later began to yield high and irregular jumps in the result. As seen in Figure 6.15, the pressure was increasing during this time period. It is therefore possible that the concrete plug have displaced due to slipping or crushing of the concrete at the top where these sensors are placed.

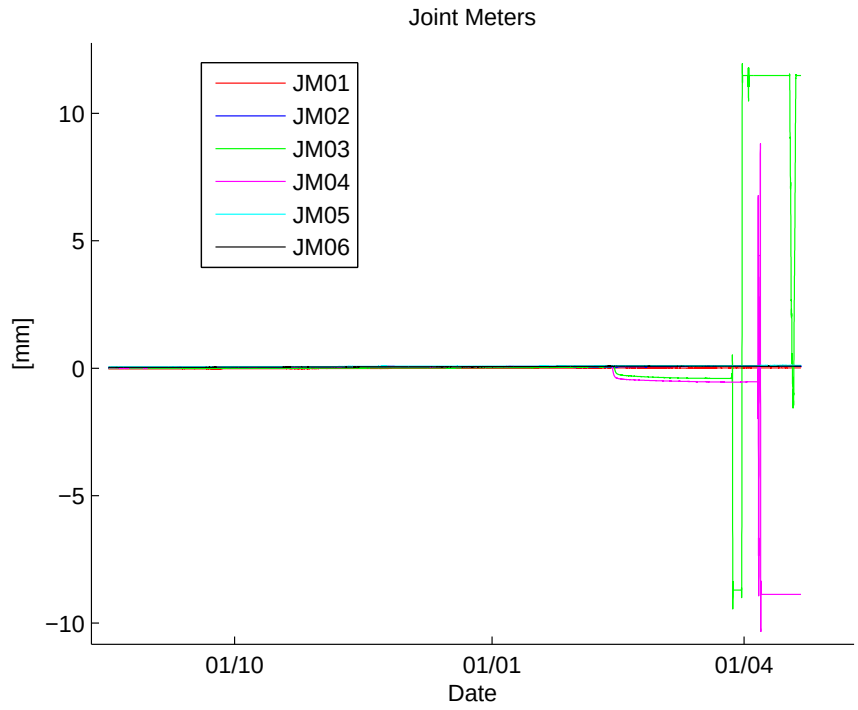

Figure 6.17: Irregular results from sensors JM03 and JM04.

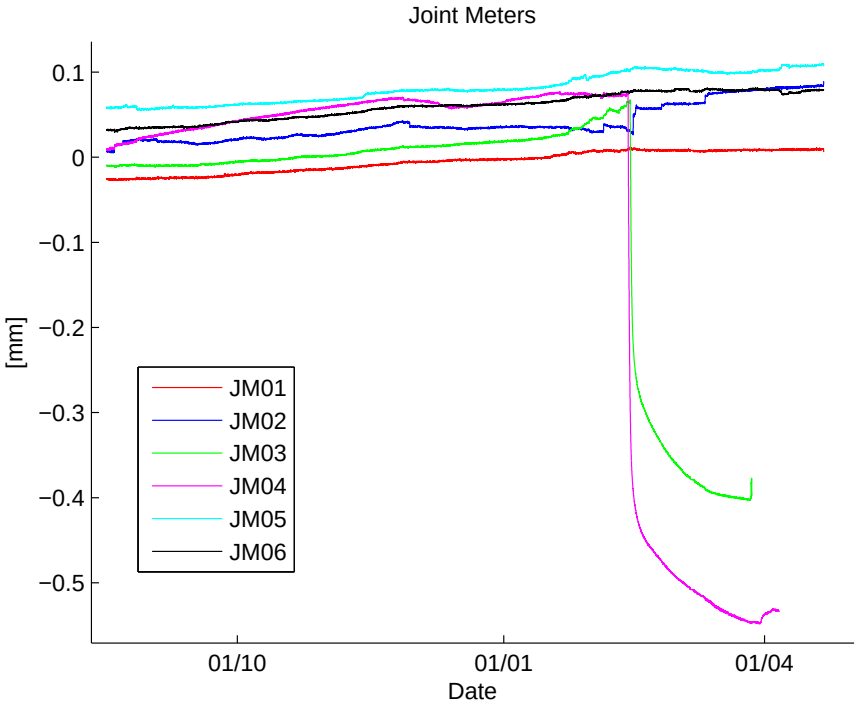

Figure 6.18: Joint meter measurements with JM03 and JM04 cut at first jump.

In Figure 6.18 sensor JM03 and JM04 are cut at the time of the first large jump. As seen in the figure, all sensors registered an increased gap in the interface. JM03 and

JM04 registered an increased gap of 0.08 mm and 0.09 mm before the drop. The other sensors registered an increased gap of 0.04-0.08 mm. Although the displacements are small, they are in the same magnitude as the measured displacements from before the concrete plug was cooled for grouting and after the concrete plug was cooled.

6.2.3 Strain

During different times of the pressurization period, sensors ST03, ST13, ST17, ST18, ST22, ST23, ST24, ST25 and ST26 were damaged and yielded large jumps in the results. The results from these sensors are therefore discarded after the failure. Result plots are shown in two figures for sensors ST01-03 and ST10-12 in this section. All result plots can be found in Appendix A. Even though the temperature stay relatively unchanged during this time period, results are presented for both of the assumption of full and no bound to examine the influence of previous stress states of the concrete plug in the FEM simulation.

Maximum, minimum and mean results of strain values and strain changes are presented with the same meaning of maximum and minimum as in Section 6.1.4. The values are presented for measured mean pressures of 1.0, 2.0 and 4.1 MPa, applied 267, 307 and 376 days after end of casting respectively, as can be seen in Figure 6.15.

Assuming no bond

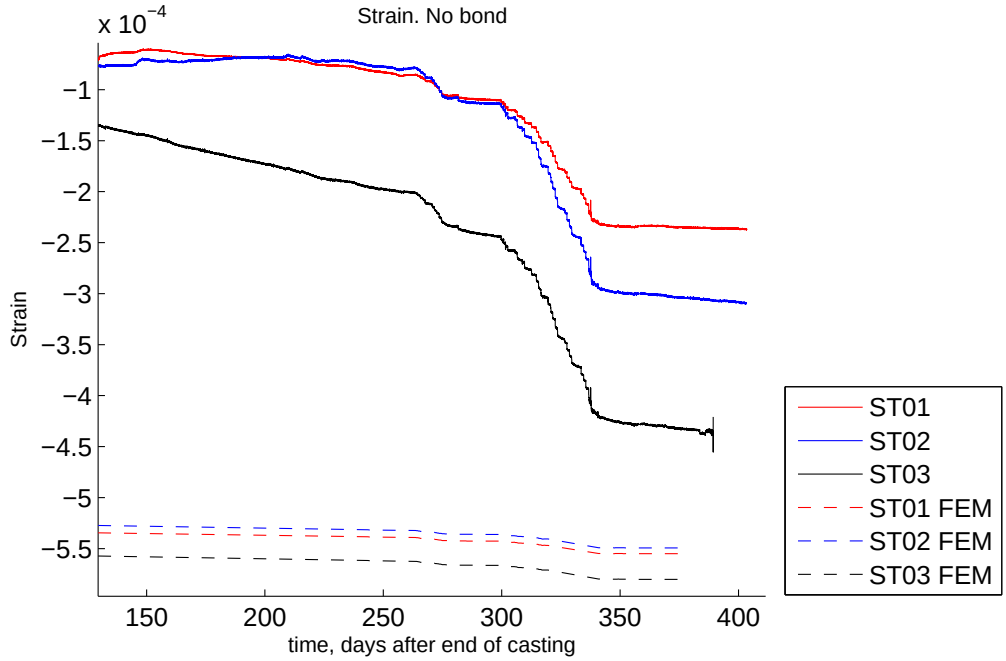

Figure 6.19: Strain for sensors ST01-03 from measurements and FE simulation assuming no bond.

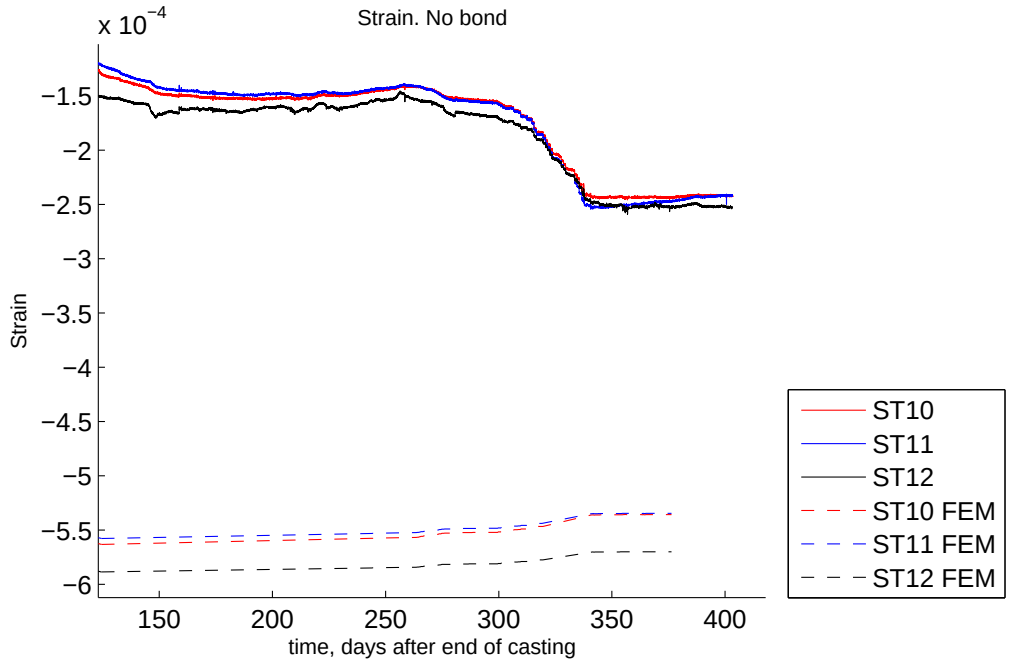

Figure 6.20: Strain for sensors ST10-12 from measurements and FE simulation assuming no bond.

As seen in Figure 6.19, sensor ST03 registered a continues strain increase even when the concrete plug was not subjected to any load. This behavior was also registered by sensor ST15. These sensors are positioned close to the upstream surface in a vertical direction.

Also as seen in Figure 6.19 and 6.20, the obtained strains from the FE simulation are small compared to the ones from measurements. This is valid for all the sensors as can be seen in Appendix A. Several of the FEM sensors indicated a tensile change of strain when the pressure was applied, for example the ones in Figure 6.20, while all measurements indicate compressive strain changes when the pressure is applied.

As seen in Table 6.11, both measurements and the FE simulation indicated compressive strains exclusively. The strain change between the applied pressures of 1.0, 2.0 and 4.1 MPa are presented in Table 6.12 with negative values representing compressive strain change. Measured tensile change of strain between the applied pressures of 1.0 to 2.0 MPa was registered by sensor ST24 only. This sensor is positioned in the concrete - rock slot at the top of the concrete plug and was later damaged. As seen in the table, the measured change of strain was in a larger magnitude than the strain change from the FE simulation.

Table 6.11: Strain at applied pressures assuming no bond.

Micro-strain at applied pressure loads.			
	1.0 MPa Load	2.0 MPa Load	4.1 MPa Load
FEM max	-295.6	-298.2	-303.7
FEM min	-819.1	-825.8	-839.9
FEM mean	-556.7	-557.2	-558.3
Measured max	-71.8	-100.3	-150.0
Measured min	-240.3	-267.0	-433.2
Measured mean	-132.9	-163.5	-269.8

Table 6.12: Change of strain between applied pressures assuming no bond.

Strain change between applied pressure loads. [micro-strain]			
	Pressure load from A to B MPa.		
	1.0 to 4.1	**1.0 to 2.0**	**2.0 to 4.1**
FEM max	20.6	6.6	14.0
FEM min	-20.8	-6.7	-14.1
FEM mean	-1.6	-0.5	-1.1
Measurements max	-51.7	0.8	-44.1
Measurements min	-226.7	-60.5	-167.3
Measurements mean	-136.7	-30.2	-104.5

Assuming full bond

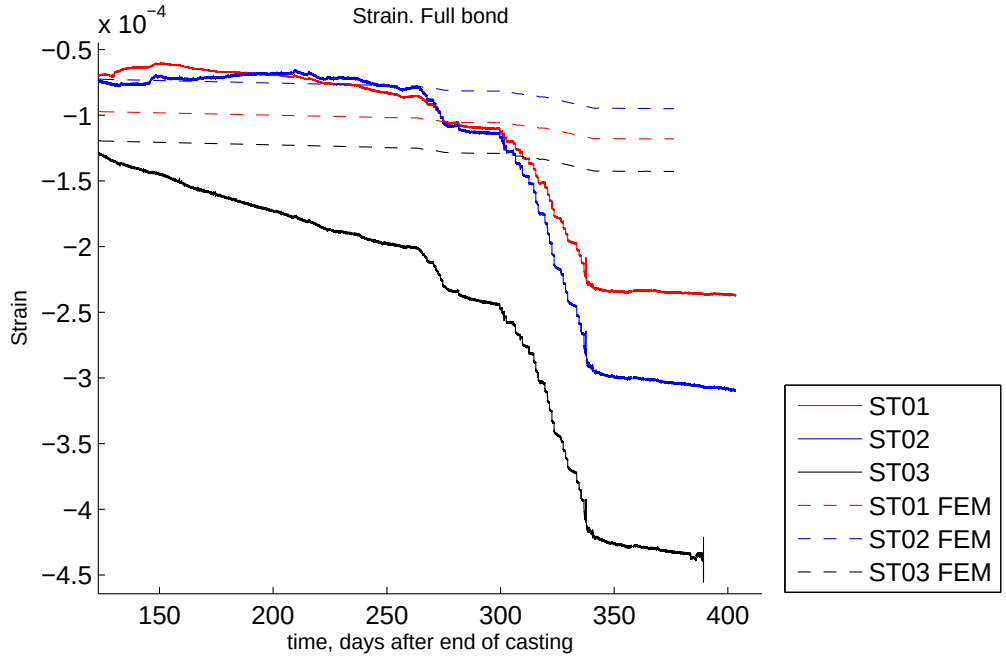

Figure 6.21: Strain for sensors ST01-03 from measurements and FE simulation assuming full bond.

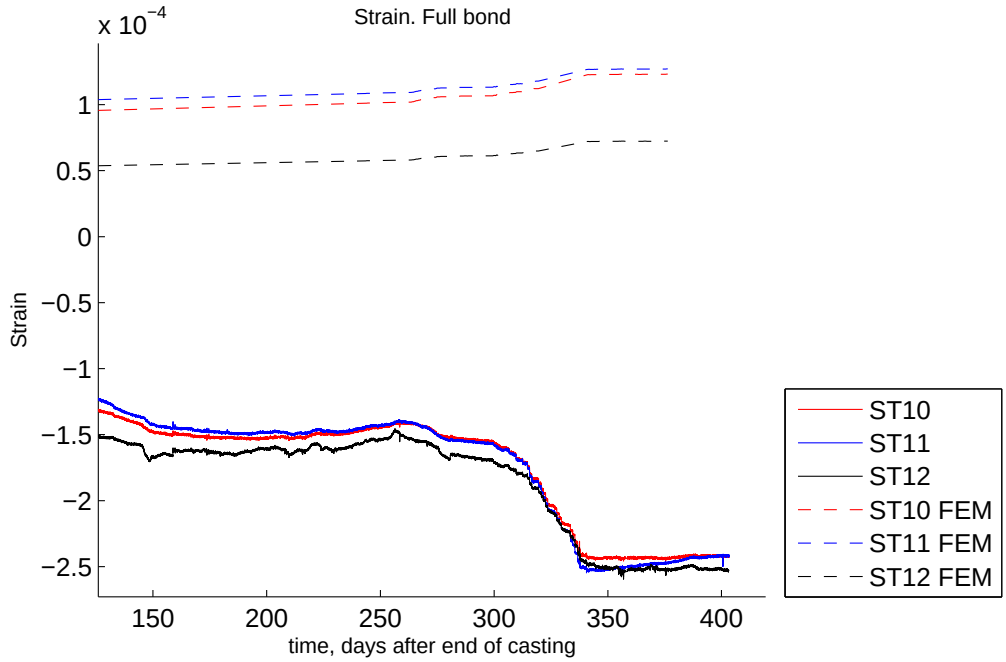

Figure 6.22: Strain for sensors ST10-12 from measurements and FE simulation assuming full bond.

As seen in Figure 6.21 and 6.22 a similar behavior was obtained for the full bond assumption as for the assumption of no bond. The change of strain between applied loads was the same as in the case of no bond. This was expected since the concrete plug is assumed to behave linear elastically. The change of strain is hence the same for both the assumptions of no and full bond. The strain results are given in Table 6.13.

Table 6.13: Strain at applied pressures assuming full bond.

Micro-strain at applied pressure loads.			
	1.0 MPa Load	2.0 MPa Load	4.1 MPa Load
FEM max	109.7	115.2	127.0
FEM min	-644.0	-650.6	-664.7
FEM mean	-123.4	-123.9	-125.0
Measured max	-71.8	-100.3	-150.0
Measured min	-240.3	-267.0	-433.2
Measured mean	-132.9	-163.5	-269.8

6.2.4 Stress

Plotted stress results are in this section presented for sensors ST01-03 and ST10-12. All stress plots can be found in Appendix B. Maximum, minimum and mean stresses and strain changes are presented with the same meaning of maximum and minimum as in Section 6.1.4. The values are presented for measured mean pressures of 1.0, 2.0 and 4.1 MPa, applied 267, 307 and 376 days after end of casting respectively, as can be seen in Figure 6.15.

Assuming no bond

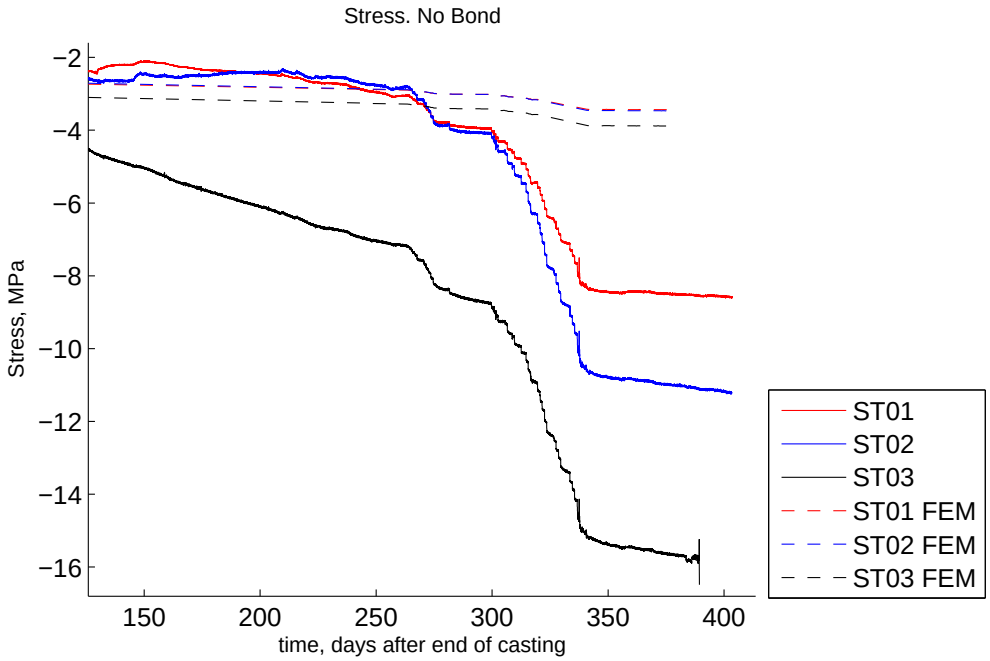

Figure 6.23: Stress for sensors ST01-03 from measurements and FE simulation assuming no bond.

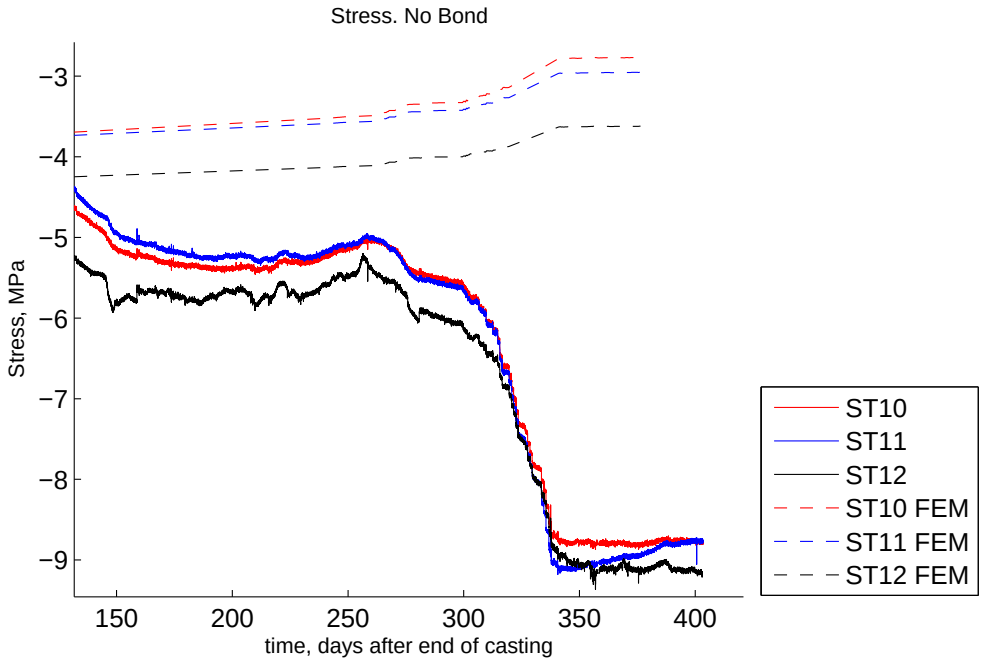

Figure 6.24: Stress for sensors ST10-12 from measurements and FE simulation assuming no bond.

The FE simulation indicated a tensile stress change for several of the sensors when the largest pressure was applied, as can be seen in Figure 6.24. Measurements however indicate compressive stress changes for all sensors. Stress changes from measurement are also larger than the ones from the FE simulation, as can be seen in Table 6.14. It should be noted that a tensile stress change between the applied pressures of 1.0 to 2.0 MPa from measurements was registered by sensor ST24 only while all other sensors indicated a compressive stress change. Sensor ST24 was later damaged and yielded large jumps in the results.

Table 6.14: Change of stress between applied pressures assuming no bond.

Stress change between applied pressure loads. [MPa]			
	Pressure load from A to B MPa.		
	1.0 to 4.1	**1.0 to 2.0**	**2.0 to 4.1**
FEM max	0.70	0.22	0.48
FEM min	-0.71	-0.23	-0.48
FEM mean	-0.06	-0.02	-0.04
Measurements max	-1.92	0.01	-1.62
Measurements min	-8.29	-2.21	-6.09
Measurements mean	-5.00	-1.11	-3.82

Table 6.15 show the stress results registered by the sensors from measurements and the FE simulation at the applied pressures of 1.0, 2.0 and 4.1 MPa. As seen in the table, both measurements and the FE simulation indicate a compressive stress state at all the sensor positions. The stresses from measurements are however much larger than the FEM stresses especially when the pressure of 4.1 MPa is applied.

Table 6.15: Stress at applied pressures assuming no bond.

Stress at applied pressure loads. [MPa]			
	1.0 MPa Load	2.0 MPa Load	4.1 MPa Load
FEM max	-1.39	-1.51	-1.65
FEM min	-4.10	-3.94	-3.88
FEM mean	-2.71	-2.73	-2.77
Measured max	-2.56	-3.60	-5.43
Measured min	-8.58	-9.59	-15.67
Measured mean	-4.75	-5.87	-9.76

Assuming full bond

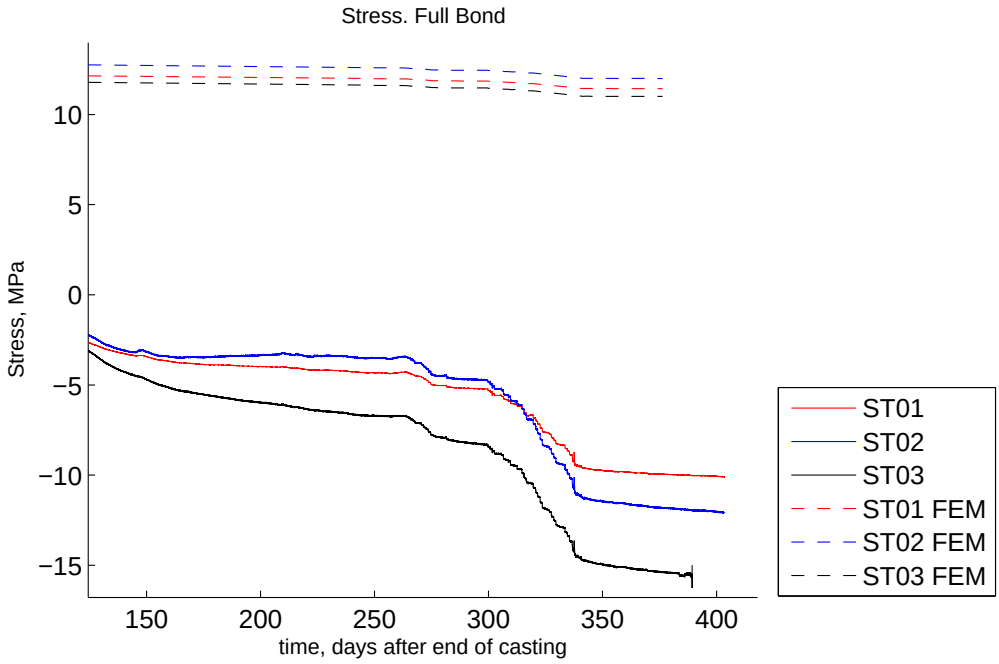

Figure 6.25: Stress for sensors ST01-03 from measurements and FE simulation assuming full bond.

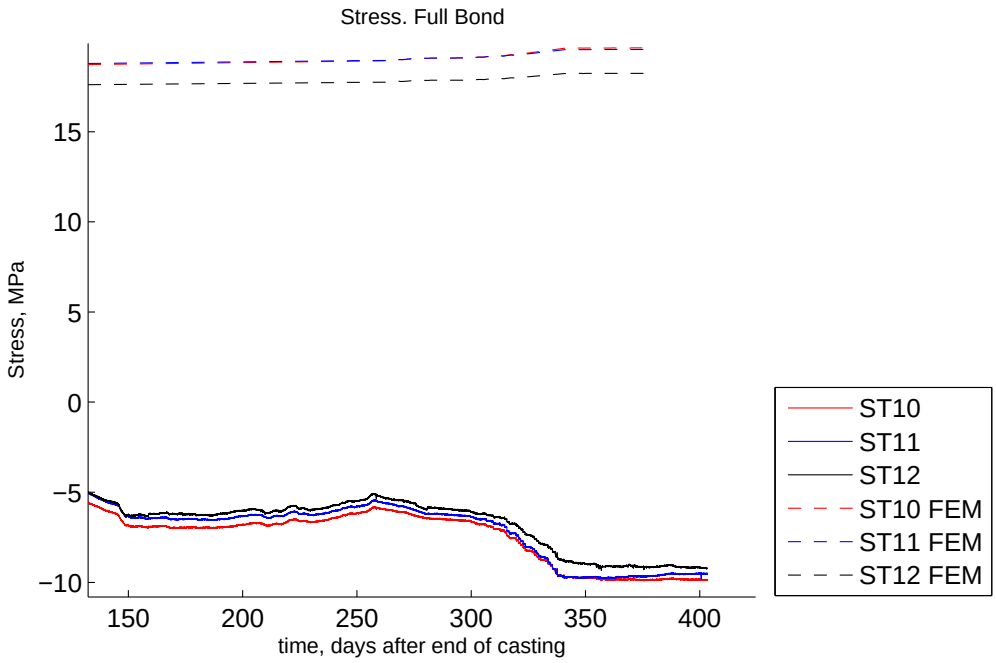

Figure 6.26: Stress for sensors ST10-12 from measurements and FE simulation assuming full bond.

Since the concrete plug is assumed to be linear elastic, the stress curves in Figure 6.25 and 6.26 are similar to the ones for the no bond assumption. Also, the change of stresses between the applied loads are the same as for the no bond assumption since the concrete plug is assumed for the same reason. The results of stress change can thus be seen in Table 6.14.

Table 6.16 show the stress results at the applied pressures of 1.0, 2.0 and 4.1 MPa. As seen in the table, the FE simulation indicate tensile stresses at all sensor positions while the measured values only indicate compressive stresses. It can also be noted that the tensile stresses from the FE simulation are higher than both the concrete tensile strength and the concrete - rock bond strength. As mentioned earlier, this would either cause cracks in the concrete plug or the concrete plug would de-bond from the rock.

Table 6.16: Stress at applied pressures assuming full bond.

Stress at applied pressure loads. [MPa]			
	1.0 MPa Load	2.0 MPa Load	4.1 MPa Load
FEM max	18.97	19.17	19.65
FEM min	4.33	4.10	3.62
FEM mean	12.03	12.01	11.98
Measured max	-3.04	-3.08	-6.92
Measured min	-9.50	-10.51	-15.43
Measured mean	-5.38	-6.53	-10.58

6.2.5 2D FEM strain result

Since the strains and stresses obtained from the 3D FEM model did not correspond to the ones from measurements, three 2D FEM simulations were performed with different conditions. Figure 6.27, shows the strain results from the 2D models at the approximate location of ST01 as well as the measured strain for the same sensor. As seen in the figure, the strain from model 4 best correspond to the measured result. In this model, the full pressure was added on the entire length of the upstream side of the slot.

With the results from the 2D FEM simulations there is reason to believe that the concrete plug is subjected to water pressure inside the slot.

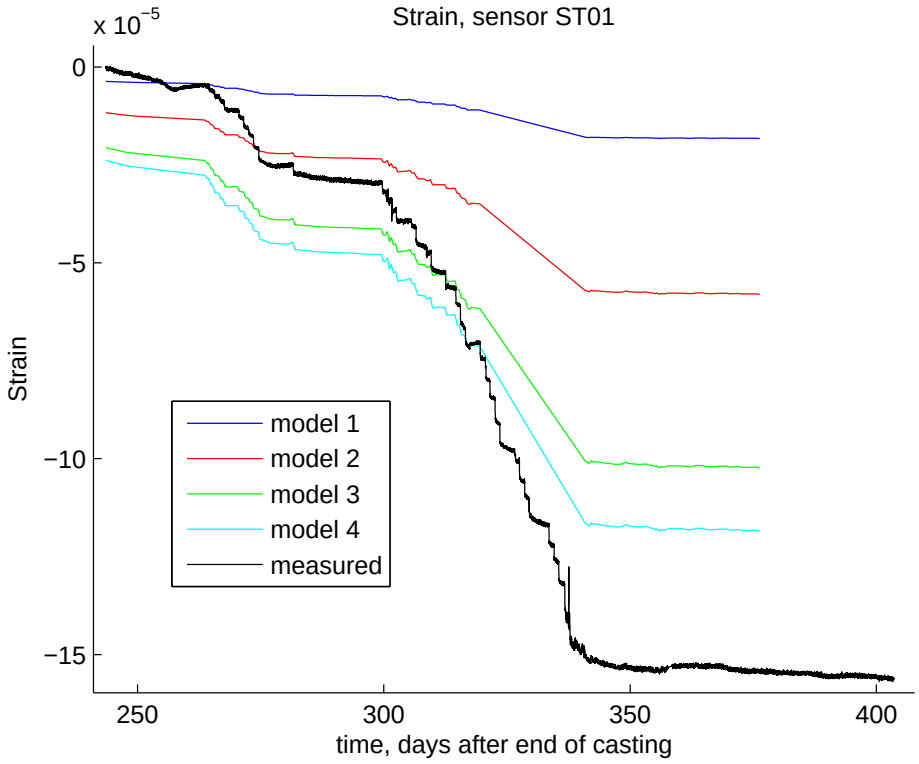

Figure 6.27: Strain results from 2D FE models and measurements for sensor ST01.

6.2.6 LVDT displacement sensors

As seen in Figure 6.28, the sensors LVDT01 and LVDT03 yield jumps in the results. The jumps were removed and plotted in Figure 6.29. As seen in Figure 6.29, LVDT01 and LVDT03 register practically no displacements during the pressurization period compared to sensor LVDT02. It is possible that the two sensors have broken or that there was a mistake in the installation.

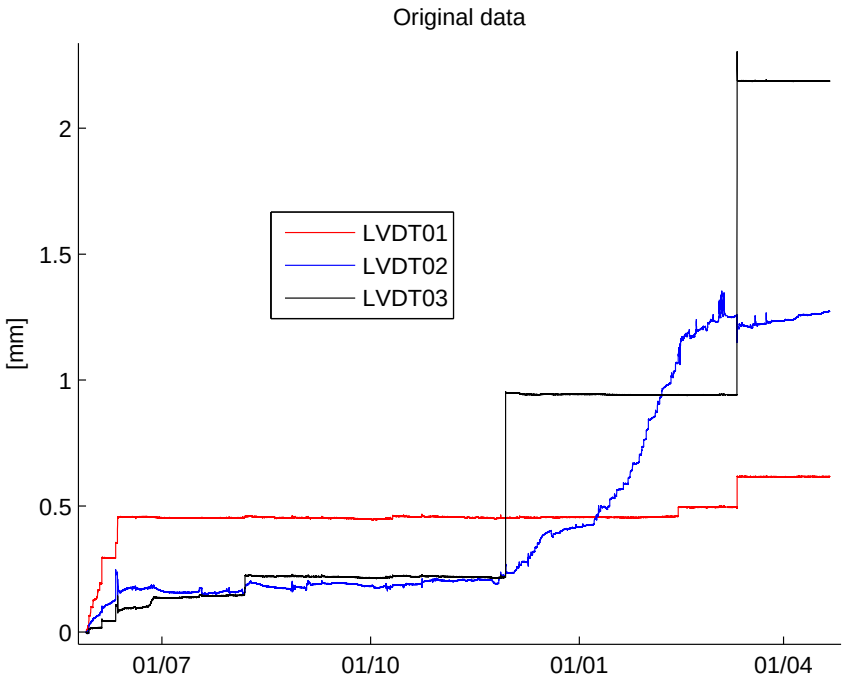

Figure 6.28: Jumps in measurements from LVDT01 and LVDT03

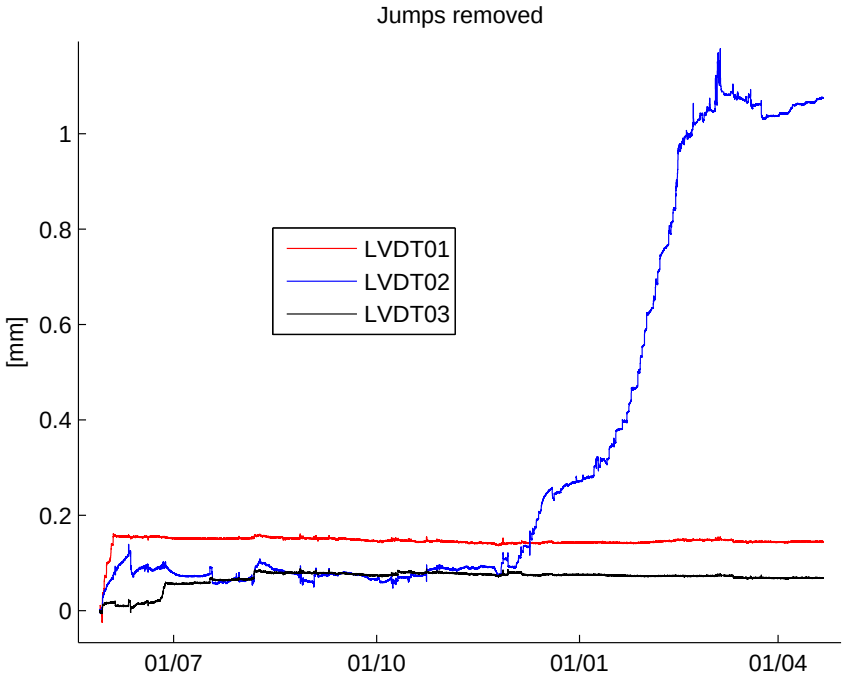

Figure 6.29: LVDT measurement results. Jumps from LVDT01 and LVDT03 removed.

From the 1st of December to the 1st of January, when the measured pressure as

presented in Figure 6.15 went from 1.0 to 1.6 MPa, LVDT02 registered a displacement of 0.18 mm. During the period of the 1st of January to the 1st of March, when the measured pressure went from 1.6 to 4.1 MPa, the same sensor registered a displacement of 0.78 mm.

Displacements from the 3D FE simulation at approximately the same positions as the LVDT sensors are presented in Figure 6.30. The displacements during the same two time periods as above are presented in Table 6.17. As seen in the results, the displacements from the FE simulation are smaller than the registered displacements by LVDT02. This gives further support to the theory that a pressure is active in the slot.

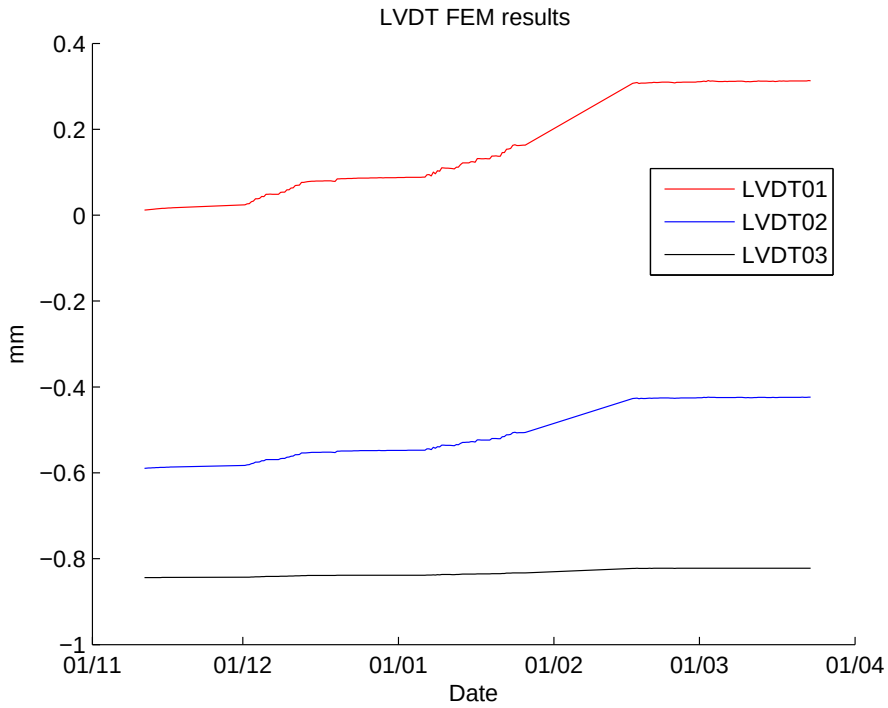

Figure 6.30: Displacements from FE simulation.

Table 6.17: Displacements from FE simulation during two time periods.

	LVDT01 [mm]	**LVDT02 [mm]**	**LVDT03 [mm]**
Dec 1 to Jan 1	0.06	0.03	0.00
Jan 1 to Mar 1	0.22	0.12	0.02

6.3 2D FEM LVDT displacement result

As seen in Figure 6.31, the measured displacement from sensors LVDT02 is larger than the obtained displacements from all the 2D FE models. The largest displace-

ment from the FE simulations is obtained from model 4, in which the pressure is applied in the entire length of the upstream side of the slot.

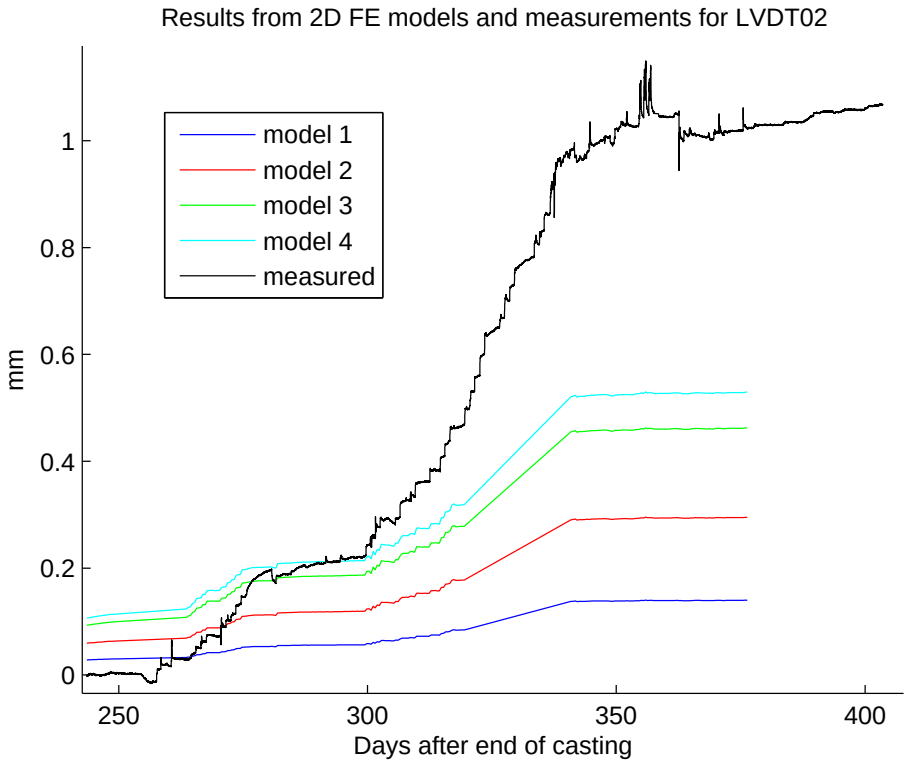

Figure 6.31: Results for sensor LVDT02 from 2D FE models and measurements.

Chapter 7

Discussion

7.1 Stress states and behavior of the concrete plug

7.1.1 Pre pressurization

During the design process, the concrete plug was assumed to de-bond from the rock and hence be stress free prior to grouting.

As mentioned in Chapter 3, in the case that the concrete plug de-bonded from the rock, the gap at the top of the concrete plug was estimated to approximately 4.2 mm (3.7 mm from autogenous shrinkage and 0.5 mm from cooling). This was close to the result from the FE simulation, indicating a gap at the top of 3.6 mm from shrinkage and roughly 1 mm from the cooling. Measurements however indicated almost no gap before the cooling with a maximum gap of 0.01 mm registered by the two sensors in the upstream direction at the sides of the concrete plug. The cooling resulted in an increased gap at the top of 0.05 mm and 0.07 mm. Sensors JM01-02 both indicated an increased gap of 0.07 mm while sensors JM05-06 indicated 0.10 mm and 0.03 mm respectively.

The joint meter indicating the largest displacement, JM05 positioned perpendicular to the rock at one of the sides, indicate a different behavior than the other sensors. During the period after the cooling during hydration and before the pre-grouting cooling, when the temperature is relatively unchanged, this sensor indicated an opening of the concrete - rock interface. One may therefore suggest that the concrete plug has de-bonded from the rock at, or close to, this position but the shrinkage is partially restrained due to concrete - rock bond at other positions. The relatively small and various gap increases might suggest that the concrete plug partially de-bonded from the rock but was restricted to fully contract due to the cooling.

The strains from the FE simulation are larger than the measured ones at many of the sensor positions. A large amount of the FEM strains occurs during the first days. This may be due to the low elastic modulus for the young concrete and the large autogenous shrinkage. The autogenous shrinkage occurring before the determined

zero levels is not included in the measurements strain results thus the measured strain will be lower than from the FE simulations. Other possible reasons is that a bond between the concrete and the rock restrain the concrete plug from shrinking or that the shrinkage was smaller than expected.

The FEM results for the no bond case, better resemble the measured ones than for the case of full bond. Based on this, it is therefore likely that the concrete plug have de-bonded from the rock. However, the measured change of strain between the first two key stages (before cooling for grouting to during grouting) was smaller than the corresponding results from the FE simulation. This may indicate that the concrete plug was partly restrained from temperature shrinkage by partial bond at the concrete-rock interface.

The sustained compressive strain after grouting would indicate that grout did penetrate into a gap between the rock and concrete plug. This would thus further indicate that the concrete plug did de-bond from the rock. The fact that sensors ST23 and ST25, positioned close to the slot, failed during grouting also indicates that grout penetrated into a gap.

In contrast to the strain results, the stress changes from measurements do not resemble the ones from the FE simulation assuming no bond as well as for the case with full bond. Compressive stress changes were however obtained between key stages 1 and 3 (from before cooling for grouting to after grouting) for both cases and for all sensors in the concrete plug. This would indicate that some prestressing of the concrete plug did take place and hence that the concrete plug had de-bonded from the rock to some degree.

The FE simulation for the case of no bond, indicated stresses between -0.62 to 0.30 MPa before the concrete plug was cooled for grouting, which can be seen as the stress range for the stress free assumption made during the design. The stresses from measurements were larger in both the cases with and without bond. In both cases, compressive stresses were obtained from measurements. This is most likely due to the shrinkage of the concrete which would further indicate that the concrete plug did de-bond from the rock to some degree.

The cooling before grouting resulted in a temperature decrease of approximately 8.5 °C. Together with a thermal dilation coefficient of $10^{-5}\,°C^{-1}$ and a Young's modulus of 33.9 GPa the thermal prestress would be approximately 2.9 MPa calculated with Equation (2.3). The FE simulation for the case of no bond, indicated a mean compressive stress change of 2.6 MPa. Calculated stress from measurements indicated a mean compressive stress change of 2.3 MPa. The prestress was hence less than estimated but still close to both the estimated value and the value from the FE simulation.

Taking all the above reasoning into account, it is likely that the concrete plug did de-bond from the rock to some extent. It is difficult to make an estimation of to what extent the concrete plug have de-bonded from the rock and hence also the stress state of the concrete plug within the time frame of this thesis. One estimation would be somewhere in between the measured values from the two cases.

7.1.2 Pressurization

The measured strains during the pressurization were large compared to the 3D FE simulations. Measurements corresponded best to the 2D model, where the full pressure was applied in the entire length of the upstream side of the slot. During the full scale test, the water leakage was too large to increase the pressure past 4.1 MPa. Also, the displacements measured by the working LVDT sensor were larger than the results from both the 2D and the 3D FE simulations. All of the above indicate that a pressure is present in the slot.

The difference between measurements and the 2D FEM results is larger for the displacement at the location of sensor LVDT02, than the strain at the location of sensor ST01. Also, the joint meters at the top of the plug failed during the pressurization. One may suggest that this is due to that the concrete plug displaced in the tunnel alignment. However, no sudden increase in displacement from sensor LVDT02 was obtained and the displacement curve is similar to the pressurization curve in Figure 6.15.

Measurements indicate that the concrete plug was in a compressive state during the whole pressurization period with a largest stress of -15.7 MPa. The mean stress when the largest pressure load was applied was -10.6 MPa.

7.2 Comparisons to previous tests

7.2.1 Prototype Repository

In the Prototype Repository test, described in Section 1.5.1, the plug was cooled in about the same degree as the concrete plug evaluated in this report. For the Prototype repository, this led to an increased concrete - rock gap of about 0.15-0.24 mm perpendicular to the rock. This was about twice as large as the results from the full scale test evaluated in this report. The evaluated stress change due to cooling in the Prototype Repository was between -1.4 to -2.2 MPa. This is compared to the stress changes between -0.77 to -3.04 MPa in the case of no bond evaluated in this report.

The gap in the concrete - rock interface was hence larger in the Prototype Repository test. The gap in the Prototype Repository was however evaluated in a more favourable way than in this report, see Dahlström (2009). With this in mind, together with the stress changes being roughly in the same magnitude in the two tests, could indicate that the concrete plug released from the rock.

7.2.2 Tunnel Sealing Experiment

Just as for the concrete plug evaluated in this report, water leakage was a problem in the TSX (described in Section 1.5.2). The measured displacement at the bulk head face was 0.25 mm during the final pressure of 4 MPa. This is compared to the displacement recorded by sensor LVDT02 of about 1 mm after the final pressure of 4.1 MPa was applied. Due to the different geometries of the two concrete plugs, a smaller displacement could be expected in the TSX than for the Äspö concrete plug. The displacement is however larger in the TSX than the evaluated displacements from the FE simulation in this report. This, in combination with the high water leakage, may suggest that there is an active pressure in the slot.

It was also concluded in the TSX that a selective de-bonding from the rock was obtained. It is plausible that the Äspö concrete plug also experienced a selective de-bonding from the rock.

7.3 Validity of results

Many of the results presented in this thesis are based on assumptions that will influence the validity of the results. Both strain and measurement results are based on the assumptions that the concrete plug has either de-bonded from the rock or not de-bonded at all. It is plausible that neither of these assumptions are true in reality. The assumptions are partly made to simplify the calculations. Also, due to the complexity of the problem, it is difficult to make any other assumption that would better capture the reality. The assumptions also represent two ideal cases, thus the real results would be somewhere in-between the results from the assumptions.

To determine the time when the sensors can be said to have bonded to the concrete (measurement reference point or zero level), proved to be a difficult task. The zero levels are determined with the assumptions that similar sensors yield similar strain results and bond to the concrete at roughly the same time. However, in the case of partial de-bonding of the rock, strain measurements from sensors at the same position but in different directions could differ more than was expected. The determined times of bonding are also not fully representative for the time that deformations start to create stresses in the concrete which has been assumed in the stress calculations. The zero levels are a large factor for the presented stress and strain results in this thesis. These results are therefore to a large extent affected by the possible faults in the zero levels.

Material parameters are of course also a source for reduced validity. Although the used material properties are the best estimate that could be made, they are evaluated on test results that do not fully represent reality and even if they did, no evaluation method is 100% accurate. Creep is not included in the stress calculations based on measurements. Creep will however, to some extent, affect the stresses in the concrete plug.

7.4 Further research

A FE model with the assumption of selective de-bonding can be made to further investigate the consequences this would have on the concrete plug. The FE model would give further knowledge about the stress state of the concrete plug, which is difficult to evaluate based on test results.

Since it is likely that a pressure is active in the slot, an investigation about the probable load case in the full scale test can be done. With this load case, one can evaluate the stress state in the concrete plug for the largest planned pressure of 10 MPa.

A study can also be done on possible ways to prevent water from entering the slot.

Bibliography

Cleveland, W., 1979. Robust locally weighted regression and smoothing scatterplots. Journal of the American Statistical Association 74 (368), 829–836.

Dahlström, L., 2009. Experiences from the design and construction of plug II in the Prototype Repository. Svensk Kärnbränslehantering AB, Stockholm, Sweden, SKB Report R-09-49.

Geokon Inc., 2013. Instruction Manual Model 4200 Series Vibrating Wire Strain Gages. Geokon Inc., Lebanon, NH, USA.

HBM, 2009. WA Inductive Standard Displacement Transducers. Hottinger Baldwin Messtechnik GmbH (HBM), Darmstadt, Germany, Data Sheet B0553-8.5 en.

Hewlett-Packard Co., 1994. The Fundamentals of Signal Analysis. Hewlett-Packard Co.

IGD-TP, 2014. DOPAS. Implementing Geological Disposal of Radioactive Waste Technology Platform, http://www.igdtp.eu/index.php/european-projects/dopas [2014-06-05].

Johannesson, L., Börgesson, L., Goudarzi, R., Sandén, T., Gunnarsson, D., Svemar, C., 2006. Prototype repository: A full scale experiment at Äspö HRL. Physics and Chemistry of the Earth 32 (1-7), 58–76.

Magnusson, J., 2013. Project meeting KBP1004 Concrete testing (low-pH), Short summary of results. NCC Construction Sverige AB, Sweden, Presentation slides.

Malm, R., 2012. Low-pH concrete plug for sealing the KBS-3V deposition tunnels. Svensk Kärnbränslehantering AB, Stockholm, Sweden, SKB Report R-11-04.

Malm, R., 2013a. Fullskaleförsök Valvplugg – Instrumentering Betongkupol. Aktivitetsplan, AP TD KBP1004-13-006, Stockholm, Sweden, SKB DokumentID 1375857.

Malm, R., 2013b. Instrumentation of the concrete dome plug DomPlu - DRAFT 2013-11-22. KTH Civil and Architectural Engineering, Stockholm, Sweden.

Malm, R., 2013c. SKB KBP 1004. Sweco, Sweden, Presentation slides.

Malm, R., 2014. Experience from the design and full-scale test of the concrete dome and bentonite seal for the KBS-3V repository. Svensk Kärnbränslehantering AB, Sweden, SKB TR-report, TR-14-XX (In preparation).

Martino, J., Dixon, D., Kozak, E., Gascoyne, M., Vignal, B., Sugita, Y., Fujita, T., Masumoto, K., 2006. The tunnel sealing experiment: An international study of full-scale seals. Physics and Chemistry of the Earth, Parts A/B/C 32, 93–107.

Orfanidis, S., 2010. Introduction to Signal Processing. Rutgers University, New Jersey, USA.

Palmer, S., Magnusson, J., 2012. Betongarbeten för kupolgjutning - Teknisk beskrivning. SKB DokumentID 1362686.

SIS, 2000. SS 137215: Concrete testing – Hardened concrete – Shrinkage. SIS Förlag AB, Stockholm, Sweden.

SIS, 2005. SS 137232: Concrete testing – Hardened concrete – Modulus of elasticity in compression. SIS Förlag AB, Stockholm, Sweden.

SKB, 2010. Design and production of the KBS-3 repository. Svensk Kärnbränslehantering AB, Stockholm, Sweden, Technical Report TR-10-12.

SKB, 2013. Dome plug in place in Äspö HRL. Svensk Kärnbränslehantering AB, Stockholm, Sweden, http://www.skb.se/Templates/Standard____35953.aspx [2014-06-05].

Swedenborg, S., 2011. PM Kontaktinjektering av betongkupol - Arbetsbeskrivning. NCC Construction Sverige AB, Göteborg, Sweden, SKB DokumentID 1353426.

TML Co., Ltd., 2013. Civil Engineering Transducers. Tokyo Sokki Kenkyojo Co., Ltd., Tokyo, Japan.

Vogt, C., Lagerblad, B., Wallin, K., Baldy, F., 2009. Low pH self compacting concrete for deposition tunnel plugs. Svensk Kärnbränslehantering AB, Stockholm, Sweden, SKB Report R-09-07.

Appendix A

Strain result plots

A.1 Casting to grouting period: Assuming no bond

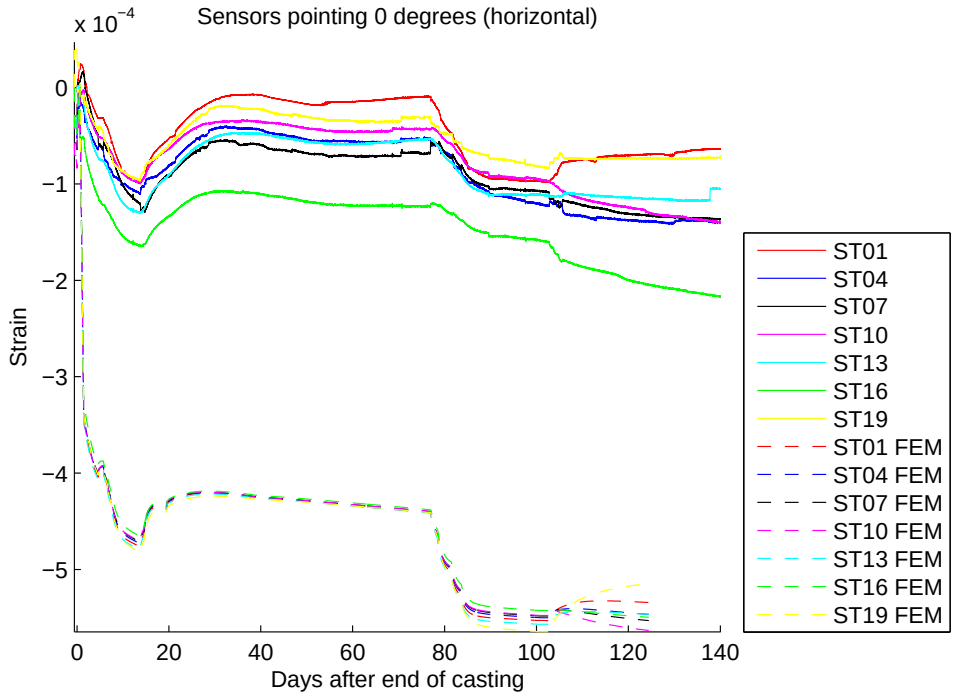

Figure A.1: Sensors pointing 0 degrees

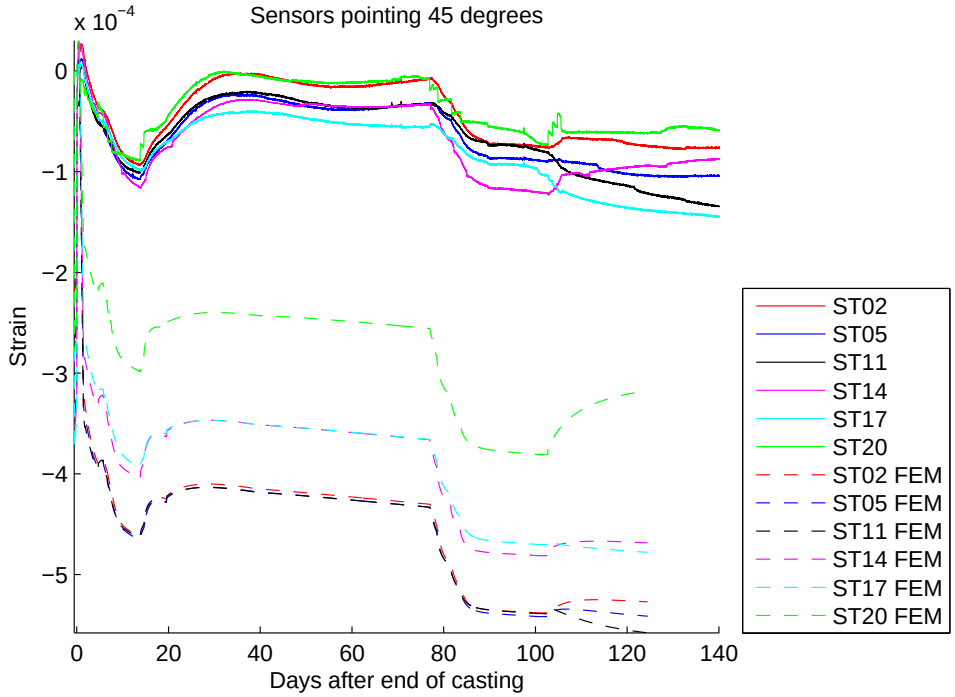

Figure A.2: Sensors pointing 45 degrees

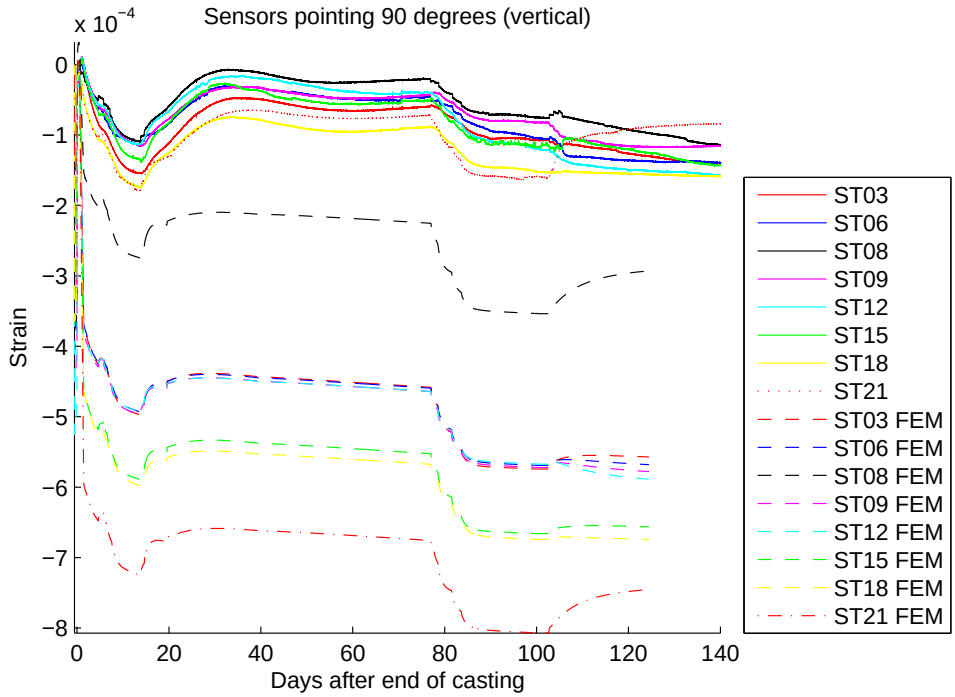

Figure A.3: Sensors pointing 90 degrees

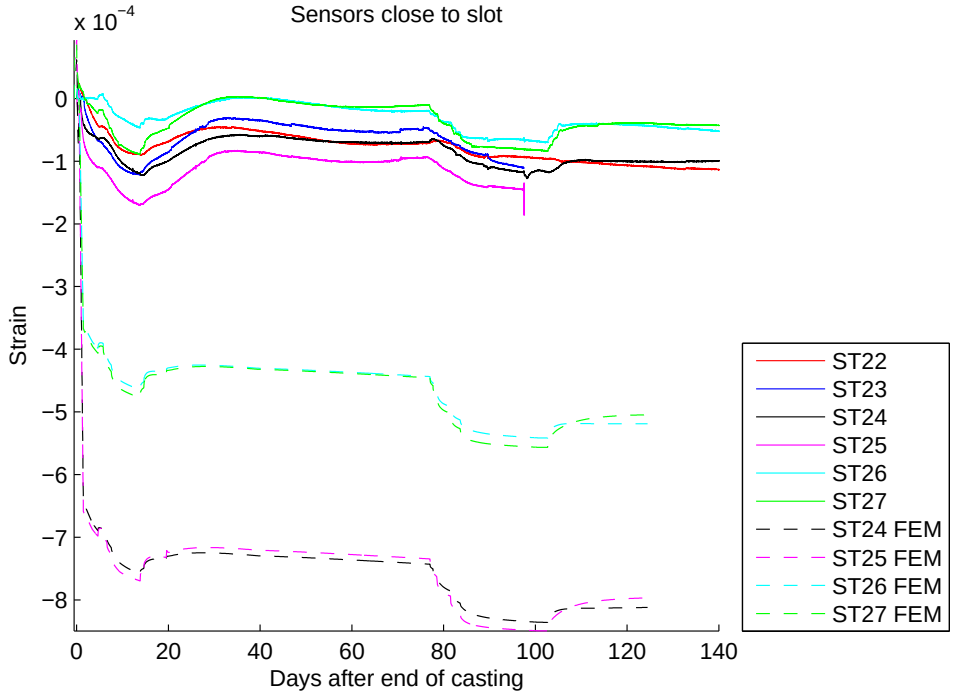

Figure A.4: Sensors close to slot

A.2 Casting to grouting period: Assuming full bond

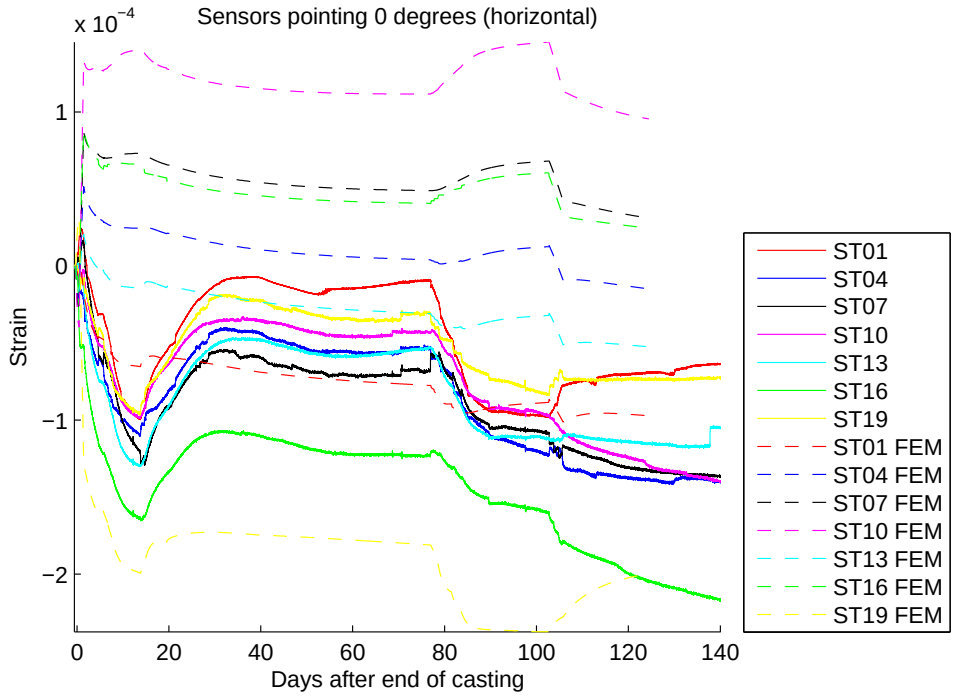

Figure A.5: Sensors pointing 0 degrees

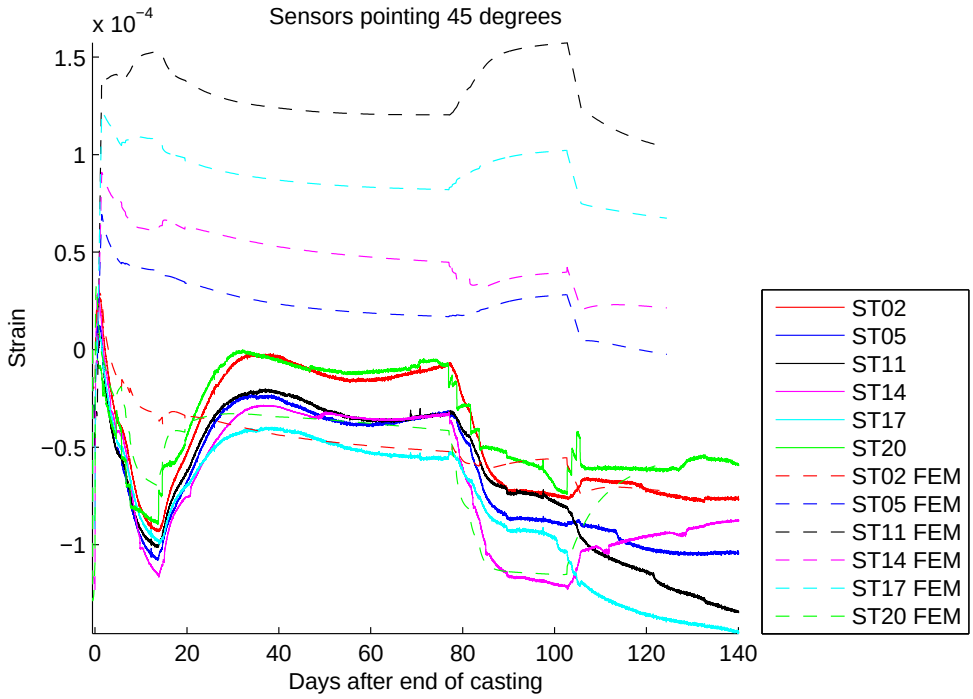

Figure A.6: Sensors pointing 45 degrees

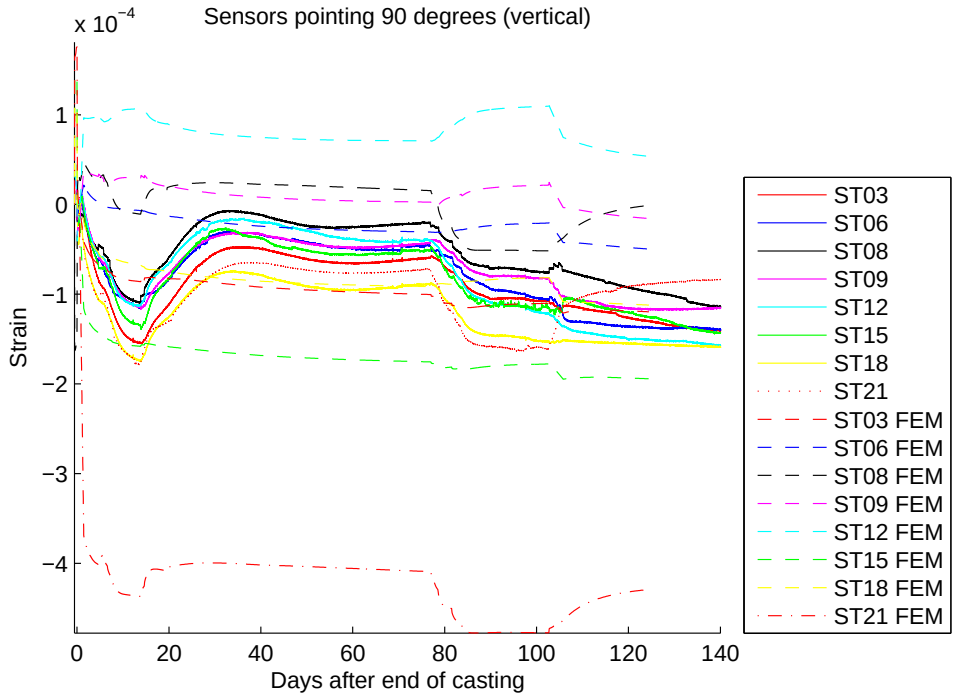

Figure A.7: Sensors pointing 90 degrees

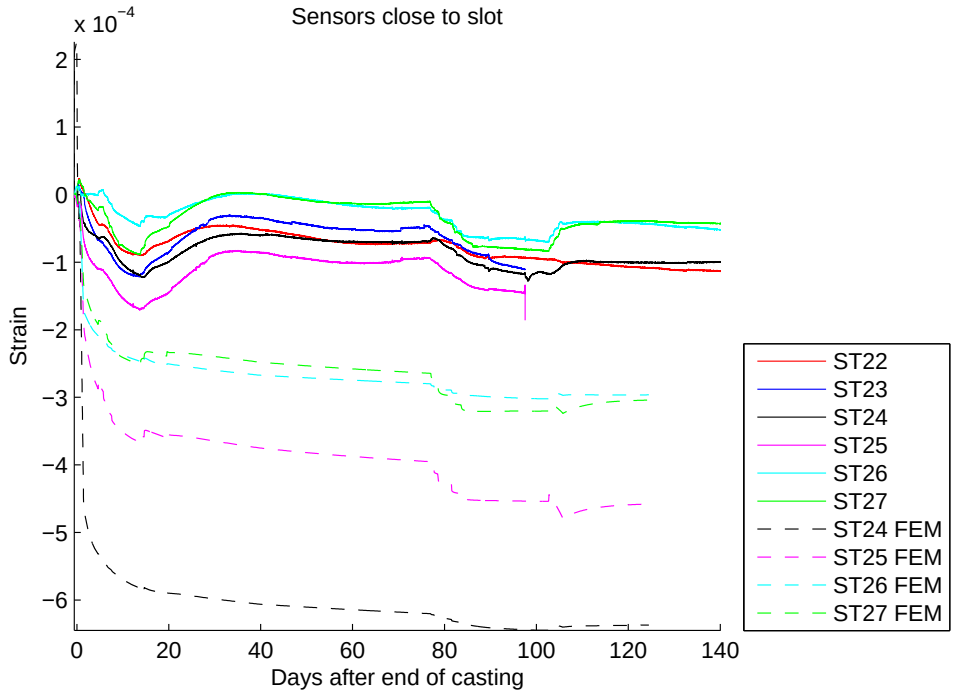

Figure A.8: Sensors close to slot

A.3 Pressurization period: Assuming no bond

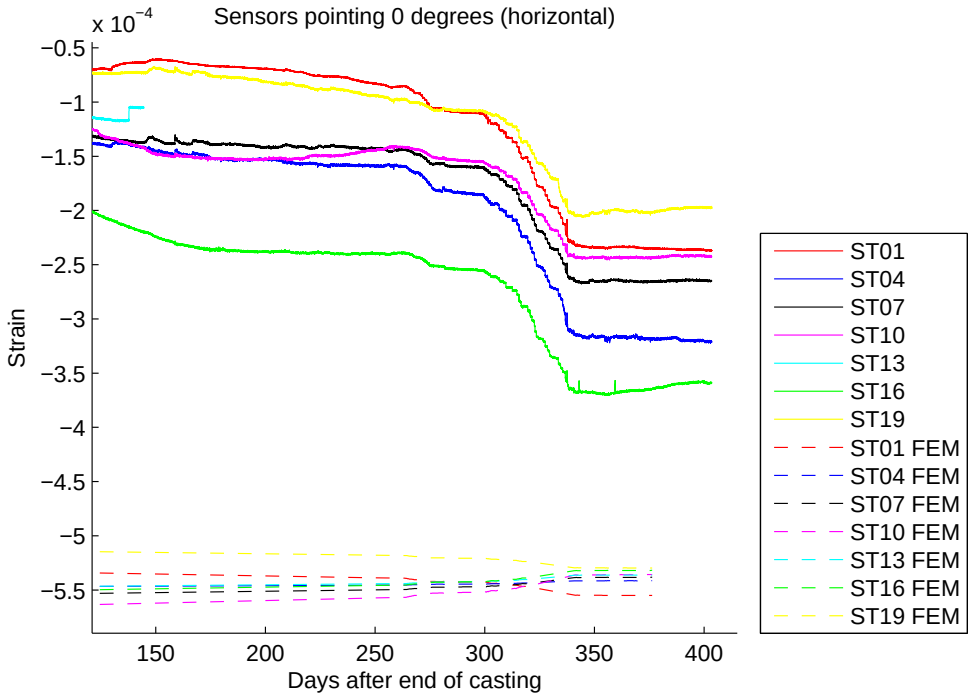

Figure A.9: Sensors pointing 0 degrees

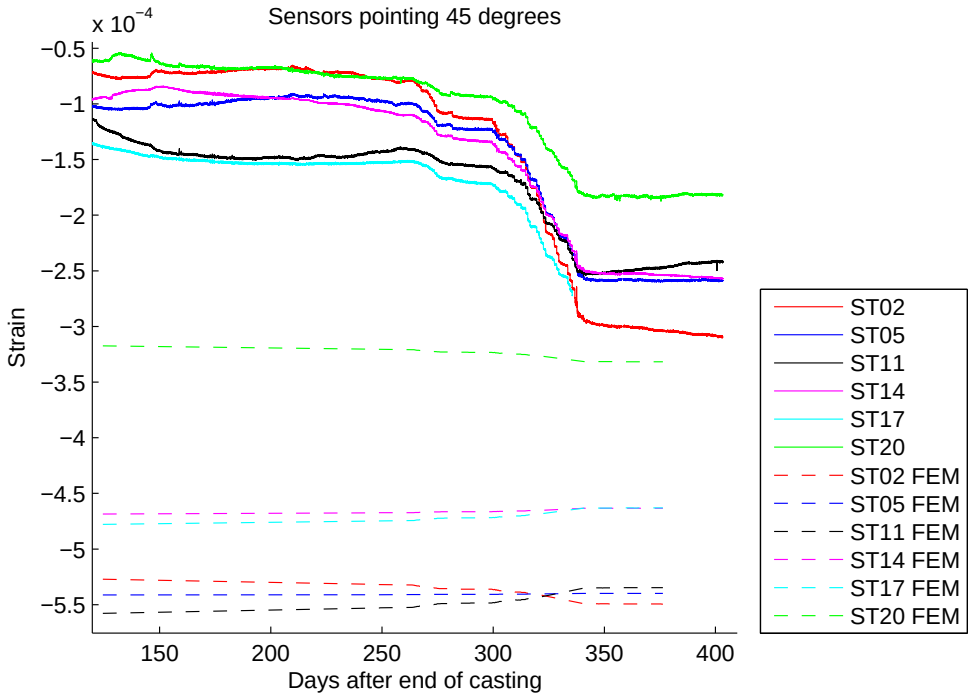

Figure A.10: Sensors pointing 45 degrees

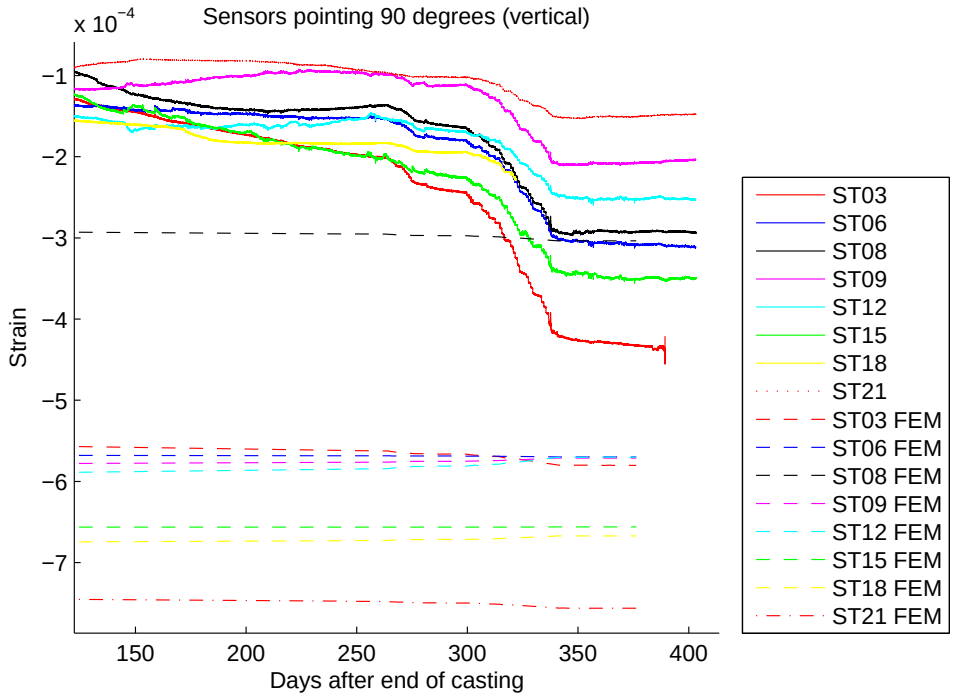

Figure A.11: Sensors pointing 90 degrees

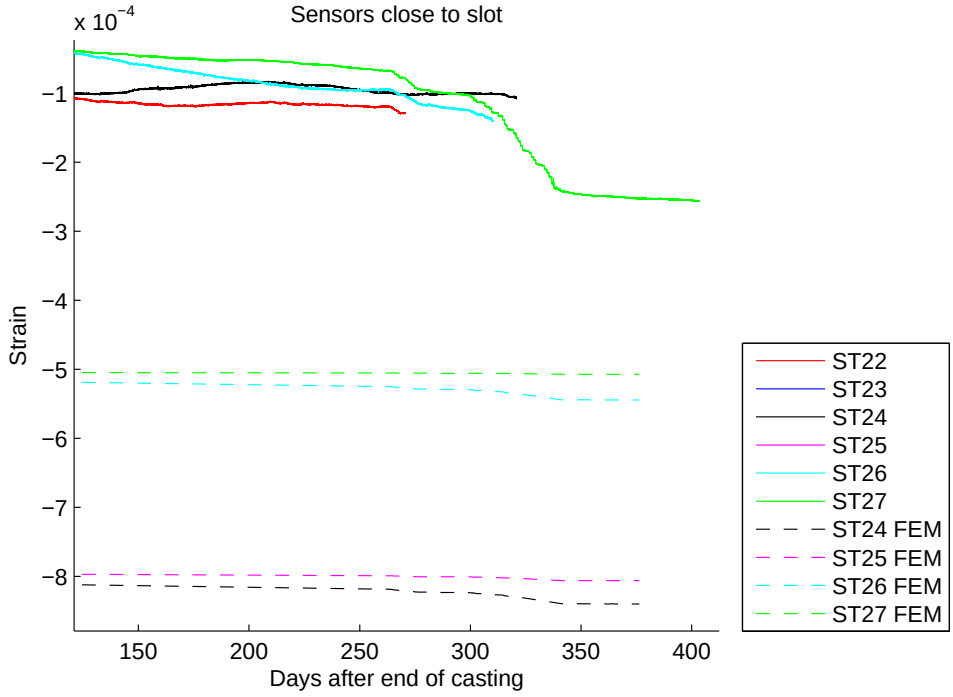

Figure A.12: Sensors close to slot

A.4 Pressurization period: Assuming full bond

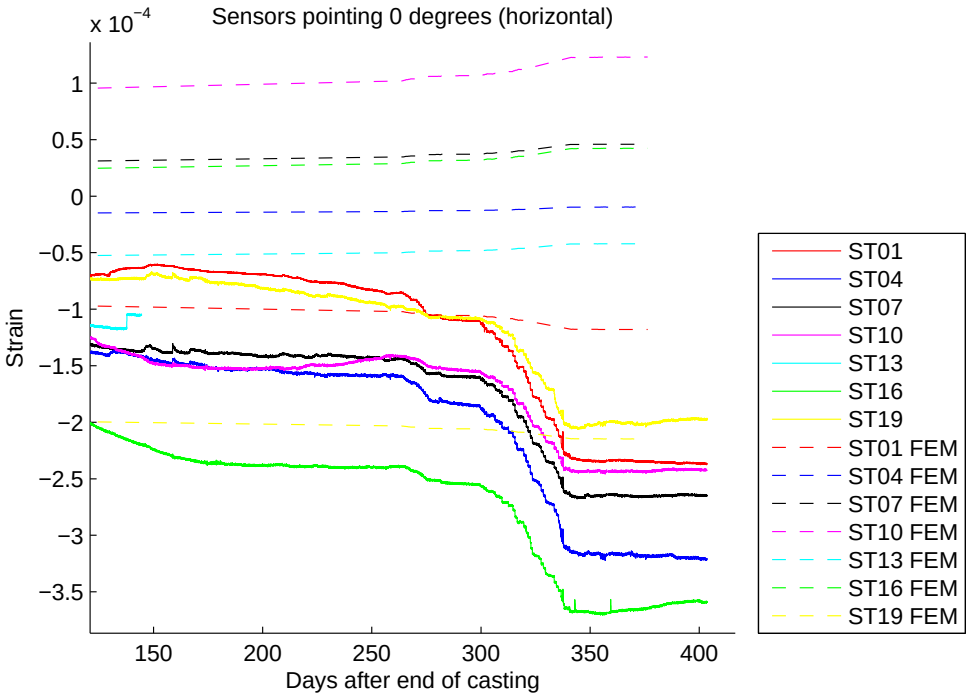

Figure A.13: Sensors pointing 0 degrees

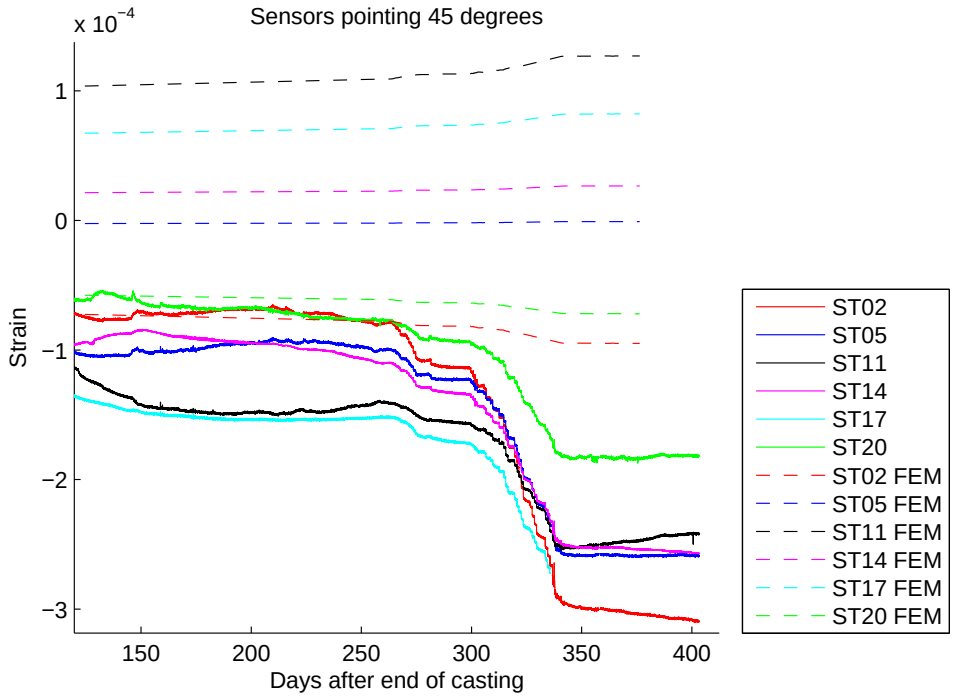

Figure A.14: Sensors pointing 45 degrees

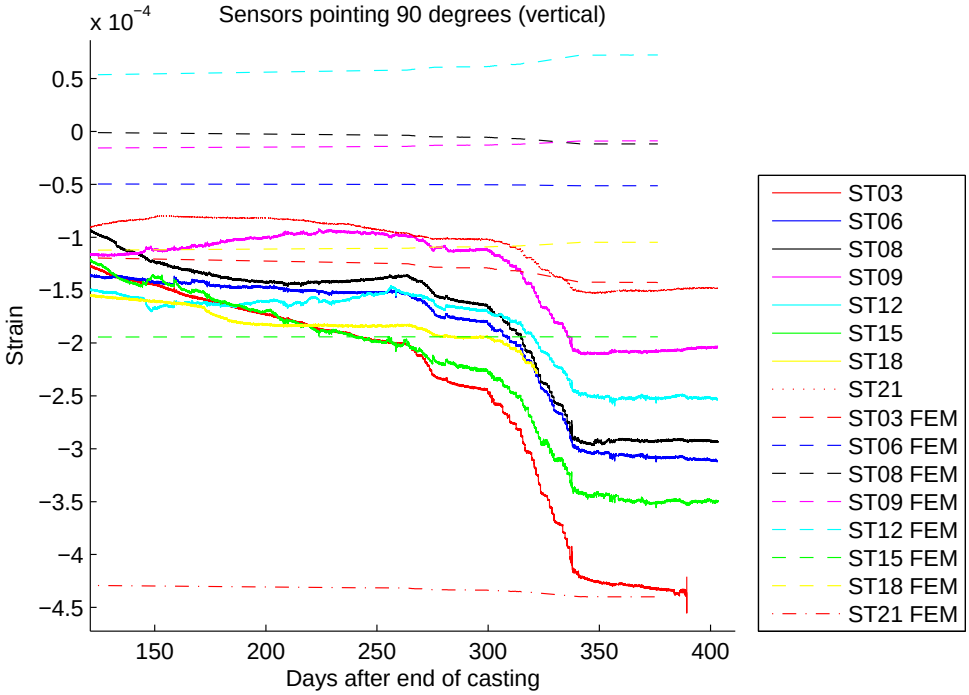

Figure A.15: Sensors pointing 90 degrees

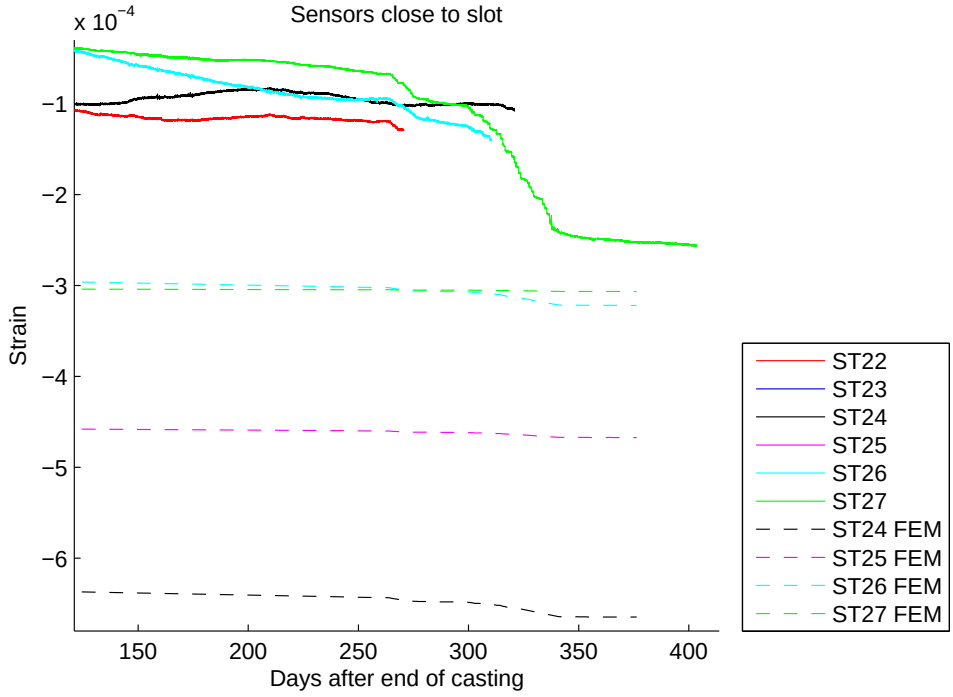

Figure A.16: Sensors close to slot

Appendix B

Stress result plots

B.1 Casting to grouting period: Assuming no bond

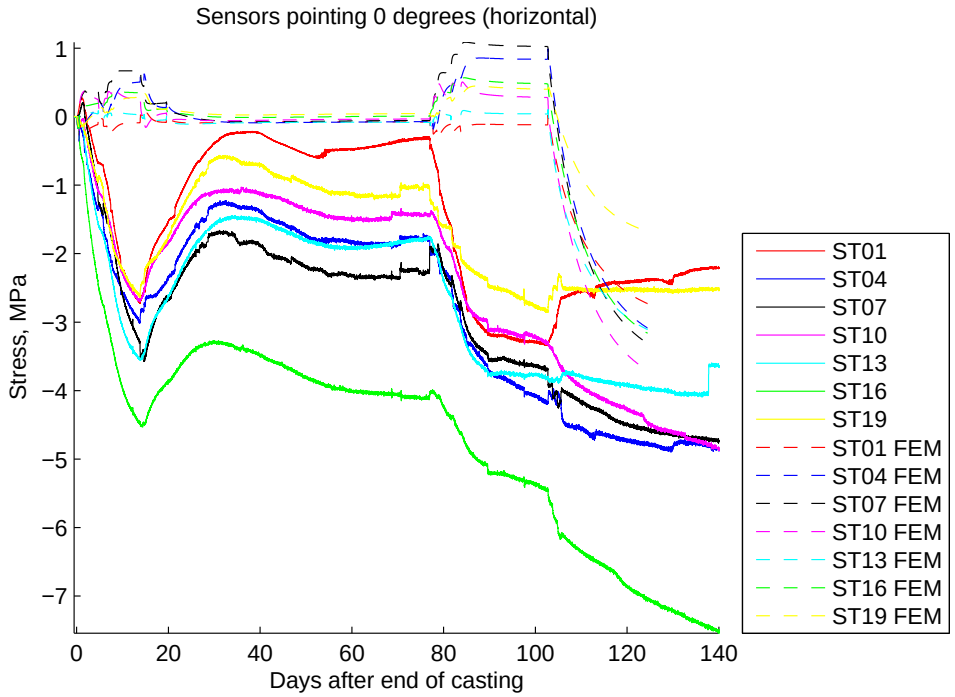

Figure B.1: Sensors pointing 0 degrees

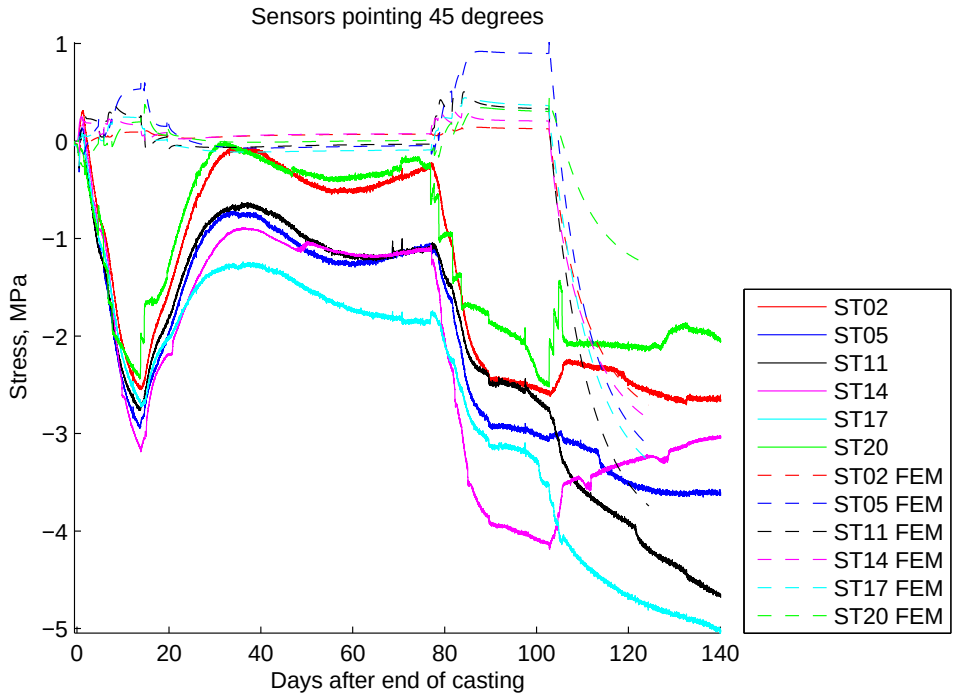

Figure B.2: Sensors pointing 45 degrees

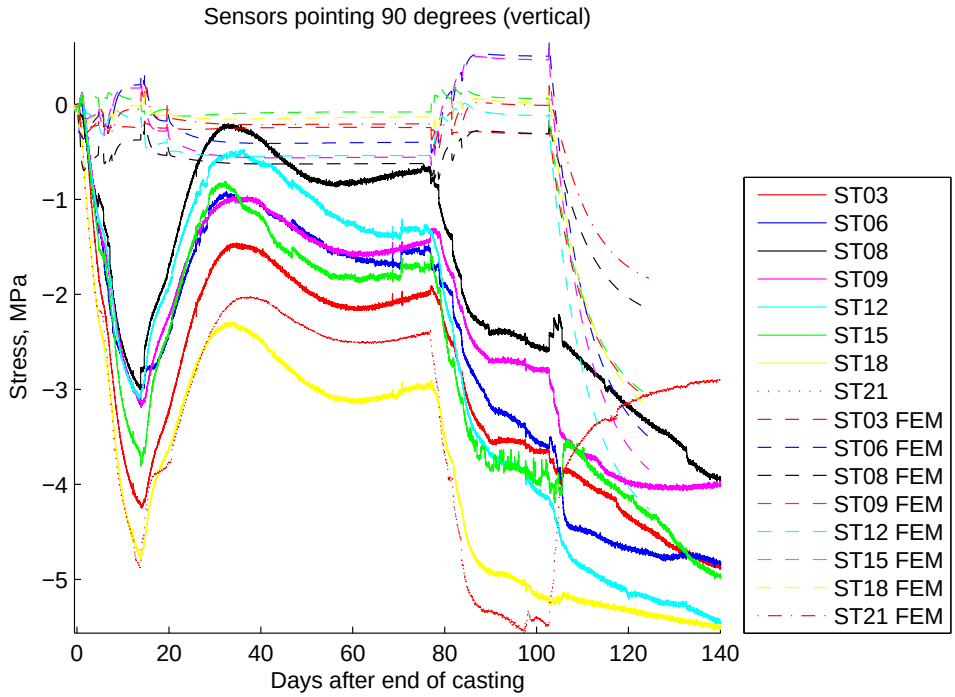

Figure B.3: Sensors pointing 90 degrees

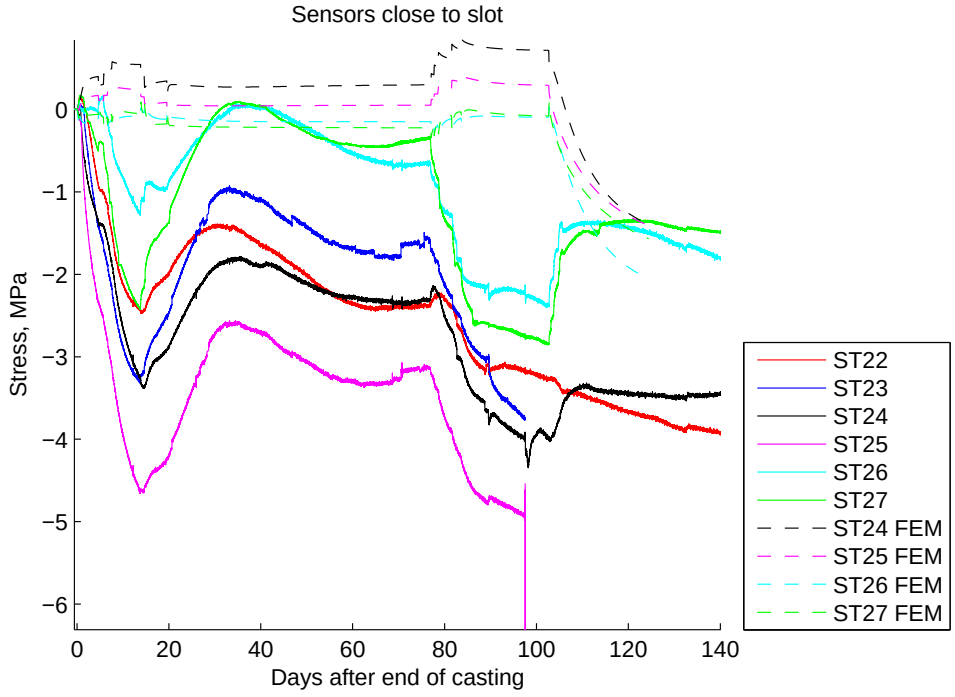

Figure B.4: Sensors close to slot

B.2 Casting to grouting period: Assuming full bond

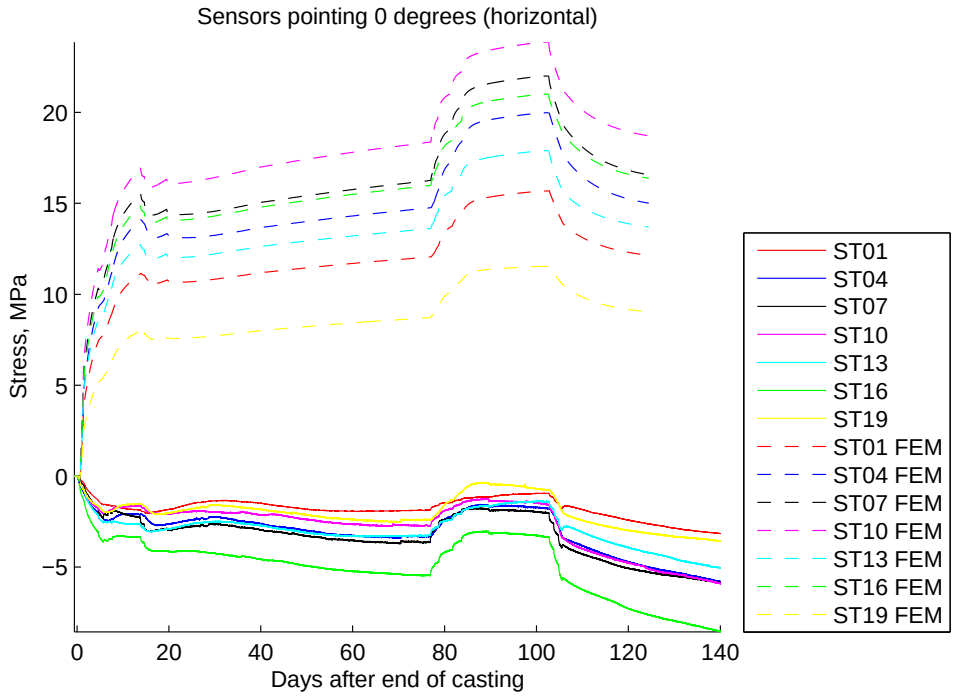

Figure B.5: Sensors pointing 0 degrees

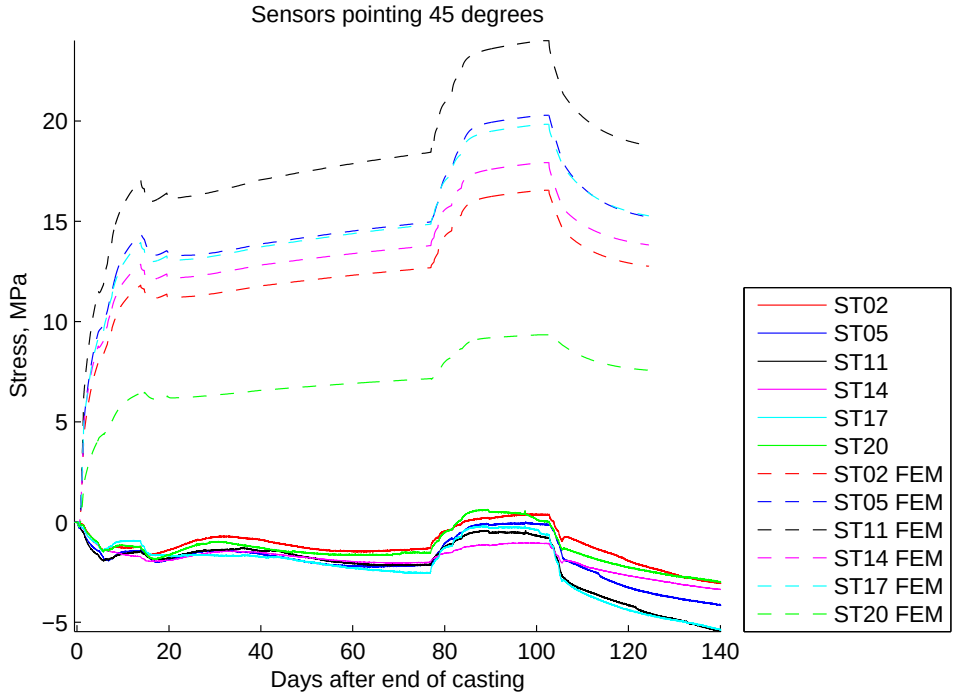

Figure B.6: Sensors pointing 45 degrees

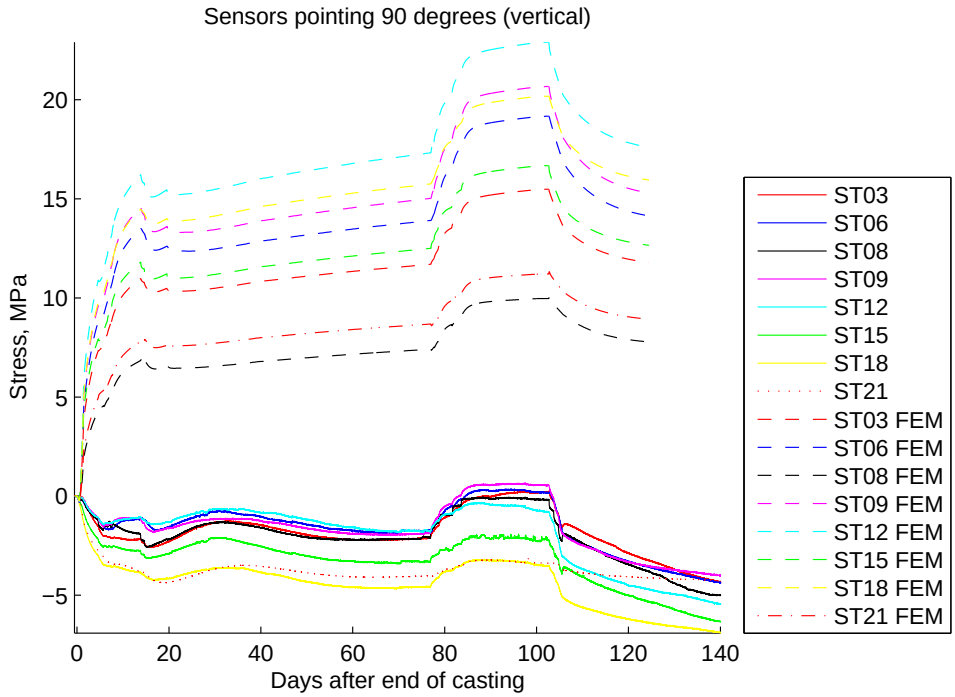

Figure B.7: Sensors pointing 90 degrees

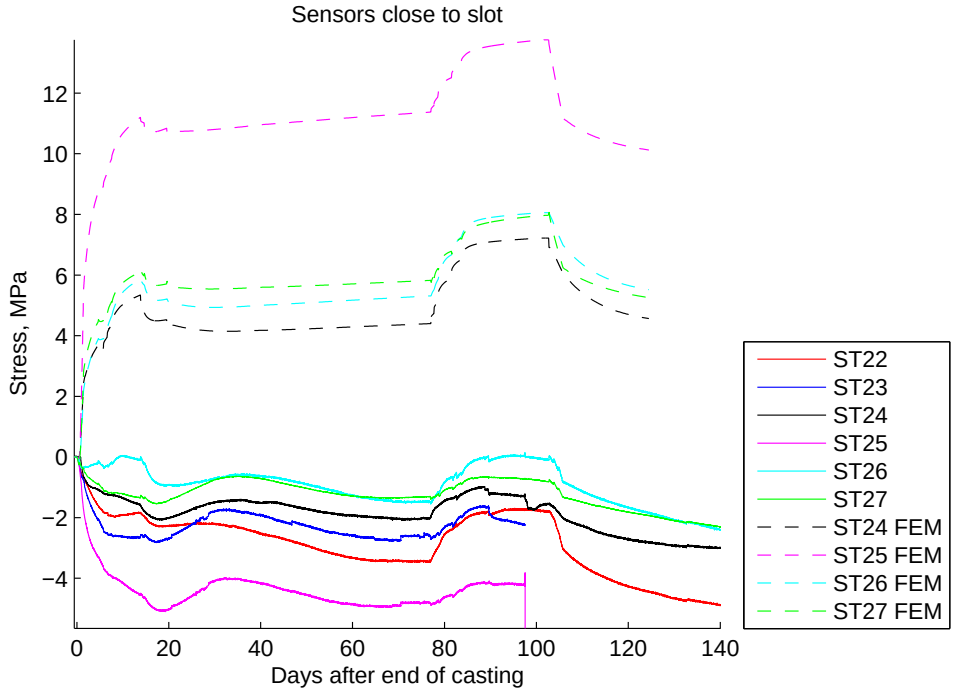

Figure B.8: Sensors close to slot

B.3 Pressurization period: Assuming no bond

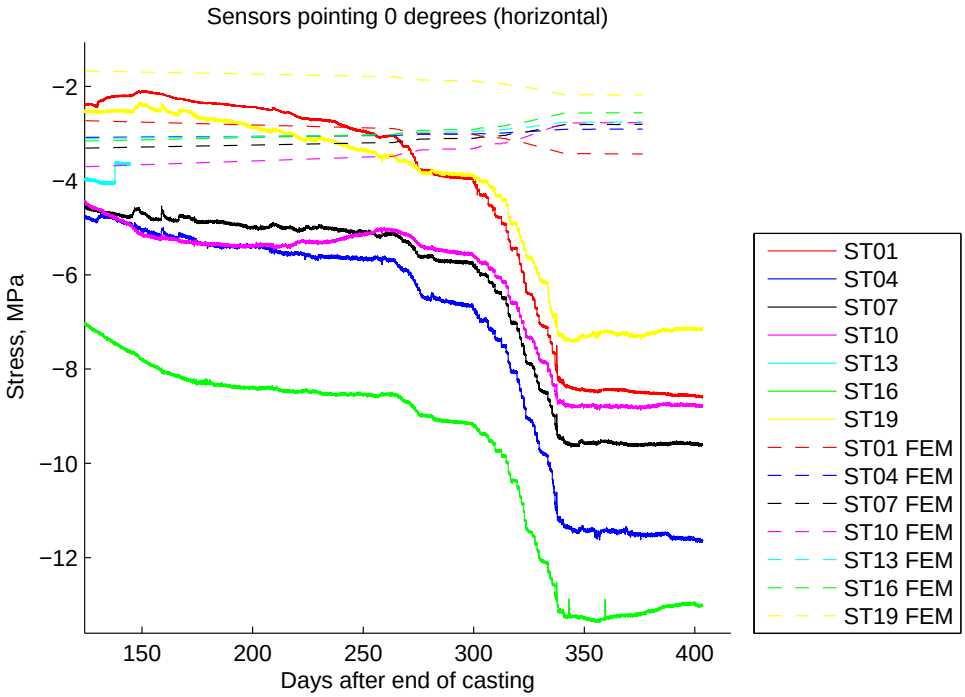

Figure B.9: Sensors pointing 0 degrees

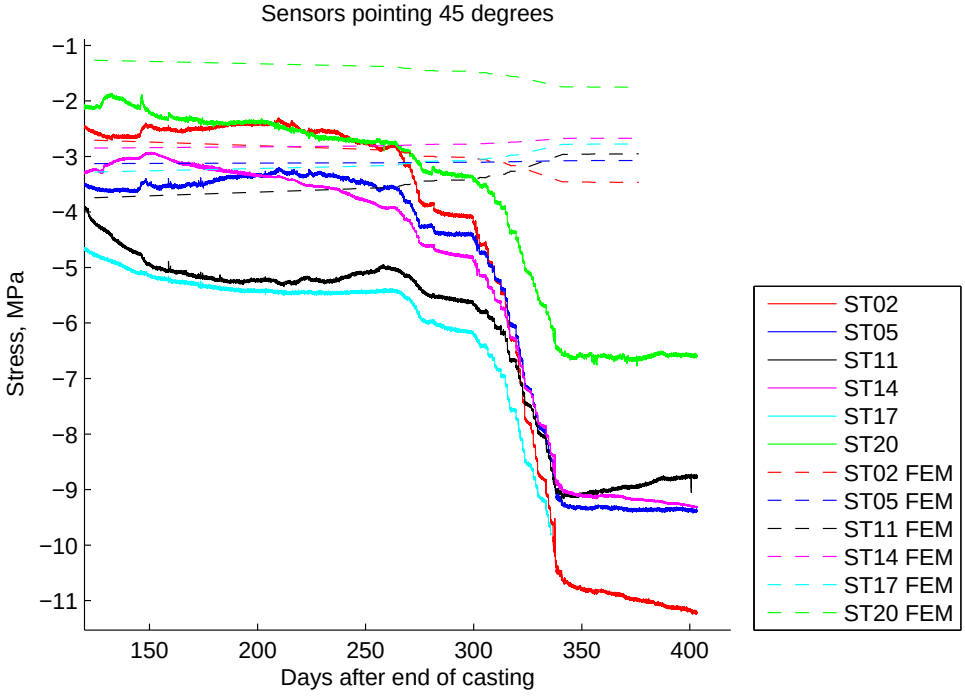

Figure B.10: Sensors pointing 45 degrees

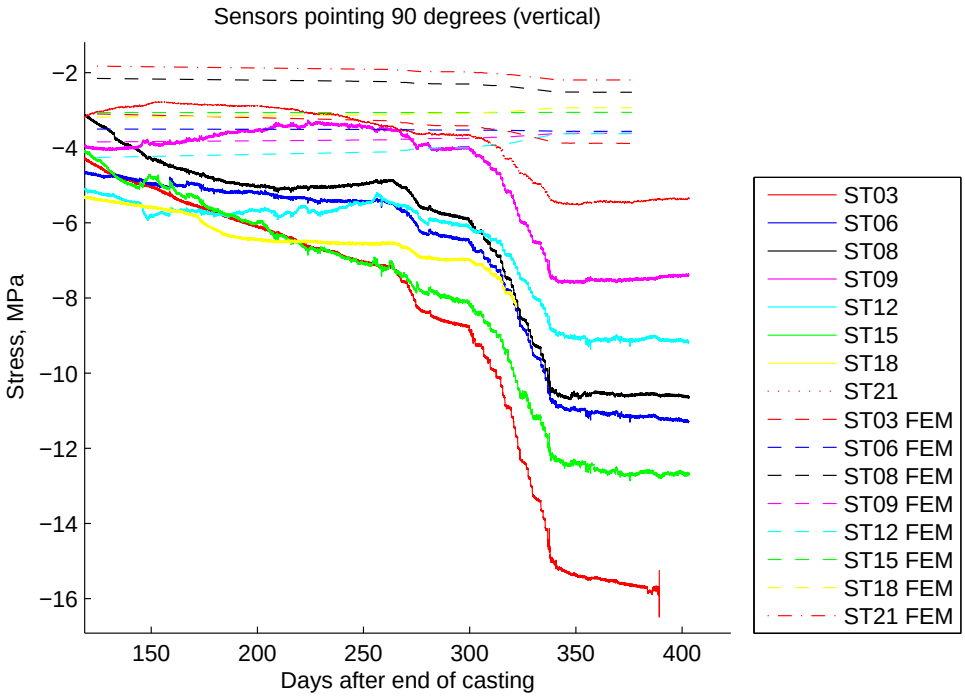

Figure B.11: Sensors pointing 90 degrees

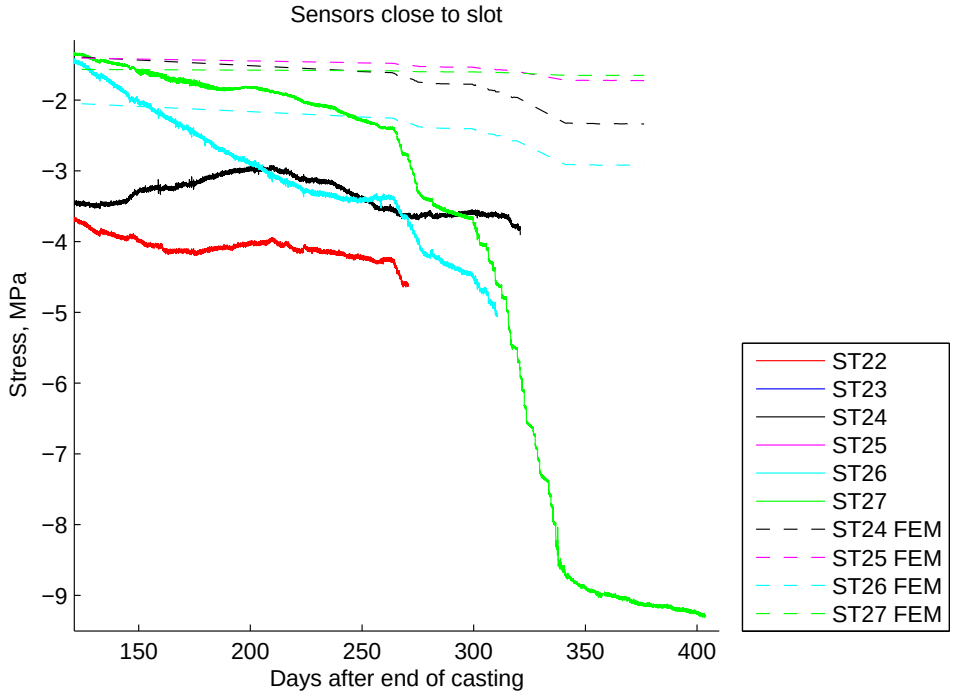

Figure B.12: Sensors close to slot

B.4 Pressurization period: Assuming full bond

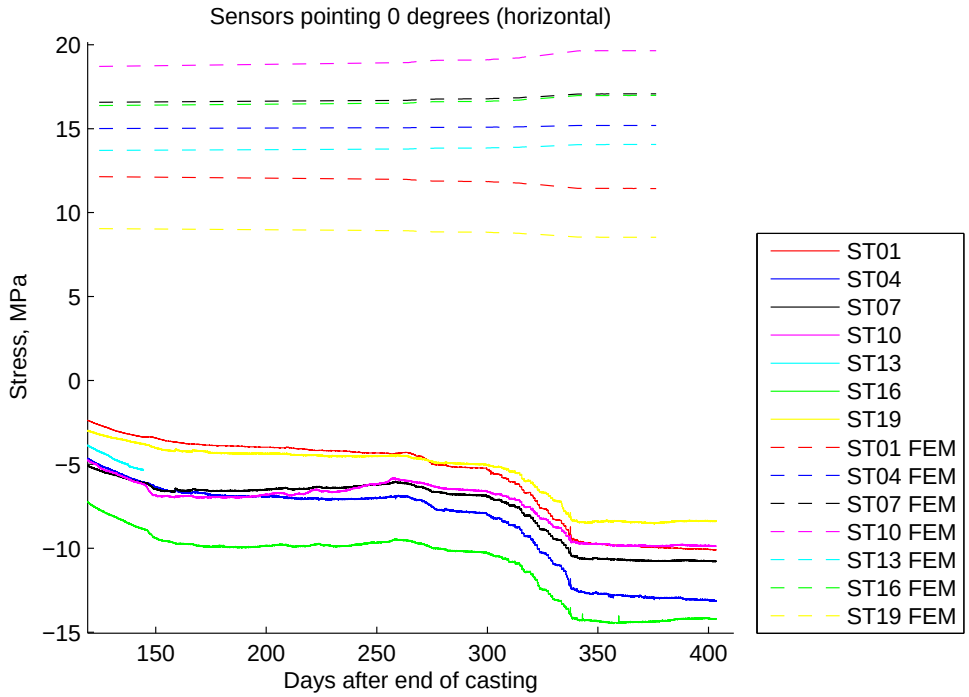

Figure B.13: Sensors pointing 0 degrees

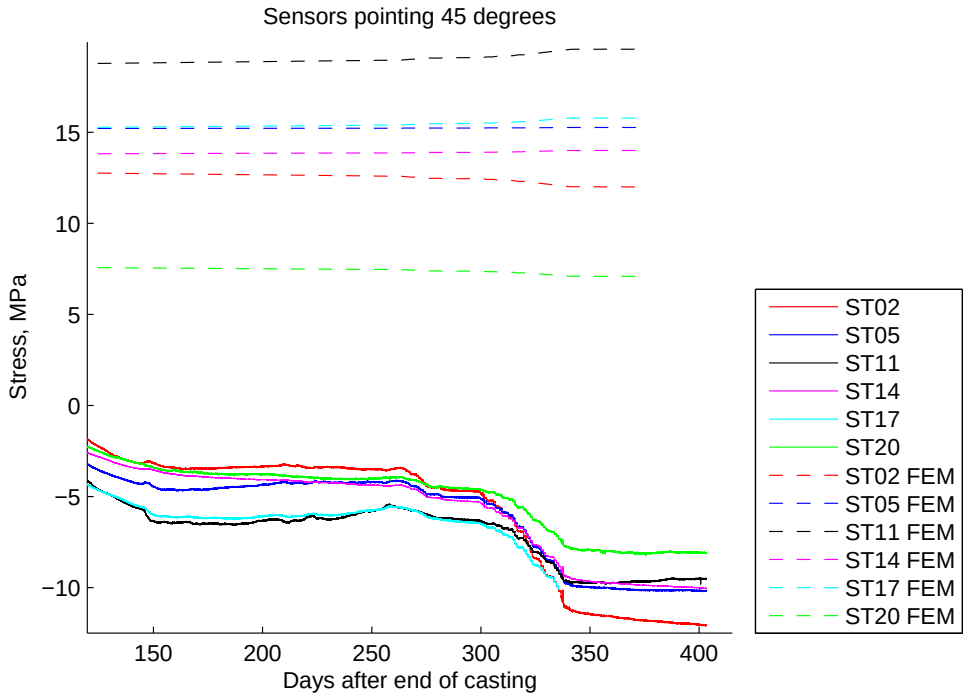

Figure B.14: Sensors pointing 45 degrees

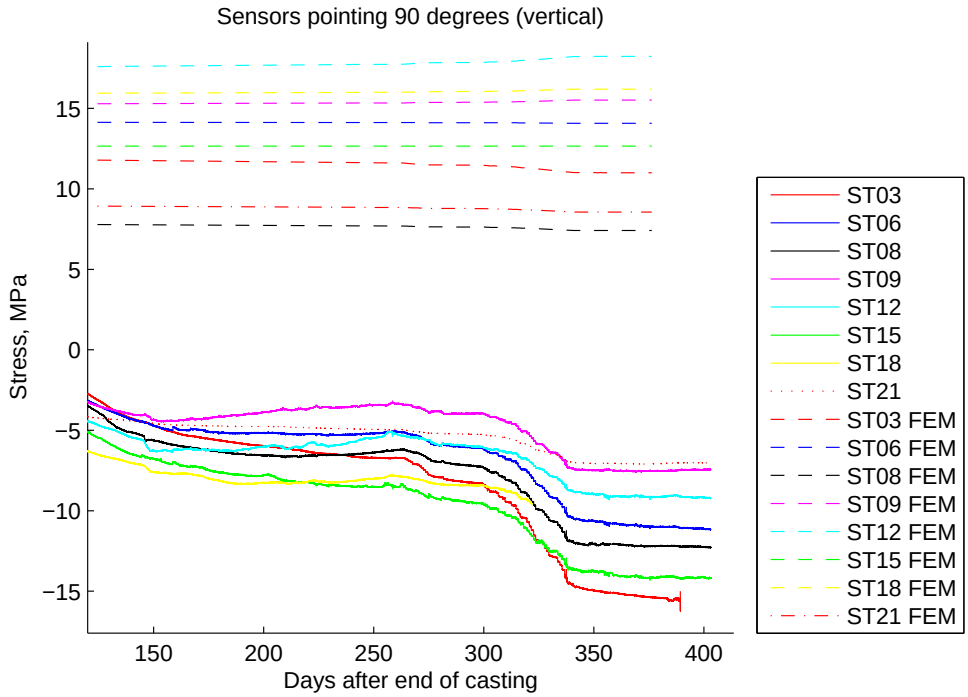

Figure B.15: Sensors pointing 90 degrees

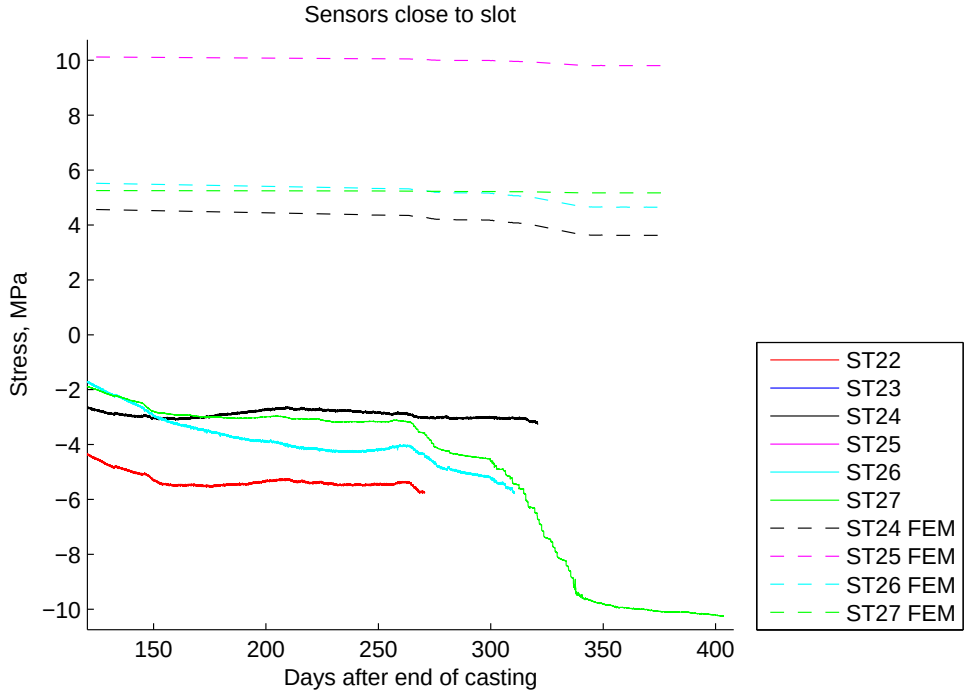

Figure B.16: Sensors close to slot

Appendix C

Cooling sequence

C.1 Cooling sequence

Cooling sequence

Cooling On/off	Date	Time	Days	Hours	Seconds	Temperature [C]
on	2013-03-13	06:54:00	0.0	0.0	0.000E+00	13
on	2013-03-14	06:54:00	1.0	24.0	8.640E+04	7
on	2013-03-15	13:54:00	2.3	57.0	2.052E+05	8
on	2013-03-18	10:54:00	5.2	126.0	4.536E+05	11
on	2013-03-19	13:54:00	6.3	153.0	5.508E+05	8
on	2013-03-20	09:54:00	7.1	173.0	6.228E+05	6
on	2013-03-21	08:54:00	8.1	196.0	7.056E+05	4
on	2013-03-27	15:54:00	14.4	347.0	1.249E+06	7
on	2013-03-28	10:54:00	15.2	366.0	1.318E+06	10
off	2013-04-02	08:54:00	20.1	484.0	1.742E+06	13
on	2013-05-29	17:54:00	77.5	1861.0	6.700E+06	11
on	2013-05-30	11:54:00	78.2	1879.0	6.764E+06	9
on	2013-05-31	08:54:00	79.1	1900.0	6.840E+06	6
on	2013-06-03	07:54:00	82.0	1971.0	7.096E+06	3
on	2013-06-05	10:54:00	84.2	2022.0	7.279E+06	1
on	2013-06-24	11:54:00	103.2	2479.0	8.924E+06	4
on	2013-06-25	11:54:00	104.2	2503.0	9.011E+06	7
on	2013-06-26	12:54:00	105.3	2528.0	9.101E+06	10
off	2013-06-27	12:54:00	106.3	2552.0	9.187E+06	13
off	2013-07-16	06:54:00	125,00	3000.0	1.080E+07	13